

Spring 2012

# Modeling Yield Surfaces of Various Structural Shapes

Oudam Meas

*Bucknell University*, [oudam.meas@bucknell.edu](mailto:oudam.meas@bucknell.edu)

Follow this and additional works at: [https://digitalcommons.bucknell.edu/honors\\_theses](https://digitalcommons.bucknell.edu/honors_theses)



Part of the [Civil and Environmental Engineering Commons](#)

---

## Recommended Citation

Meas, Oudam, "Modeling Yield Surfaces of Various Structural Shapes" (2012). *Honors Theses*. 119.  
[https://digitalcommons.bucknell.edu/honors\\_theses/119](https://digitalcommons.bucknell.edu/honors_theses/119)

This Honors Thesis is brought to you for free and open access by the Student Theses at Bucknell Digital Commons. It has been accepted for inclusion in Honors Theses by an authorized administrator of Bucknell Digital Commons. For more information, please contact [dcadmin@bucknell.edu](mailto:dcadmin@bucknell.edu).

# Modeling Yield Surfaces of Various Structural Shapes

By

**Oudam Meas**

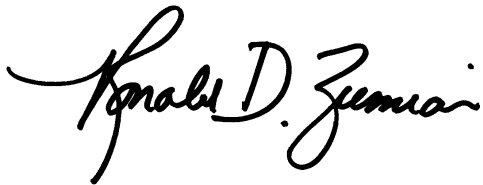
A Thesis Submitted to the Honors Council

For Honors in Civil Engineering

at Bucknell University

May 10<sup>th</sup>, 2012

Approved by:

A handwritten signature in black ink, reading "Ronald D. Ziemian". The signature is written in a cursive style with a large initial 'R' and a distinct 'Z'.

---

Adviser: Dr. Ronald D. Ziemian



## ACKNOWLEDGEMENTS

I wish to acknowledge the following individuals for their contributions to my insight and knowledge in completing this thesis. First, I wish to express gratitude to Dr. Ronald Ziemian for his instruction and tremendous help throughout the research and preparation for this thesis. His affection for structural engineering could hardly be matched and this gives me inspiration to explore more in this area. Second, I wish to thank my family for their support and care both during this project and my life at Bucknell University.

## TABLE OF CONTENTS

<b>Introduction.....</b>	<b>1</b>
<b>1.1 Objective .....</b>	<b>1</b>
<b>1.2 Scope.....</b>	<b>2</b>
<b>2 Background .....</b>	<b>3</b>
<b>2.1 Theory .....</b>	<b>3</b>
2.1.1 Yield Surface .....	3
2.1.2 Role of a Yield Surface in Inelastic Analysis.....	6
<b>2.2 History .....</b>	<b>7</b>
2.2.1 The Development of Yield Surfaces .....	7
2.2.2 Chen and Atsuta’s Yield Surfaces .....	9
2.2.3 Orbison’s Yield Surface .....	9
2.2.4 MASTAN2’s Yield Surface .....	10
<b>3 Discussion.....</b>	<b>11</b>
<b>3.1 Methodology .....</b>	<b>11</b>
<b>3.2 Generating Theoretical Yield Surface (<math>m_x, m_y, p</math>).....</b>	<b>12</b>
3.2.1 Moment Arms.....	26
<b>3.3 Weighting Factors .....</b>	<b>28</b>
<b>3.4 Regression Analysis.....</b>	<b>33</b>
<b>3.5 Concavity Test .....</b>	<b>39</b>
<b>3.6 Analysis .....</b>	<b>42</b>
<b>4 Methods and Results.....</b>	<b>45</b>
<b>4.1 Solid Rectangular Section.....</b>	<b>45</b>
4.1.1 Method.....	45
4.1.2 Results .....	56
<b>4.2 Hollow Rectangular Section .....</b>	<b>59</b>
4.2.1 Method.....	59
4.2.2 Results .....	65
<b>4.3 Solid Circular Section .....</b>	<b>68</b>
4.3.1 Method.....	68
4.3.2 Results .....	70
<b>4.4 Hollow Circular Section .....</b>	<b>72</b>
4.4.1 Method.....	72
4.4.2 Results .....	75
<b>4.5 Wide-Flange Section .....</b>	<b>77</b>
4.5.1 Method.....	77
4.5.2 Results .....	81
<b>5 Conclusions.....</b>	<b>88</b>
<b>Bibliography .....</b>	<b>89</b>
<b>Appendices.....</b>	<b>91</b>

## ABSTRACT

This study investigates the possibility of custom fitting a widely accepted approximate yield surface equation (Ziemian, 2000) to the theoretical yield surfaces of five different structural shapes, which include wide-flange, solid and hollow rectangular, and solid and hollow circular shapes. To achieve this goal, a theoretically “exact” but overly complex representation of the cross section’s yield surface was initially obtained by using fundamental principles of solid mechanics. A weighted regression analysis was performed with the “exact” yield surface data to obtain the specific coefficients of three terms in the approximate yield surface equation. These coefficients were calculated to determine the “best” yield surface equation for a given cross section geometry. Given that the exact yield surface shall have zero percentage of concavity, this investigation evaluated the resulting coefficient of determination ( $R^2$ ) and the percentage of concavity of the customized yield surface in comparison to those of the widely accepted yield surface.

Based on the results obtained, only the customized yield surface equations for wide-flange sections fit the corresponding theoretical yield surfaces better than the widely accepted yield surface equation. For other sections, the  $R^2$  was either very small, negative, or zero for both the customized yield surface equation and the widely-accepted yield surface equation. By using the concavity test developed in this study, the theoretical yield surface was found to have a small percent of concavity, which can be attributed to the high sensitivity of the convexity test to rounding off errors. In these

cases, a negligible degree of concavity was consistently observed at these points. Therefore, the percentage of concavity of the exact yield surface was subsequently used as an offset for assessing the concavity of both the widely accepted yield surface and the customized yield surface equations. With this approach, both the widely accepted and customized yield surfaces were shown to be completely convex for all sections except for hollow circular sections. With regard to both improving  $R^2$  values and maintaining the continuous and convex characteristics of a yield surface, only the widely accepted yield surface equation could be customized to fit the theoretical yield surfaces for wide-flange sections.

# INTRODUCTION

## 1.1 OBJECTIVE

Most of today's structural design is based on an analysis that does not account for the possibility of the material failing, either by excessive yielding or fracture. To assure that these failure modes will not govern, the capacity of members are significantly increased when they are designed. Such an approach has proven to be safe and reliable, but in many cases it can be very conservative and subsequently, less economical. Over the past twenty years, research has continued in developing more advanced structural analysis methods that can account for material yielding and thereby allow forces within the structure to redistribute away from members that are yielding and on towards members with reserve capacity. Such analysis approaches provide for improved economy and a better representation of the actual structural performance. With this in mind, the American Institute of Steel Construction (AISC), which is the governing body for the design of hot-rolled steel buildings in the U.S., recently released an updated specification (AISC, 2010) that contains new rules (Appendix 1 – *Design by Inelastic Analysis*) that allows engineers to take advantage of the actual material nonlinear behavior (termed inelasticity) that will occur as a structure reaches its limit state of strength. Unfortunately, very few of today's commercially available analysis software packages provide such functionality. One of the difficulties in developing such software



is providing an analysis that is accurate and can be completed within a reasonable or even acceptable amount of time (i.e., within minutes, not hours or days).

A key component of such an analysis is the device that is used to determine when full yielding will occur. This device, commonly referred to as a yield surface, is in theory a function of each member's cross sectional shape. As a result, it is unique to each type of member used. To maintain an efficient analysis, software developers have been using a single yield surface equation to represent all cross sections (e.g., I-beams, box sections, pipes, etc.). Unfortunately, this approach can in many cases provide unconservative results and most engineers agree that a scheme for efficiently incorporating custom fit yield surfaces within structural analysis software is needed before design by inelastic analysis will become more common. In this regard, this research explores the possibility of custom fitting a single general form yield surface to the characteristics and dimensions of individual structural shapes.

## 1.2 SCOPE

The scope of this project consists of custom fitting a widely accepted yield surface equation to all wide-flange, solid and hollow rectangular, and solid and hollow round shapes. For example, the coefficients (3.5, 3.0, and 4.5) used in the general expression for a single all-purpose yield surface, shown below as:

$$p^2 + m_x^2 + m_y^4 + \underline{3.5}p^2m_x^2 + \underline{3.0}p^6m_y^2 + \underline{4.5}m_x^4m_y^2 = 1.0 \quad \text{Eq. (1)}$$

could be individually tailored to best match the unique theoretical yield surface for a given cross section. The expected outcome from this study will be a computational algorithm, based on regression analysis, that determines the best numerical coefficients to be used in the above yield surface equation for any given shape (e.g. I-beam) and its corresponding dimensions (such as height, width, and wall thicknesses). The optimum numerical coefficients will be determined based on the respective  $R^2$  and concavity of the yield surface. Note that only one quadrant of the yield surface needs to be studied because each quadrant is assumed for isotropic material to be identical to the others.

## **2 BACKGROUND**

### **2.1 THEORY**

#### **2.1.1 YIELD SURFACE**

The yield surface is a “hypersurface” of the combined effects defining a yield criterion. This can be viewed as combinations of multidirectional stress in a structural member that result in stresses equal to the yield stress of the material [5]. Theoretically, a yield surface is a six-dimensional surface, corresponding to the six generalized stress components. In the plastic-hinge analysis of ductile frames, the specified yield surface is a stress resultant yield surface that only needs be three-dimensional [1]. The surface is a non-dimensional function of axial force and bending moments about two axes, all of which produce normal stress in the direction of the length axis of the member. The surface is represented by the function:

$$\phi(m_x, m_y, p)$$

where:

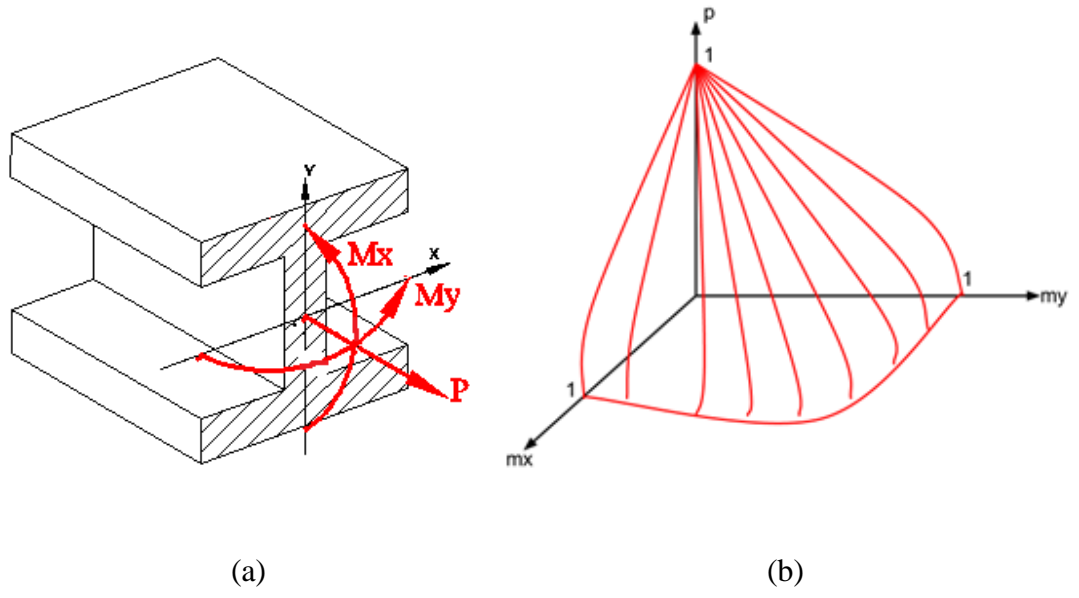
$p = P/P_y$ , the ratio of the axial force to the squash (axial yield) load,

$m_x = M_x/M_{px}$ , the ratio of the major-axis bending moment to the corresponding plastic moment, and

$m_y = M_y/M_{py}$ , the ratio of the minor-axis bending moment to the corresponding plastic moment.

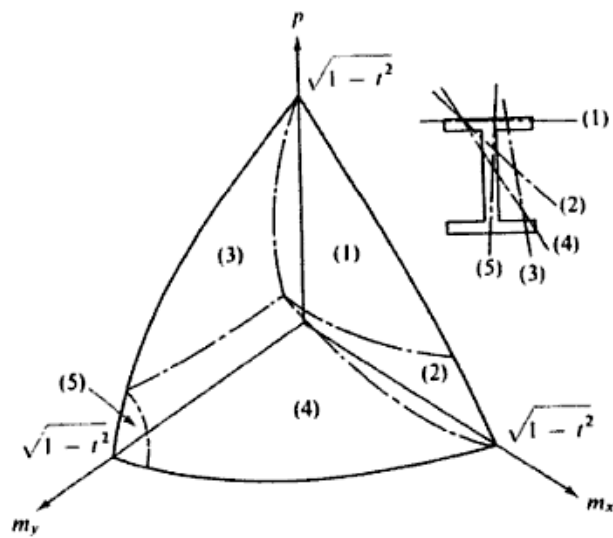
The squash load  $P_y$  is the product of the cross-sectional area,  $A$ , and the material yield stress,  $F_y$ . The plastic moment,  $M_p$ , about a principle axis is the product between the plastic section modulus,  $Z$ , about the corresponding axis and the material yield stress,  $F_y$ . Figure 1.a shows an example of a plastic-hinge at a wide-flange section that is subjected to combined axial force and bending moments about two principal axes and Figure 1.b shows the traces of a typical yield surface.

The reasoning and justification for adopting a three-dimensional yield surface instead of a six-dimensional surface are presented in Section 2.2.1. The theoretically exact representation of a yield surface is a multi-faced surface (composed of multiple equations) as shown in Fig. 1.c. Single-equation yield surfaces, however, are needed because such forms satisfy the computational requirement of “being a continuous function” while multi-faced surfaces do not [4].



(a)

(b)



(c) [Reference 4]

Figure 1. (a) Wide-flange section under combined axial and bending loads (b) sketch of a wide-flange yield surface (c) Chen and Atsuta's multi-faced wide-flange yield surface.

The theoretical yield surface can be calculated for a given shape, dimensions, and material of a cross section based on cross-sectional equilibrium [1].

### **2.1.2 ROLE OF A YIELD SURFACE IN INELASTIC ANALYSIS**

The yield surface is a device that can indicate when plastic hinging occurs. Yielding is typically defined as a loss of stiffness at a location within a cross section where any additional stress is redistributed to the neighboring unyielded parts that still have stiffness. Initial yielding occurs at the beginning of the stress redistribution; complete yielding or a plastic hinge is the limit at which a cross-section can resist any additional applied loading. Therefore, plastic hinging serves as an important component of an inelastic analysis, in which the main goal can be considered as designing members to use of all their reserved capacity just before the strength limit of the system is reached. Practically, the yield surface is a benchmark for the design that attempts to maximize the economy of structural members without exceeding the design strengths. The combined axial and bending moments that are resisted by a member (after being normalized by the member's squash load and plastic moments) is compared with the yield surface of the member's cross-section to assess whether or not a plastic hinge has formed. For inelastic analysis software to perform efficiently it is ideal to employ a yield surface that formatted into an appropriate single continuous equation.

## **2.2 HISTORY**

### **2.2.1 THE DEVELOPMENT OF YIELD SURFACES**

In principle, a stress-resultant yield surface is a six-dimensional surface, which includes all possible degrees of freedom at a typical member end. Possible member or element types include the beams, columns, and braces found in a typical structure. These six degrees of freedom account for the effects of axial force, two directions of shear force, two directions of bending moment, and torsion. An example of a wide-flange cross-section of such an element is shown in Fig. 2 [5].

For a stress resultant yield surface, only normal stresses are typically considered. Normal stresses are the result of axial force and bending moments about two principle axes, which define the three attributes of the yield surfaces explored in this study. As a result, this means that the effects of shear force in two directions and torsion are neglected. By doing so, the following two assumptions must be made:

- (a) Material is elastic-perfectly plastic, and
- (b) Plane sections remain plane before and after load s are applied.

Elastic-perfectly plastic behavior means that there are no transitions between elastic and plastic states. Figure 3 is the stress-strain diagram for typical carbon steel. The stress-strain diagram for an elastic-perfectly plastic material differs from that of the typical carbon steel in that the transition between elastic and plastic range and strain hardening are not included. Figure 4 is the normal stress diagram over the depth of a

cross section. For an elastic-perfectly plastic material, the transitional state of stress occurs between initial yielding and full plastic hinge are ignored. Thus, the cross-section is either fully elastic or completely plastic.

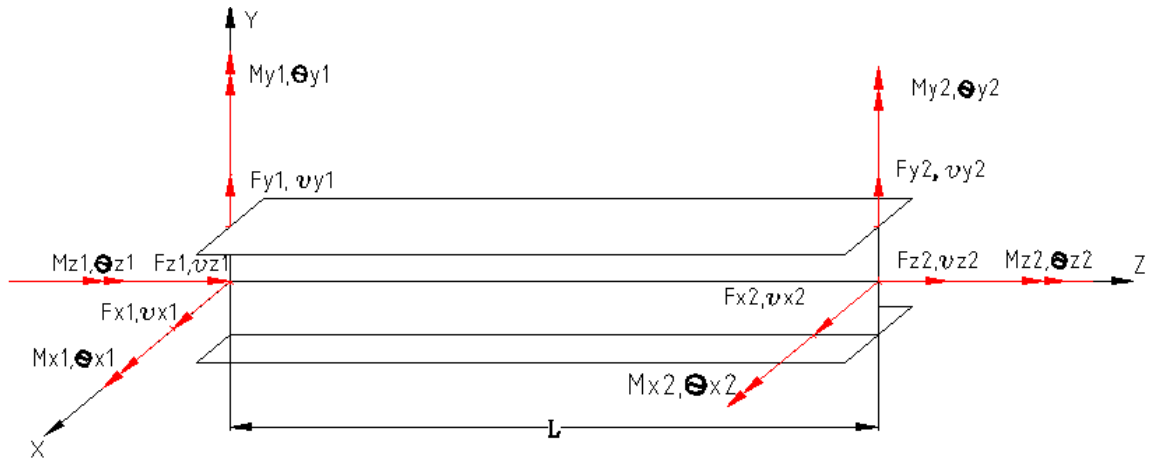


Figure 2 (adopted from reference [5])

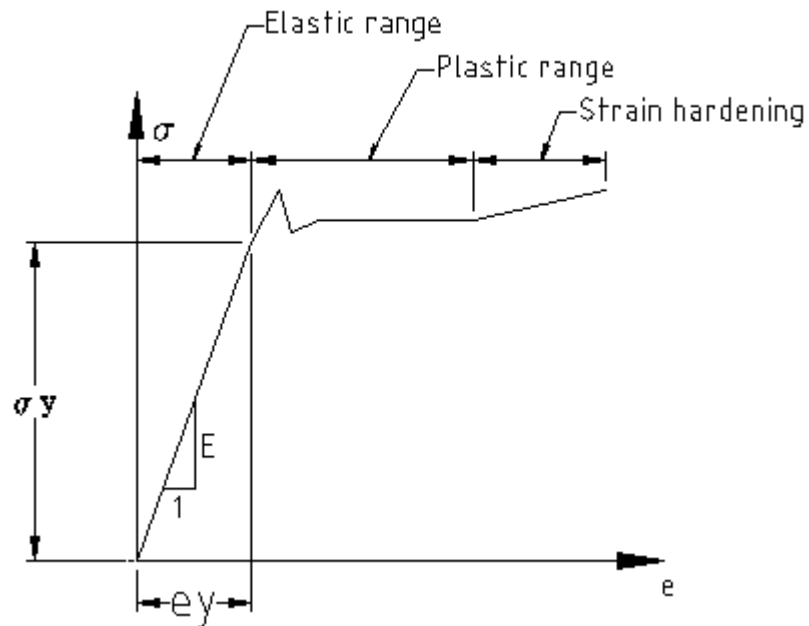
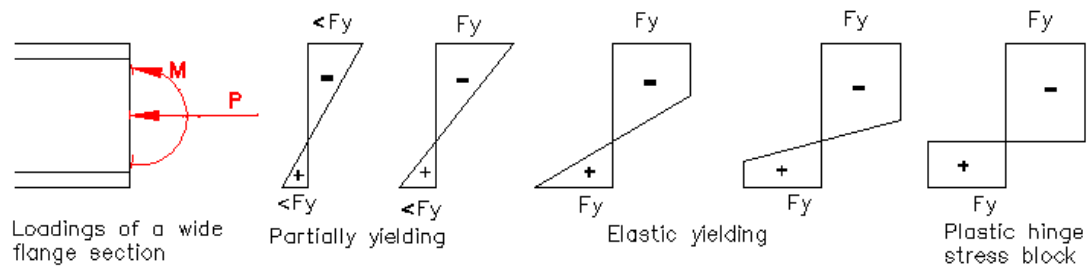


Figure 3 (adopted reference [4])



**Figure 4 (adopted reference [4])**

### 2.2.2 CHEN AND ATSUTA'S YIELD SURFACES

Using equilibrium on the cross-section geometry, Chen and Atsuta successfully derived each exact expression of the interaction equation (yield surface) relating axial force and biaxial bending moments acting on rectangular or circular sections under the fully yielding condition. Based on the concept of superposition, Chen and Atsuta provided methods of analysis to calculate the exact expression of the interaction equation for other double web and doubly symmetrical cross sections, including wide-flange and hollow rectangular shapes. This was achieved by treating entire cross-sections as assemblages of rectangles. Unfortunately, their interaction equations always contain non-integer exponents, which produce slope discontinuities on their respective yield surfaces. These discontinuities in slope can provide computational errors in inelastic analysis due to the potential for numerical instability [4].

### 2.2.3 ORBISON'S YIELD SURFACE

Based on the work of Chen and Atsuta, Orbison developed a single-equation yield surface to represent the behavior of W12x31, which can also be used to approximate the



behavior of light-to-medium-weight American shapes. Orbison's equation (Eq. 2) was developed through a process of trial and error curve fitting and is given by the criterion

$$1.15p^2 + m_x^2 + m_y^4 + 3.67p^2m_x^2 + 3.0p^6m_y^2 + 4.65m_x^4m_y^2 = 1.0 \quad \text{Eq. (2)}$$

where  $p$ ,  $m_x$ , and  $m_y$  are defined as above. This objective of this equation is to “a) conform closely to a realistic, physically derived surface, b) be continuous and convex, and c) be amenable to efficient computer implementation.” [4].

#### 2.2.4 MASTAN2'S YIELD SURFACE

MASTAN2 is structural engineering software developed by Ziemian and McGuire (MASTAN2, 2011). MASTAN2 intended for educational use and can account for both linear and nonlinear structural behavior. Available analysis options include “first- or second-order elastic or inelastic analyses of two- or three-dimensional frames and trusses subjected to static loads” (MASTAN2, 2011). Similar to other available structural analysis software, the yield surface in MASTAN2 was modeled by a general single continuous equation. The yield surface equation used in MASTAN2 is Eq. 1 shown above. The equation was based on Orbison's yield surface equation with the 1.15 modified to 1.0 so that the full axial yield load of a truss element could be achieved.

This study uses the yield surface equation of MASTAN2 to custom fit to the real yield surfaces of selected shapes by modifying the coefficients of the cross-terms  $p^2m_x^2$ ,  $p^6m_y^2$ , and  $m_x^4m_y^2$ .

## 3 DISCUSSION

### 3.1 METHEDODOLOGY

The process of custom fitting the MASTAN2 yield surface equation to a given shape defined in terms of its geometric dimensions of height, width, and wall thicknesses can be divided into the following four main stages, which are also illustrated in Fig. 5.

(1) Using principles of solid mechanics, a theoretically “exact” but overly complex representation of the cross section’s yield surface,  $(m_x, m_y, p)$ , is initially obtained.

(2) Data weighting factors for use in the latter regression analysis are developed from this representation.

(3) With both the weighting factors and theoretical yield surface data, the approximate yield surfaces using the form of Eq. 1 are subsequently obtained. Essentially these “exact” data points are utilized within a weighted regression analysis to obtain the three aforementioned coefficients and to determine the “best” yield surface equation of the form given in Eq. 1.

(4) For the convexity requirement of a yield surface, each yield surface obtained through regression analysis is tested for concavity and compared to the MASTAN2 yield surface.

It should be noted that all of the work completed in this research is based on MATLAB, which is computational software that was readily available to the author and permits routines to be written in module form for any required analysis processes.

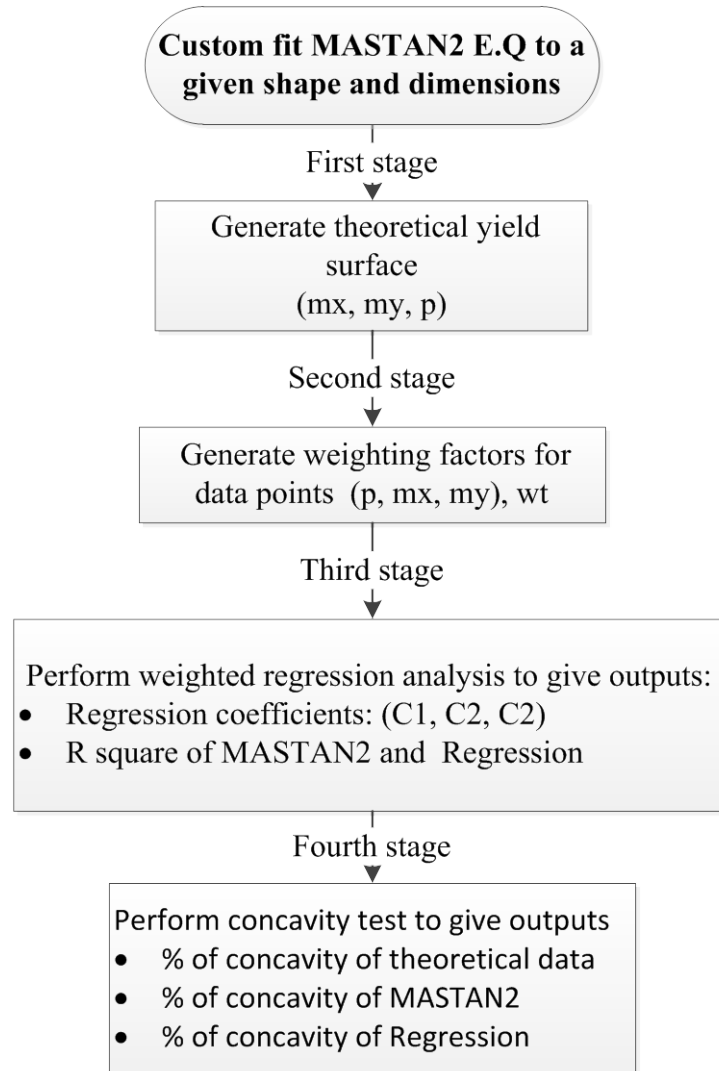
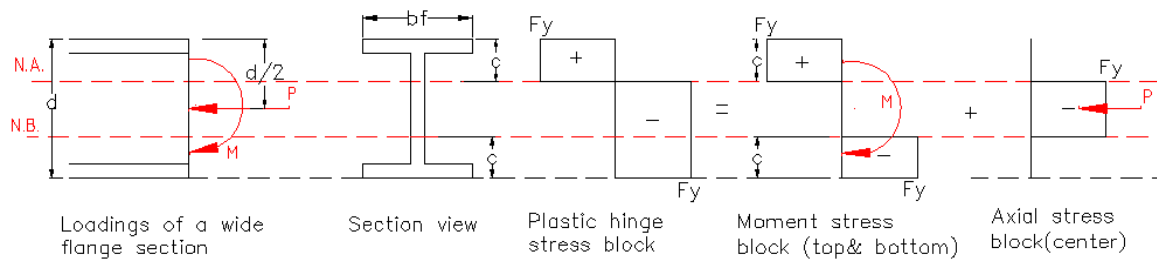


**Figure 5. General analysis flow chart.**

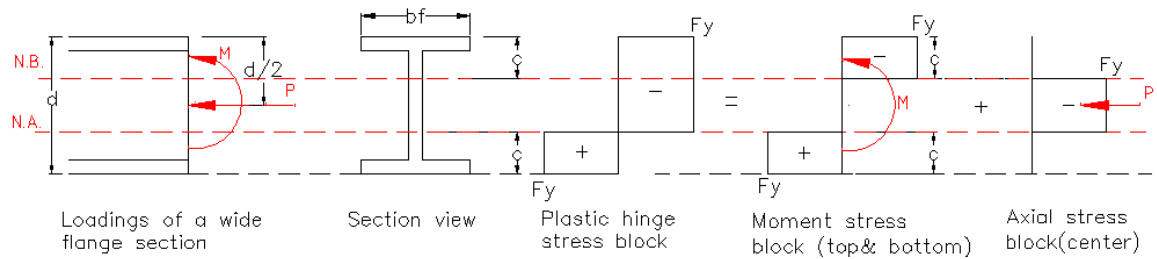
### **3.2 GENERATING THEORETICAL YIELD SURFACE $(m_x, m_y, p)$**

Consider the wide-flange section that is under combined axial force and bending moment and its plastic hinge diagram shown in Fig. 6. The plastic hinge stress block diagram is modeled the same way for all types of cross sections, where the yield stress of material is reached throughout the depth of the cross section. The defined neutral axis

(N.A.) divides the cross-section into compression (-) and tension (+) regions. The Section Assemblage Concept defines that the plastic hinge stress block diagram can be represented by the combination of a moment stress block diagram (above and below the neutral axis) and axial stress block diagram (neighboring the neutral axis). With N.B. defined as the reflection line of N.A. about the center of the cross-section, the position of N.A. is that of N.B. if the moment changes direction.



**(a) Negative moment.**



**(b) Positive moment.**

**Figure 6. Plastic hinge stress block diagram. (Wide-flange section)**

Following this stress distribution, stresses contributed by axial forces and bending moments can be represented by axial area  $A_p$  and bending moment area  $A_m$ . Therefore, the cross-sectional area  $A$  can be considered as the sum of the axial and bending moment

areas:  $A = A_p + A_m$ . Based on cross-section equilibrium, the ratio of the axial area to the cross-sectional area is  $p = P/P_y = A_p F_y / A F_y = A_p / A$  and the ratio of the bending moment area to cross-sectional area is  $(1 - p) = A_m / A$ .

If  $P$ ,  $M_x$ , and  $M_y$  are the given axial force, the major-axis bending moment (x-axis) and minor-axis bending moment (y-axis), respectively, and  $P_y$ ,  $M_{px}$ , and  $M_{py}$  are the squash load, major-axis plastic bending moment, and minor-axis plastic bending moment, respectively, then the ratios  $p = P/P_y$ ,  $m_x = M_x/M_{px}$ , and  $m_y = M_y/M_{py}$  are dimensionless components of the yield surface.

Given that a cross-section can be subjected to both axial force and bending moments and such force and moments can be applied about various axes, there is an undefined number of different locations for the N.A. (Fig. 7). In addition, a given location of the plastic neutral axis corresponds to a single point  $(m_x, m_y, p)$  on the theoretical yield surface. The location of the N.A. needs to be varied widely so that a well-distributed cloud of sampling data points  $(m_x, m_y, p)$  can be obtained that is intended to represent the theoretical yield surface. An adequate number of points, here, does not imply a specific number but rather a large enough number of data points that allows a reasonable calculation time and will not improve the results significantly when a larger number of data points is used. Generating a cloud of uniformly distributed data points can be a challenge. Weighting factors, however, can be used to ameliorate this distribution problem when performing the regression analysis. The determination of such weighting factors is presented in Section 3.3.

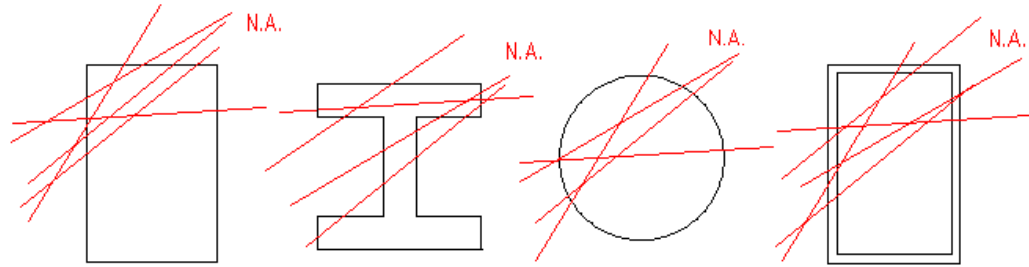
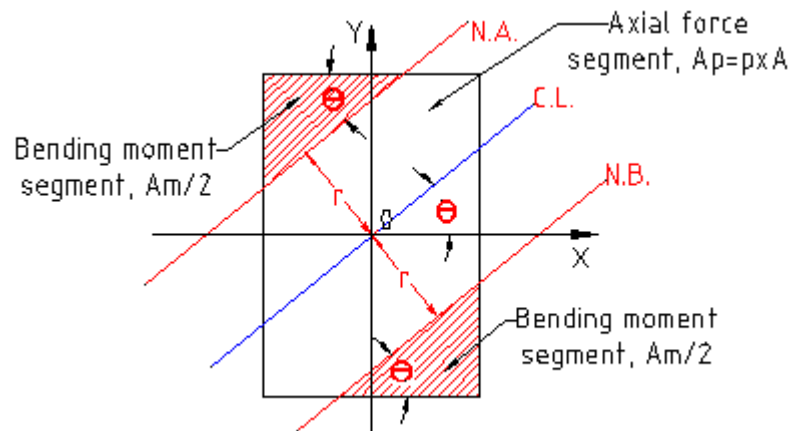


**Figure 7. Different cases of neutral axis (N.A.)**

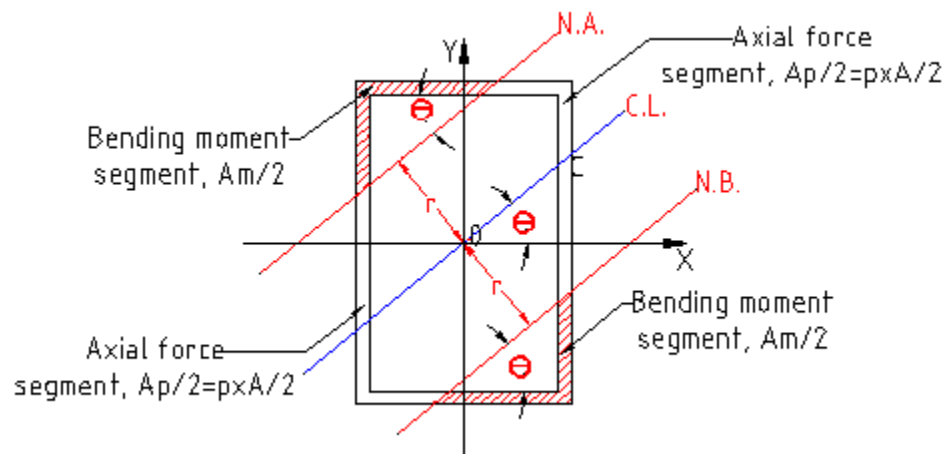
The value of  $p$  at a given point  $(m_x, m_y, p)$  and the location of the N.A., which can be represented by the angle made by N.A. and the horizontal x-axis  $\theta$ , can be used as controlling factors of the distribution of the data points. This is because  $p$  is the vertical component of each data point and the other two components ( $m_x$  and  $m_y$ ) are only functions of  $\theta$ . To allow variables  $p$  and  $\theta$  to be the controlling factors, the below strategy that is based on the Section Assemblage Concept defined above is used for all shapes and dimensions investigated in this research (refer to Fig.8):

- Let the origin be at the center of the cross-section.
- Let  $\theta$  be the angle made by the neutral axis and the horizontal x-axis.
- The cross-section can be divided into (1) an axial force segment, which is the region subjected to axial force and (2) a bending moment segment, which is the region subjected to the major- and minor-axis bending moments, by using the following process:
  - 1.) Draw a center line C.L. through the center of the cross-section and parallel to N.A.

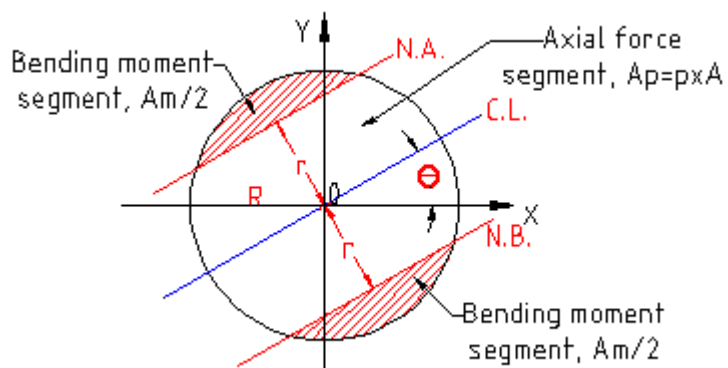
- 2.) Draw N.B., the inflection line of N.A. about C.L. and make  $r$  an equal distance from C.L. to N.A. and N.B.
- 3.) Make the axial force segment be the region on the cross-section between N.A. and N.B. This region has an area  $A_p$ .
- 4.) Make the two regions (shaded) on the other side of N.A. and N.B. be the bending moment segment. They are geometrically symmetric and each of an area  $A_m/2$ .
- 5.) The value of  $p$  and  $\theta$  then will dictate the shape of these three segments.



**(a) Solid rectangular section**

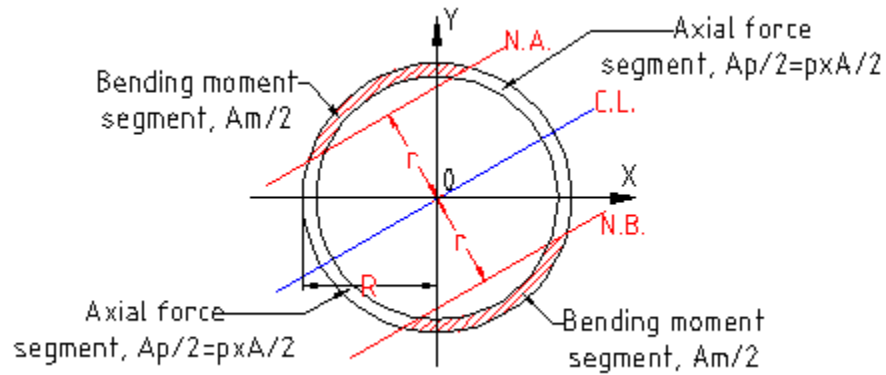


**(b) Hollow rectangular section**

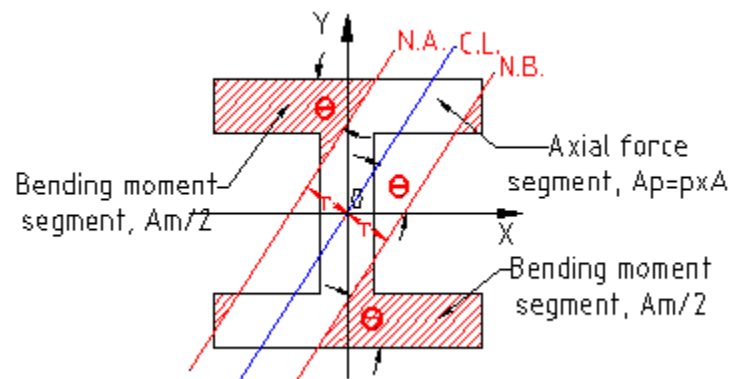


**(c) Solid circular section**





(d) Hollow circular section



(e) Wide-Flange section

**Figure 8. Partitioning of different cross-section shapes:**

- (1) Region subjected to Moments above N.A. of area  $A_m/2$ .**
- (2) Region subjected to Moments below N.A. of area  $A_m/2$ .**
- (3) Region subjected to Axial Forces of area  $A_p$ .**

For a given  $p$  and  $\theta$ , normalized moments  $m_x$  and  $m_y$  can then be calculated as follows.

Plastic bending moments  $M_{px}$  and  $M_{py}$  are previously defined as the products between their respective plastic section modulus  $Z$  and material yield stress,  $F_y$ , where  $Z$  is a function of cross-section shape and dimensions:

$$M_{px} = Z_x F_y, \quad (\text{Eq.3})$$

$$M_{py} = Z_y F_y.$$

Bending moment about a particular axis is defined as the product between the areas of bending moment segment  $A_m$  and the moment arm  $C$  about the axis of interest:

$$M_x = A_m \times C_x, \quad (\text{Eq.4})$$

$$M_y = A_m \times C_y,$$

where  $A_m$  can be calculated from the given value of  $p$  as previously defined and moment arms  $C_x$  and  $C_y$  about the x-axis and y-axis can be determined from the coordinates of the vertices of the polygon defining the bending moment segment. The calculation of moment arms for different shapes of bending moment segment is presented in Section 3.2.1.

Coordinates of vertices of different shapes of the bending moment segment can be derived mathematically for different cross-section shapes (rectangular, circular, wide-flange, etc.) and dimensions using geometry and an interpolating technique in MATLAB. Vertices and other information defining the bending moment segment are presented in Section 4 for each cross-section shape.

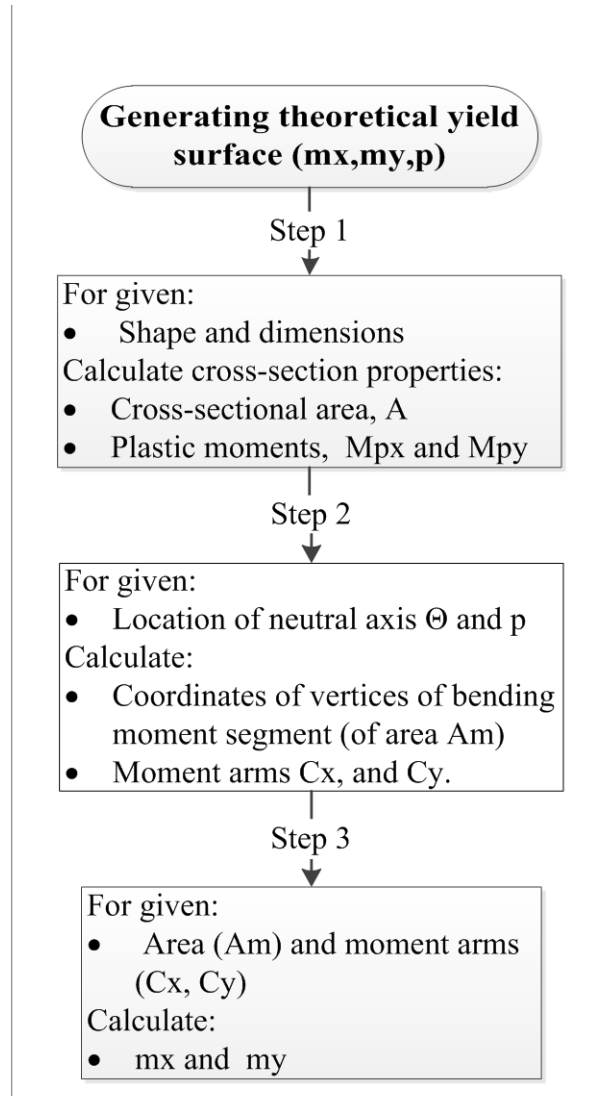


**Figure 9. General steps of generating theoretical yield surface.**

Overall, the three routines---“Moment Arms”, “Weighting Factors” and “Regression Analysis”---are determined in the same way regardless of shapes and dimensions. The only routine whose method of determination is unique for different shapes is “Generating Theoretical Data Points ( $m_x, m_y, p$ )”. The general steps of generating data points

$(m_x, m_y, p)$  are presented in Fig.9 and the more detailed methods for different shapes are presented in Section 4.

### 3.2.1 MOMENT ARMS

#### POLYGONS

The major- and minor-axis moment arms of a given polygon are the distances from the centroid of the polygon to the x-axis and y-axis, respectively (Fig.10). The position of the centroid of the polygon is given as the following:

$$C_x = \frac{1}{6A_{polygon}} \sum_{i=0}^{N-1} (x_i + x_{i+1})(x_i y_{i+1} - x_{i+1} y_i) \quad \text{Eq. (5)}$$

$$C_y = \frac{1}{6A_{polygon}} \sum_{i=0}^{N-1} (y_i + y_{i+1})(x_i y_{i+1} - x_{i+1} y_i)$$

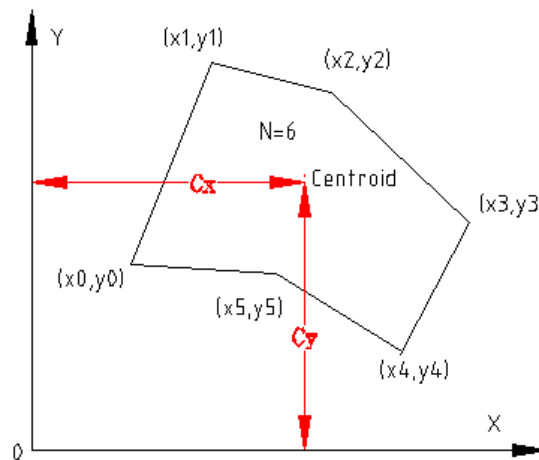


**Figure 10. Centroid of a polygon.**

where,  $A_{polygon}$  is the area of the polygon, which in the case of bending moment segment is  $A_m/2$ ,  $(x_i, y_i)$  are coordinates of a given vertex  $i$ , and  $N$  is the number of vertices as shown in Fig. 10.

### CIRCULAR SEGMENTS

For a circular segment shown in Fig. 11, its centroid can be determined according to Eq. 6:

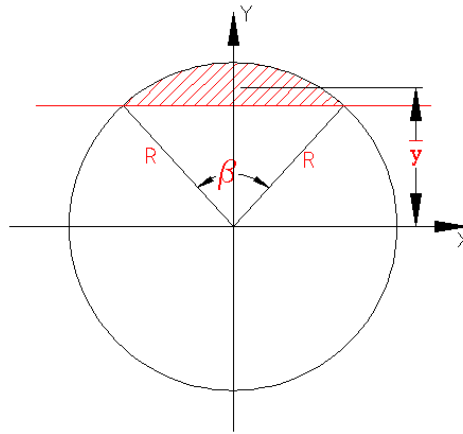


**Figure 11. Centroid of a circular segment.**

- Horizontal component of the centroid:  $\bar{x} = 0$  Eq. (6)
- Vertical component of the centroid:  $\bar{y} = \frac{4R \sin(\frac{\beta}{2})^3}{3(\beta - \sin(\beta))}$ ,

where  $R$  is the radius of the circle and  $\beta$  is the radius angle of the circular segment.

### 3.3 WEIGHTING FACTORS

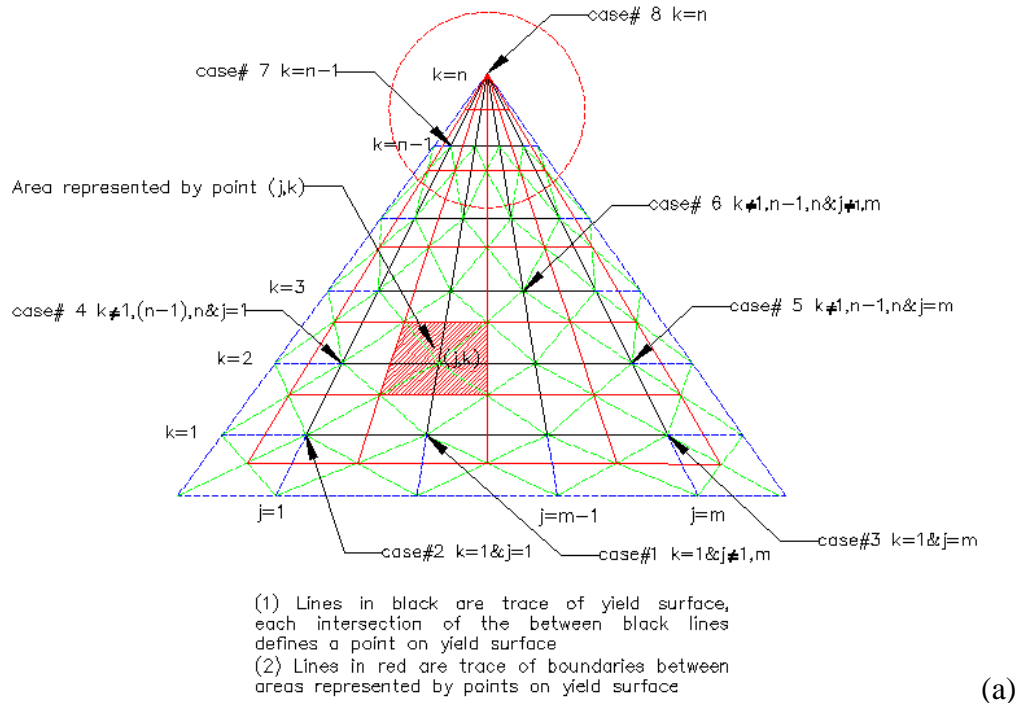
This study explored two methods of defining weighting factors that can be used to help rectify a point distribution problem within the yield surface data points. Generally, a weighting factor is the value that is assigned to each point on the surface to reflect the amount of exact surface area to be represented by the point while performing regression analysis.

The first method defined boundaries between approximated areas represented by all points and these areas are used as weighting factors. This type of weighting factor method is termed “area weighting factors.” Note that, because the yield surface data points are not in the same plane in three-dimensional space, the calculated area represented by each point is the approximation of the area of the corresponding point on the exact yield surface. What matters here, however, is the relative size between areas represented by all points rather than the actual values of exact areas themselves. For visualization purposes, one quadrant of the yield surface was flattened out onto a plane as shown in Fig. 12. Lines in black are traces of the yield surface, where each intersection between these lines defines a point on theoretical yield surface:  $O(j, k)$ . Lines in red are traces of the boundaries between areas represented by points on yield surface. Lines in green are diagonals of the three-dimensional quadrangle<sup>1</sup>. Lines in blue are traces of neighboring quadrants of the yield surface.

---

<sup>1</sup> A three-dimensional quadrangle here is defined as a quadrangle whose vertices are not on the same plane in three-dimensional space.

For the points whose  $k$ -coordinate is not  $n$  or  $(n - 1)$ , the area represented by a given point  $O(j, k)$  was calculated with the following strategy. For each point, eight immediate neighboring points are identified:  $A(j - 1, k)$ ,  $B(j, k - 1)$ ,  $C(j, k + 1)$ ,  $D(j + 1, k)$ ,  $E(j - 1, k - 1)$ ,  $F(j + 1, k - 1)$ ,  $G(j - 1, k + 1)$  and  $H(j + 1, k + 1)$  as shown in Fig. 13a. Because all these nine points are not on the same plane in three-dimensional space, the area represented by a given point  $O$  is approximated as the summation of four triangles ROS, SOT, TOU, and UOR, where R, S, T, and U are defined as the “virtual intersection points” between the diagonals of three-dimensional quadrangle AGCO, CHDO, DFBO, and BEAO, respectively. A “virtual intersection point” is the mid-point of the shortest line drawn between two skew diagonals of a three-dimensional quadrangle (Fig. 13b).



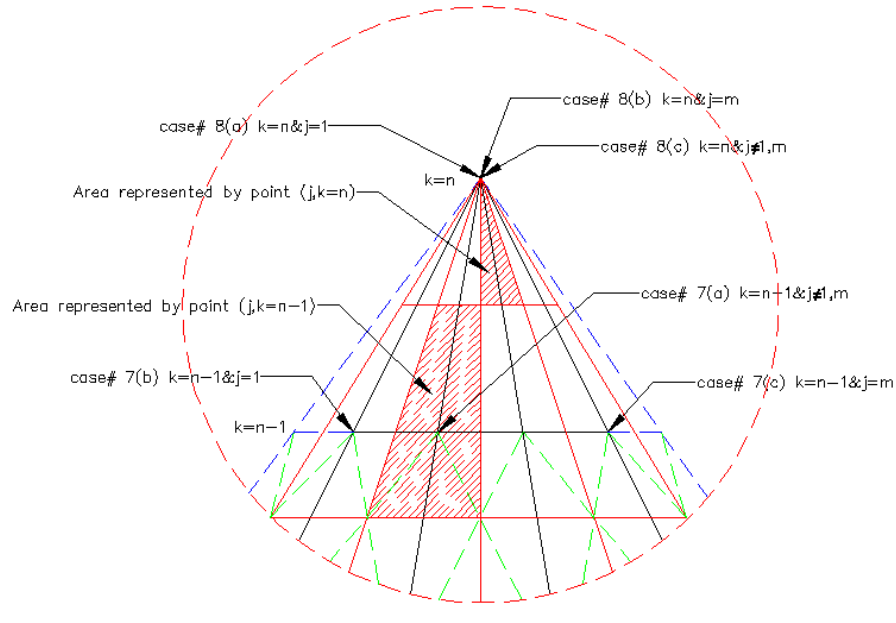


**Figure 12. Area weighing factors.**

For points whose  $k$ -coordinate is  $(n - 1)$ , the same strategy that is used with points whose  $k$ -coordinate is not  $n$  or  $(n - 1)$  applies except that  $R$  and  $S$  for  $k = (n - 1)$  are defined differently from above (Fig. 14.c). The point  $R$  for  $k = (n - 1)$  is defined as the midpoint of the line connecting  $AO_{(k=n)}$  and  $O_{(k=n-1)}O_{(k=n)}$  at their respective midpoints. Point  $S$  for  $k = (n - 1)$  is defined as the midpoint of the line connecting  $O_{(k=n-1)}O_{(k=n)}$  and  $DO_{(k=n)}$  at their respective midpoints.

For points whose  $k$ -coordinate is  $n$ , the interest area is the area of triangle  $RSO_{k=n}$  where  $R$  and  $S$  belong to their corresponding  $O_{k=(n-1)}$  point (Fig. 13c). Note that points along the edges of one quadrant of the yield surface are shared with one to three other quadrants. Therefore, the areas that the edge points are representing are beyond those in



only one quadrant of the yield surface. For this reason, there are eight cases of points whose calculations of area are distinguishable from each other's as shown in Fig. 12.

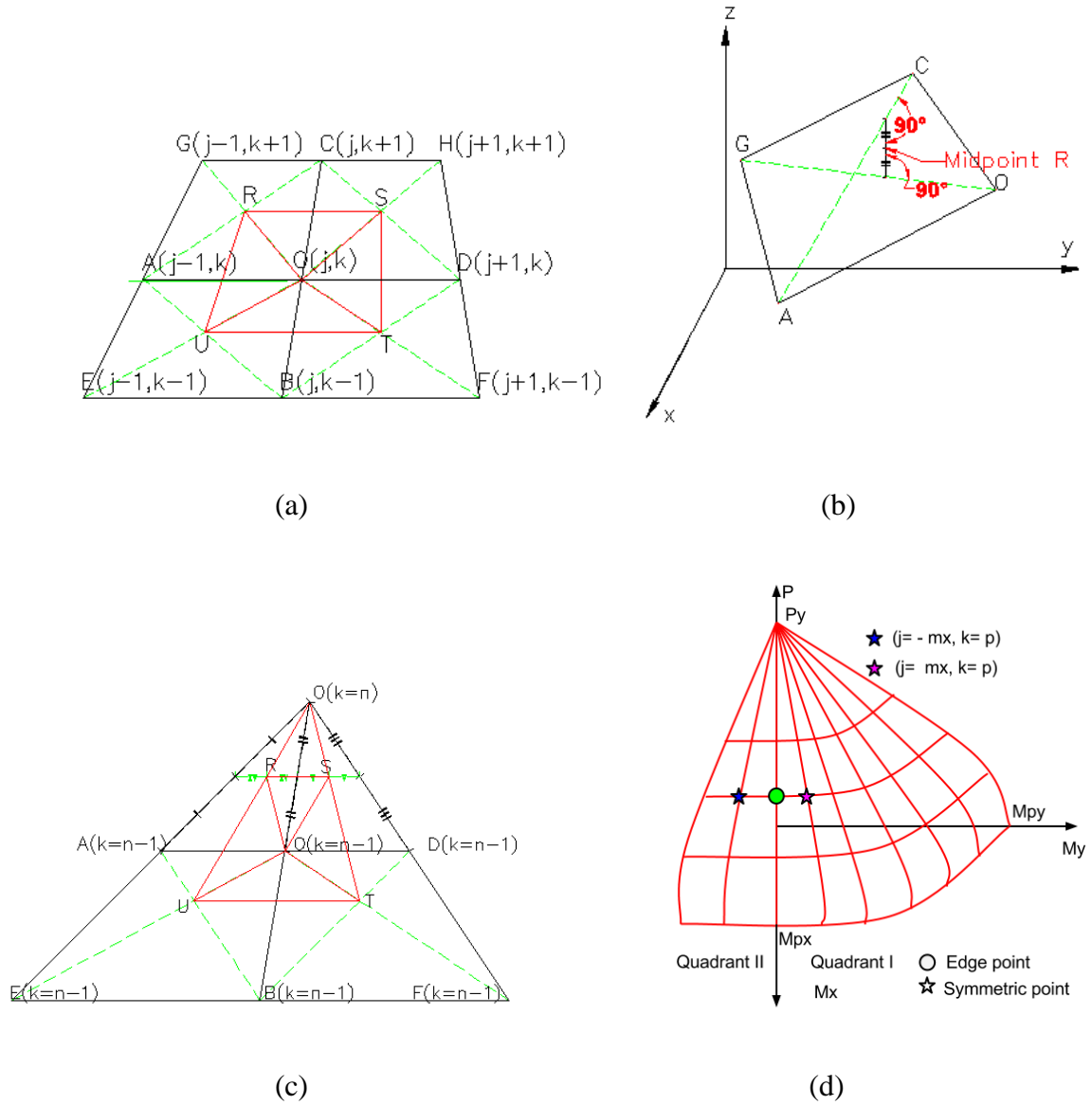


**Figure 13. (a) A given point  $O$  for  $k \neq n - 1, n$ . (b) Defining a virtual intersection point. (c) A given point  $O$  for  $k = n - 1$  and  $O$  for  $k = n$ . (d) Edge points and Symmetric points.**

The rule of thumb for cases where the edge points of one quadrant of yield surface that can be shared by two or more quadrants is: the immediate neighboring points of an edge point of one quadrant are geometrically symmetric to those of the other quadrants, with which the edge point being shared, about the axis the edge of yield surface that contains the edge point lies on (Fig. 13d). The different cases of points are listed below.

- Case #1,  $k = 1 \& j \neq 1, m$
- Case #2,  $k = 1 \& j = 1$
- Case #3,  $k = 1 \& j = m$
- Case #4,  $k \neq 1, n - 1, n \& j = 1$
- Case #5,  $k \neq 1, n - 1, n \& j = m$
- Case #6,  $k \neq 1, n - 1, n \& j \neq 1, m$
- Case #7,  $k = n - 1$ 
  - (a)  $k = n - 1 \& j \neq 1, m$
  - (b)  $k = n - 1 \& j = 1$
  - (c)  $k = n - 1 \& j = m$
- Case #8,  $k = n$ 
  - (a)  $k = n \& j = 1$
  - (b)  $k = n \& j = m$
  - (c)  $k = n \& j \neq 1, m$

As a second method for calculating weighting factors, the area represented by each point is calculated by means of determining the “crowdedness” of that point.

Crowdedness of a point is represented by the ratio of (i) the area of a circle whose radius is the average distance from the interest point to the eight immediate neighboring points to (ii) the sum of the areas of all circles (Fig.14). The same strategy used for neighboring points of an edge point of the area weighting factors is also used for computing crowdedness-weighting factors.

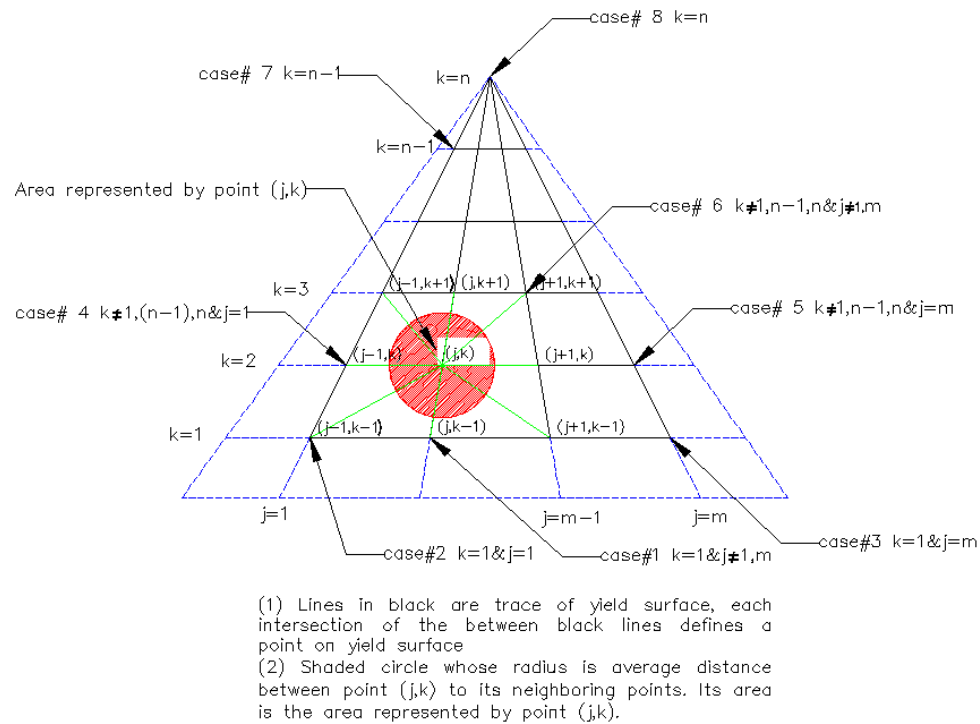


**Figure 14. Crowdedness weighting factors.**

### 3.4 REGRESSION ANALYSIS

After the exact representation of the yield surface is obtained, a regression analysis can be performed. There are two goals in this regression analysis. The first is to determine the “best fit” coefficients  $c_1, c_2, c_3$  in the general yield surface equation Eq. 7.

$$\phi = p^2 + m_x^2 + m_y^4 + c_1 p^2 m_x^2 + c_2 p^6 m_y^2 + c_3 m_x^4 m_y^2 \quad \text{Eq. (7)}$$

For a general yield surface point  $i$ , Eq. (7) can be re-arranged as

$$y_i = c_1 z_{i1} + c_2 z_{i2} + c_3 z_{i3} \quad \text{Eq.(8)}$$

where

$$y_i = (\Phi - p^2 - m_x^2 - m_y^4)_i$$

$$z_{i1} = (p^2 m_x^2)_i$$

$$z_{i2} = (p^6 m_y^2)_i$$

$$z_{i3} = (m_x^4 m_y^2)_i$$

and  $y_i$  is the general component of a column vector  $\{Y\}$  of length  $n$ , where  $n$  is the total number of yield surface points generated and  $\{Y\}$  is a defined property of the theoretical yield surface because it is only a function of theoretical yield surface data points  $(m_x, m_y, p)$ , and  $\Phi$  theoretically equals 1.00. Variables  $z_{i1}$ ,  $z_{i2}$ , and  $z_{i3}$  are the general components of matrix  $[Z]$  of size  $n \times 3$ , which is also a property of the theoretical yield surface. In least-squares regression, if the right-hand side expression  $c_1 z_{i1} + c_2 z_{i2} + c_3 z_{i3}$  is the linear model of the left hand side dependent variable  $y_i$ , then the difference between  $y_i$  and  $c_1 z_{i1} + c_2 z_{i2} + c_3 z_{i3}$  is the residual  $e_i$ .

$$e_i = y_i - c_1 z_{i1} - c_2 z_{i2} - c_3 z_{i3} \quad \text{Eq.(9)}$$

The objective of a least-squares regression approach is to minimize the sum of the squares of the residuals  $S_r$  between measured  $y$  and calculated  $y$  with the linear model.

$$S_r = \sum_{i=1}^n e_i^2 = \sum_{i=1}^n (y_{i,measured} - y_{i,model})^2 \quad \text{Eq.(10)}$$

$$S_r = \sum_{i=1}^n (y_i - z_{i1}c_1 - z_{i2}c_2 - z_{i3}c_3)^2$$

Differentiating with respect to each of the unknown coefficients,

$$\frac{\partial S_r}{\partial c_1} = -2 \sum (y_i - z_{i1}c_1 - z_{i2}c_2 - z_{i3}c_3)(z_{i1}) = 0$$

$$\frac{\partial S_r}{\partial c_2} = -2 \sum (y_i - z_{i1}c_1 - z_{i2}c_2 - z_{i3}c_3)(z_{i2}) = 0$$

$$\frac{\partial S_r}{\partial c_3} = -2 \sum (y_i - z_{i1}c_1 - z_{i2}c_2 - z_{i3}c_3)(z_{i3}) = 0$$

and performing algebra results in

$$\sum z_{i1}(z_{i1}c_1 + z_{i2}c_2 + z_{i3}c_3) = \sum(z_{i1})(y_i)$$

$$\sum z_{i2}(z_{i1}c_1 + z_{i2}c_2 + z_{i3}c_3) = \sum(z_{i2})(y_i)$$

$$\sum z_{i3}(z_{i1}c_1 + z_{i2}c_2 + z_{i3}c_3) = \sum(z_{i3})(y_i)$$

These equations can be expressed in matrix form as

$$\begin{bmatrix} \sum z_{i1}z_{i1} & \sum z_{i1}z_{i2} & \sum z_{i1}z_{i3} \\ \sum z_{i2}z_{i1} & \sum z_{i2}z_{i2} & \sum z_{i2}z_{i3} \\ \sum z_{i3}z_{i1} & \sum z_{i3}z_{i2} & \sum z_{i3}z_{i3} \end{bmatrix} \begin{Bmatrix} c_1 \\ c_2 \\ c_3 \end{Bmatrix} = \begin{Bmatrix} \sum(z_{i1})(y_i) \\ \sum(z_{i2})(y_i) \\ \sum(z_{i3})(y_i) \end{Bmatrix}$$

With

$$\{RHS\} = \underbrace{\begin{bmatrix} z_{11} & z_{21} & z_{31} & z_{41} & \dots & z_{n1} \\ z_{12} & z_{22} & z_{32} & z_{42} & \dots & z_{n2} \\ z_{13} & z_{23} & z_{33} & z_{43} & \dots & z_{n3} \end{bmatrix}}_{[Z]^T} \begin{Bmatrix} y_1 \\ y_2 \\ y_3 \\ \vdots \\ y_n \end{Bmatrix}$$

$$\{LHS\} = \underbrace{\begin{bmatrix} z_{11} & z_{21} & z_{31} & z_{41} & \dots & z_{n1} \\ z_{12} & z_{22} & z_{32} & z_{42} & \dots & z_{n2} \\ z_{13} & z_{23} & z_{33} & z_{43} & \dots & z_{n3} \end{bmatrix}}_{[Z]} \underbrace{\begin{bmatrix} z_{11} & z_{12} & z_{13} \\ z_{21} & z_{22} & z_{23} \\ z_{31} & z_{32} & z_{33} \\ \vdots & \vdots & \vdots \\ z_{n1} & z_{n2} & z_{n3} \end{bmatrix}}_{[Z]}$$

The resulting regression equation is

$$[Z]^T [Z] \{C\} = \{[Z]^T \{Y\}\}$$

where  $\{C\}$  is the coefficient vector of size  $3 \times 1$  and whose components are  $c_1, c_2, c_3$ . By using Gaussian elimination,  $\{C\}$  can be calculated as:

$$\{C\} = [[Z]^T [Z]]^{-1} \{[Z]^T \{Y\}\} \quad \text{Eq.(11)}$$

The second goal of the regression analysis is to find the coefficient of determination  $R^2$  of MASTAN2 equation,  $R^2_{MASTAN2}$ , and that of the regression equation,  $R^2_{Regression}$ . In general, the coefficient of determination can be calculated as

$$R^2 = (S_t - S_r) / S_t, \quad \text{Eq.(12)}$$

where  $S_t$  is the total sum of the squares around the mean for independent variable ( $y_i$ ), which can be calculated as

$$S_t = \sum_{i=1}^n (y_i - y_{ave})^2, \quad \text{Eq.(13)}$$

in which  $y_{ave}$  is the mean of  $y_i$ , defined as the arithmetic average of  $y_i$ .

To incorporate the weighting factors into the regression analysis, the same steps as shown above are employed with the weighting factor  $w_i$  of each data point incorporated as follows

$$S_r = \sum_{i=1}^n w_i e_i^2 = \sum_{i=1}^n w_i (y_{i,measured} - y_{i,model})^2 \quad \text{Eq.(14)}$$

$$S_r = \sum_{i=1}^n w_i (y_i - z_{i1}c_1 - z_{i2}c_2 - z_{i3}c_3)^2$$

Differentiating with respect to each of the unknown coefficients,

$$\frac{\partial S_r}{\partial c_1} = -2 \sum w_i (y_i - z_{i1}c_1 - z_{i2}c_2 - z_{i3}c_3)(z_{i1}) = 0$$

$$\frac{\partial S_r}{\partial c_2} = -2 \sum w_i (y_i - z_{i1}c_1 - z_{i2}c_2 - z_{i3}c_3)(z_{i2}) = 0$$

$$\frac{\partial S_r}{\partial c_3} = -2 \sum w_i (y_i - z_{i1}c_1 - z_{i2}c_2 - z_{i3}c_3)(z_{i3}) = 0$$

which can be expressed as

$$\sum w_i z_{i1} (z_{i1}c_1 + z_{i2}c_2 + z_{i3}c_3) = \sum w_i (z_{i1})(y_i)$$

$$\sum w_i z_{i2} (z_{i1}c_1 + z_{i2}c_2 + z_{i3}c_3) = \sum w_i (z_{i2})(y_i)$$

$$\sum w_i z_{i3} (z_{i1}c_1 + z_{i2}c_2 + z_{i3}c_3) = \sum w_i (z_{i3})(y_i)$$

In matrix form is

$$\begin{bmatrix} \Sigma w_i z_{i1} z_{i1} & \Sigma w_i z_{i1} z_{i2} & \Sigma w_i z_{i1} z_{i3} \\ \Sigma w_i z_{i2} z_{i1} & \Sigma w_i z_{i2} z_{i2} & \Sigma w_i z_{i2} z_{i3} \\ \Sigma w_i z_{i3} z_{i1} & \Sigma w_i z_{i3} z_{i2} & \Sigma w_i z_{i3} z_{i3} \end{bmatrix} \begin{Bmatrix} c_1 \\ c_2 \\ c_3 \end{Bmatrix} = \begin{Bmatrix} \Sigma w_i(z_{i1})(y_i) \\ \Sigma w_i(z_{i2})(y_i) \\ \Sigma w_i(z_{i3})(y_i) \end{Bmatrix}$$

With

$$\{RHS\} = \begin{bmatrix} w_1 z_{11} & w_2 z_{21} & w_3 z_{31} & w_4 z_{41} & \dots & w_n z_{n1} \\ w_1 z_{12} & w_2 z_{22} & w_3 z_{32} & w_4 z_{42} & \dots & w_n z_{n2} \\ w_1 z_{13} & w_2 z_{23} & w_3 z_{33} & w_4 z_{43} & \dots & w_n z_{n3} \end{bmatrix} \begin{Bmatrix} y_1 \\ y_2 \\ y_3 \\ \vdots \\ y_n \end{Bmatrix}$$

$$\{LHS\} = \begin{bmatrix} w_1 z_{11} & w_2 z_{21} & w_3 z_{31} & w_4 z_{41} & \dots & w_n z_{n1} \\ w_1 z_{12} & w_2 z_{22} & w_3 z_{32} & w_4 z_{42} & \dots & w_n z_{n2} \\ w_1 z_{13} & w_2 z_{23} & w_3 z_{33} & w_4 z_{43} & \dots & w_n z_{n3} \end{bmatrix} \underbrace{\begin{bmatrix} z_{11} & z_{12} & z_{13} \\ z_{21} & z_{22} & z_{23} \\ z_{31} & z_{32} & z_{33} \\ \vdots & \vdots & \vdots \\ z_{n1} & z_{n2} & z_{n3} \end{bmatrix}}_{[Z]}$$

and

$$\begin{bmatrix} w_1 & 0 & 0 & 0 & 0 \\ 0 & w_2 & 0 & 0 & 0 \\ 0 & 0 & w_3 & 0 & 0 \\ \vdots & \vdots & \vdots & \ddots & \vdots \\ 0 & 0 & 0 & 0 & w_n \end{bmatrix} \begin{Bmatrix} y_1 \\ y_2 \\ y_3 \\ \vdots \\ y_n \end{Bmatrix} = \begin{Bmatrix} w_1 y_1 \\ w_1 y_2 \\ w_1 y_3 \\ \vdots \\ w_1 y_n \end{Bmatrix}$$

*[W] is the diagonal of column vector of weighted factor*

the resulting system of equations is

$$[Z]^T [W] [Z] \{C\} = [Z]^T [W] \{Y\}$$

And again by employing Gaussian elimination, the coefficients are computed from



$$\{C\} = [[Z]^T[W][Z]]^{-1}\{[Z]^T[W]\{Y\}\} \quad \text{Eq.(15)}$$

### 3.5 CONCAVITY TEST

A concavity test was derived in this study to check the required convex behavior of a yield surface. The results of a concavity test on a yield surface are defined by the percentage and degree of concavity of the yield surface. The percentage of concavity can be obtained as the percentage of number of concave points among the total data points. The degree of concavity of a yield surface may be represented by the depth of depression at the concave point. The depth of depression can be related to the slopes falling from the neighboring points to the center of the depression, which is the location of the concave point. The steeper the slopes are, the higher the degree of concavity.

A concavity test that is capable of differentiating the concave points from the total data points and approximating the slopes falling from the neighboring points to the concave point was developed based on a MATLAB function called “*SURFNORM*.” The syntax for *SURFNORM* function is

$$[N_x, N_y, N_z] = \text{SURFNORM}(X, Y, Z).$$

*“This function returns the components of the three-dimensional normal vector for the surface defined by point arrays (X,Y,Z). The result is normalized to length 1”* (MathWorks, 2012). The direction of *SURFNORM* surface normal at every point is the

same, that is they are all either pointing inward or outward. This direction, however, can be reversed by applying transpose to the inputs as shown below

$$[N_x, N_y, N_z] = SURFNORM(X', Y', Z')$$

When applied to this study, the cloud of points  $(m_x, m_y, p)$  that make up a yield surface, are included as follows

$$[N_x, N_y, N_p] = SURFNROM(m_x, m_y, p)$$

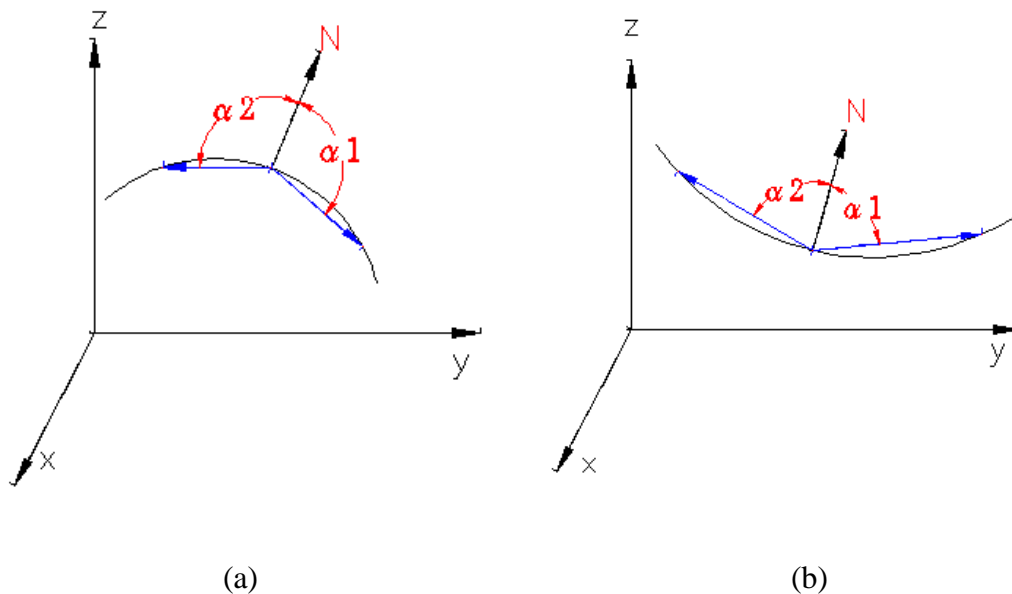


**Figure 15. SURFNORM surface normal N pointing in positive vertical direction (a) at a convex point. (b) at a concave point.**

The routine returns an array of the components of the three-dimensional yield surface normal at each yield surface point, which each has a length of 1 and its direction can be manipulated to either point inward or outward. If the surface normal at each is directed to

point in a known vertical direction the dot-products between the surface normal  $\mathbf{N}$  and the vector  $\mathbf{v}$  that originates at the interest point and ends at each neighboring point can indicate whether this given point is a concave or convex point on the surface. This statement is illustrated in Fig. 15.

For example, suppose that each surface normal  $\mathbf{N}$  is to point in the positive vertical direction. If  $\mathbf{N}$  belongs to a convex point (Fig. 15a), the angle ( $\alpha$ ) made by  $\mathbf{N}$  and the individual vectors  $\mathbf{v}$  must be obtuse. In other words, the dot-product between  $\mathbf{N}$  and  $\mathbf{v}$  gives a negative value. Instead, if  $\mathbf{N}$  belongs to a concave point (Fig. 15b),  $\alpha$  must be acute and the dot-product between  $\mathbf{N}$  and  $\mathbf{v}$  gives a positive value. If  $\mathbf{N}$  is to be reversed in direction, the above rules also need to be reversed.

In summary, a point can be classified as a concave or convex point by only checking the signs of the dot-products between  $\mathbf{N}$  and the  $\mathbf{v}$ 's with respect to the specified direction of  $\mathbf{N}$ . The largest magnitude of dot-products is termed the "concavity coefficient." The degree of concavity of a given point can be related to the concavity coefficient. The larger the negativity or positivity of the concavity coefficient of a point is, the greater the degree of concavity at that point.

On the other hand, the percentage of concavity of the yield surface ( $\%con$ ) can be obtained as the percentage of concave points out of the total data points of the yield surface. Weighting factors can also be incorporated into the calculation of the percentage of concavity.

$$\%con = \frac{\sum w_{i,con}}{\sum w_i} \times 100\% \quad \text{Eq.(16)}$$

where  $w_{i,con}$  is the weighting factor corresponding to the yield surface point  $(m_{ix}, m_{iy}, p_i)$  that tested as concave.

The validity of the concavity test was verified by running this test with the theoretical yield surface data. The results show that the theoretical yield surface, which shall be entirely convex or have a zero percent of concavity, contains a certain percent of concavity. Because this should not be occurring, the appearance of a small percent of concavity in the theoretical yield surface was deemed due to the round-off error. This conclusion was made by three-dimensional plotting and observation of the degrees of concavity at the points on theoretical yield surface that tested concave. Due to the fact that some parts of the yield surface are almost flat or almost have zero degree of convexity, the differences between being convex and concave are almost negligible. Therefore, to test the customized yield surface, the concavity test are calibrated using the percentage of concavity that exists in the corresponding theoretically exact yield surface.

### 3.6 ANALYSIS

There are two options of analysis that were investigated in this study, including (1) with area weighting factors, and (2) with crowdedness weighting factors. Initially, these two different sets of analysis were done for selected dimensions from all cross section shapes. The results of these two sets of analysis were then compared to each other with respect to the  $R^2$  value and percentage of concavity. The weighting factors in the set of analysis that

on average provides better  $R^2$  and smaller percentage of concavity would be used within the regression analysis and concavity test for the remaining shapes and dimensions.

The general steps of analysis of both sets for all shapes and dimensions are the same. The only difference is the weighting factors that are used. Figure 16 shows the detail flowchart of custom fitting MASTAN2 equation to the theoretical yield surface of a wide-flange shape by using area weighting factors. First, the dimensions of the wide-flange shapes are called from the database (“*Wshape.mat*”). Then, the algorithm that is required to calculate the theoretical yield surface and its corresponding weighting factors is called (“*wshapeyld.m*”). With this information, weighted regression analysis is performed to find the best coefficients. With the coefficients found,  $R^2$  of both regression and MASTAN2 equations are determined. Before the concavity test can be performed on either regression or MASTAN2 equation, the offset value must first be determined by performing concavity test on the theoretical data. Two separate but similar algorithms were created for testing percentage of concavity of theoretical yield surface and approximate yield surfaces. One algorithm takes an array of yield surface points as inputs (“*yldsurf\_data\_concavetest.m*”) and the other algorithm takes coefficients within the form of Eq. (1) as inputs (“*yldsurf\_eq\_concavetest.m*”). Finally, a summary of required results is made available for record. A similar flowchart, which is not shown here, is also used for the set that uses crowdedness weighting factors. This analysis process is used for all shapes. Only the routine that is required to generate the theoretical yield surface that is unique to each shape.

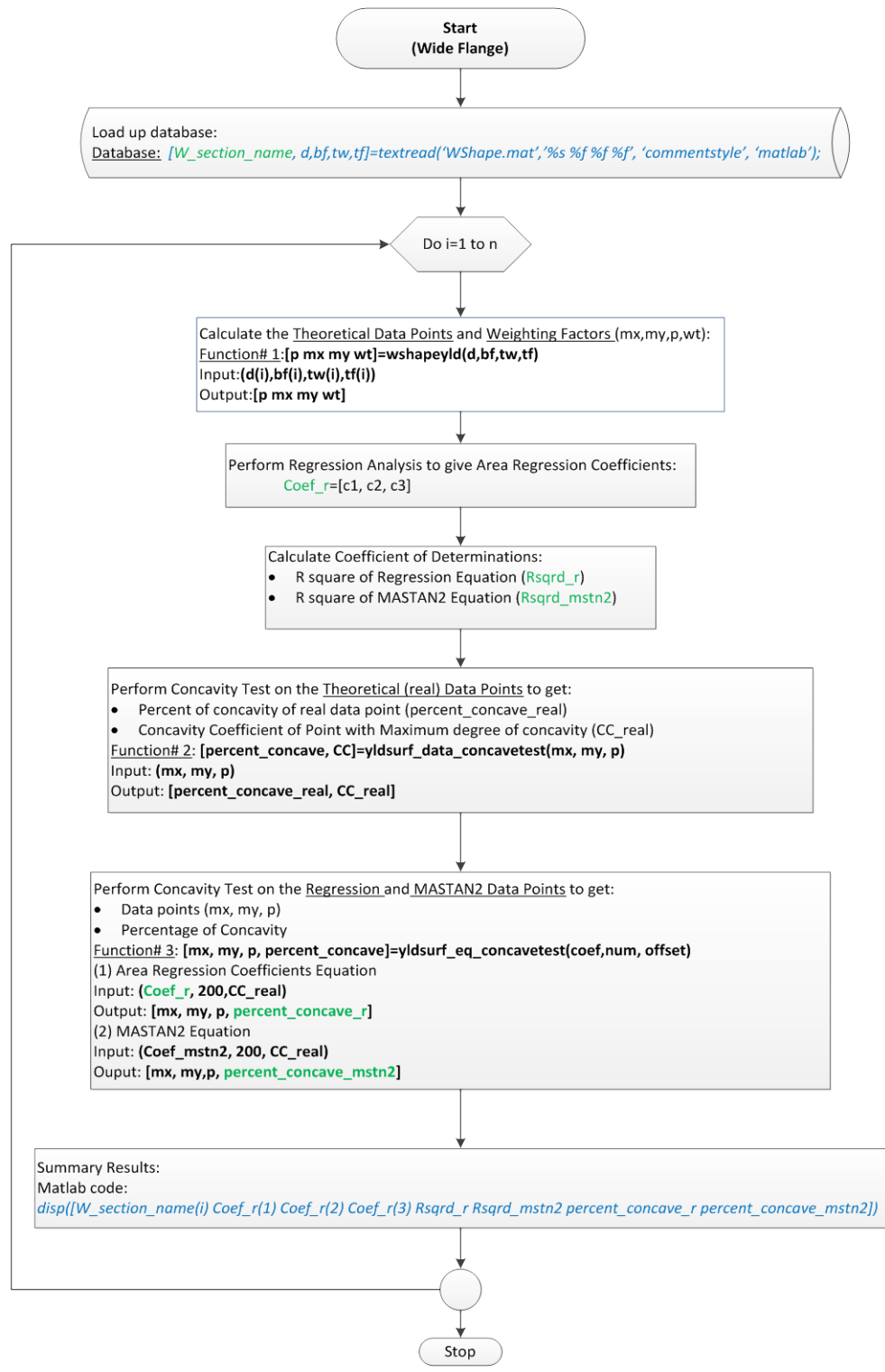


Figure 16. Detail flowchart of analysis for wide-flange sections.

## 4 METHODS AND RESULTS

In the following sections, the input dimensions of each cross-section shape are defined. By referring to the flowchart in Fig.9, the formulas required for calculating cross section properties and derivation of bending moment segments that contribute to the steps for generating theoretical yield surface for each cross-sectional shapes are provided in their respective sections. The results of the analysis and the discussion are also included.

### 4.1 SOLID RECTANGULAR SECTION

#### 4.1.1 METHOD

Inputs: cross-section dimensions:

$h$  = depth of the shape

$b$  = width of base

$F_y$  = yield strength of material

Output: arrays of  $p$ ,  $m_x$ , and  $m_y$ .

**STEP #1 CROSS SECTION PROPERTIES ( $A$ ,  $M_{px}$ ,  $M_{py}$ )**

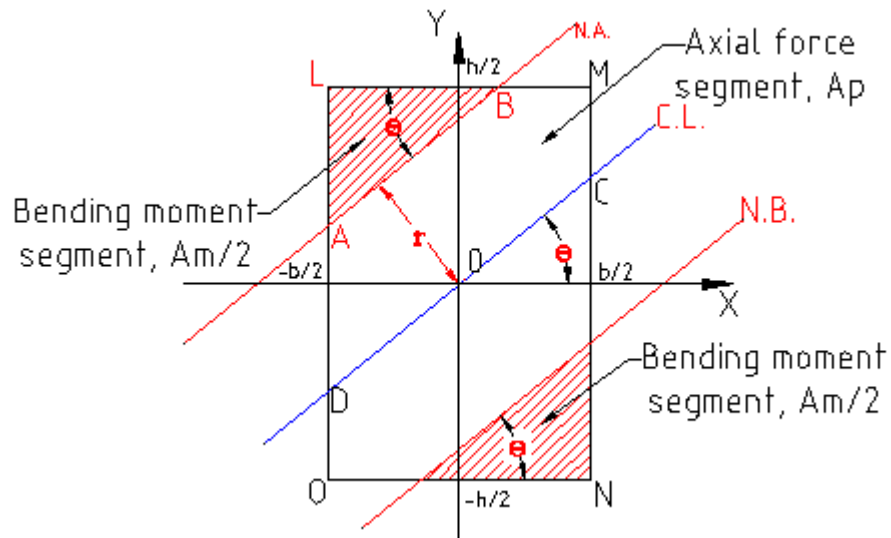


**Figure 17. Solid rectangular section**

For rectangular section:

- Cross-sectional area,  $A = bh$  Eq.(17)
- Plastic Moment,  $M_p = F_y \frac{bh^2}{4}$

### **STEP #2 BENDING SEGMENT'S VERTICES AND CENTROID**

By studying the possible locations of N.A. on a solid rectangular section, there are three cases for which the N.A. can be located to give different cases when defining the bending moment segment (Fig.18). These three cases of the bending moment segment are distinguished by two different cases of critical angles  $\theta_c$ . These two critical angles need to be determined before the study of different cases of bending moment segment can be done.



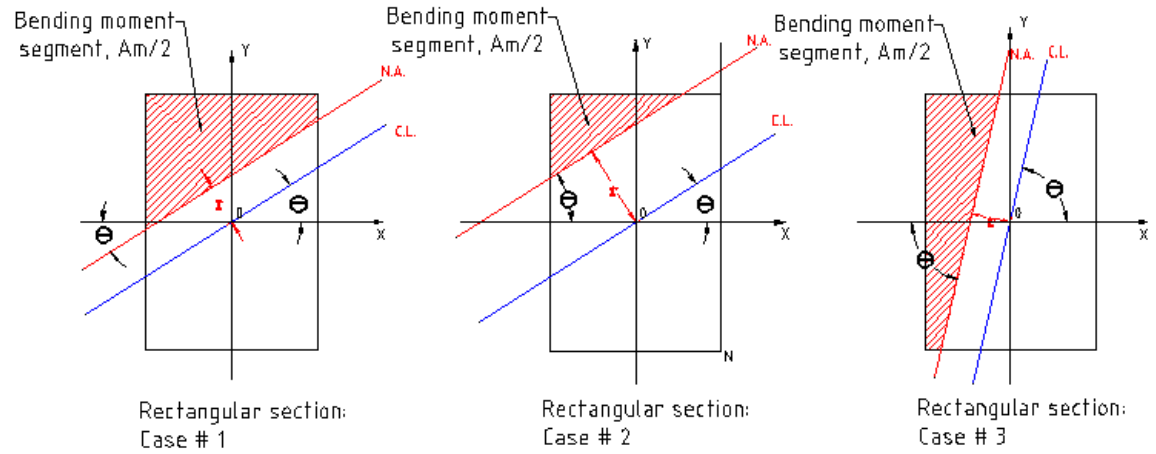


**Figure 18. Different cases of the shape of the bending moment segment for solid rectangular section.**

**FIND CRITICAL ANGLES:**

- The first critical angle  $\theta_{c1}$  occurs when  $B$  is over lapsed with  $M$  (Fig.19).

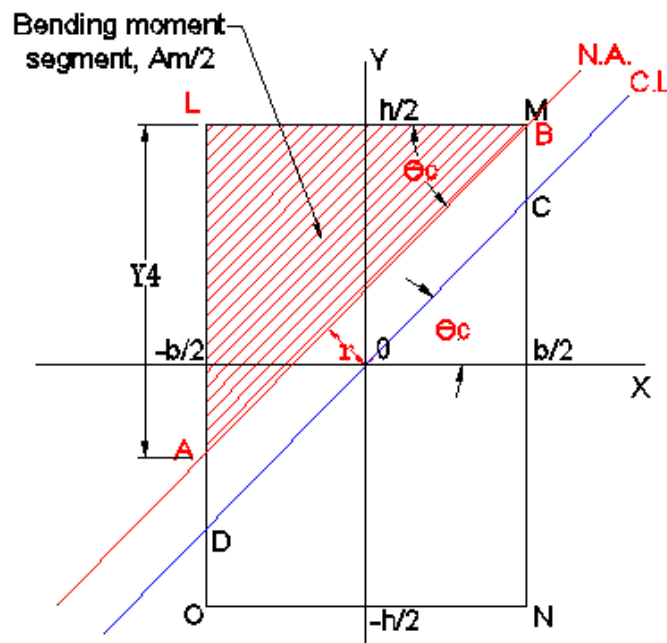


**Figure 19. Critical angle, case #1**

Observe:  $\Delta_{ALM}$

$$\Delta_{ALM} = \frac{1}{2} y_4 b = \frac{1}{2} b^2 \tan(\theta)$$

$\Delta_{ALM}$  is also equal to half of the area subjected to moment  $A_m$ .

Thus,

$$\tan(\theta) = A_m/b^2$$

$$\theta_{c1} = \text{atan}(A_m/b^2) \quad \text{Eq.(18)}$$

The second critical angle  $\theta_{c2}$  occurs when A is overlapped with O (Fig. 20).

Observe:  $\Delta_{OLB}$

$$\Delta_{OLB} = \frac{1}{2} x_4 h = \frac{1}{2} h^2 \cot(\theta)$$

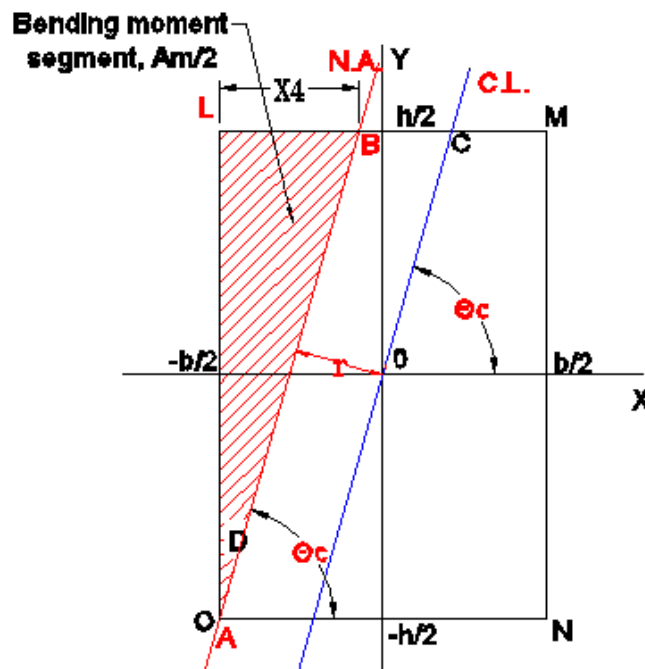


Figure 20. Critical angle, case #2

$\Delta_{OLB}$  is also equal to half of the area subjected to moment  $A_m$ .

Thus,

$$\cot(\theta) = A_m/h^2$$

$$\theta_2 = \cot(A_m/h^2) \quad \text{Eq.(19)}$$

### DIFFERENT CASES OF BENDING MOMENT SEGMENT:

#### CASE#1, $\theta \leq \theta_1$

The bending moment segment in this case is polygon  $ALMB$ . Its vertices can be calculated as:

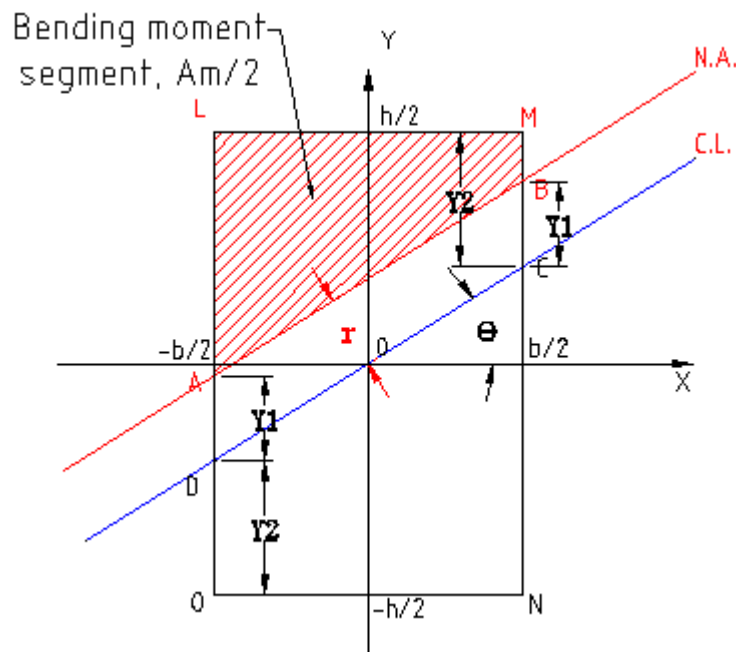


Figure 21. Solid rectangular section, case #1

- $L(x_L, y_L) = (-\frac{b}{2}, \frac{h}{2})$

- $M(x_M, y_M) = (\frac{b}{2}, \frac{h}{2})$

- $A(x_A, y_A)$

$$x_A = -\frac{b}{2}$$

$$y_A = OD + AD$$

$$y_A = y_1 + y_2$$

But,  $y_1 = r/\cos(\theta)$

Find R

$$Area_{ABCD} = CD \times r$$

But,

$$CD = b/\cos(\theta)$$

And,

$$Area_{ABCD} = A_p/2$$

Then,

$$r = \frac{A_p \cos(\theta)}{2b}$$

So,

$$y_1 = \frac{A_p}{2b}$$

$$y_2 = (h - b \tan(\theta))/2$$

Hence,

$$y_A = \frac{A_p}{2} + (h - b \tan(\theta))/2$$

- $B(x_B, y_B)$

$$x_B = b/2$$

$$y_B = y_A + CD \times \sin(\theta)$$

$$y_B = \frac{A_p}{2} + \frac{h - b \tan(\theta)}{2} + b \sin(\theta) / \cos(\theta)$$

**CASE#2:  $\theta_1 < \theta < \theta_2$**

The interest region in this case is the triangle  $ALB$ . Its vertices can be calculated as

- $L(x_L, y_L) = (-\frac{b}{2}, \frac{h}{2})$

- $A(x_A, y_A)$

$$x_A = -\frac{b}{2}$$

$$y_A = h - y_4$$

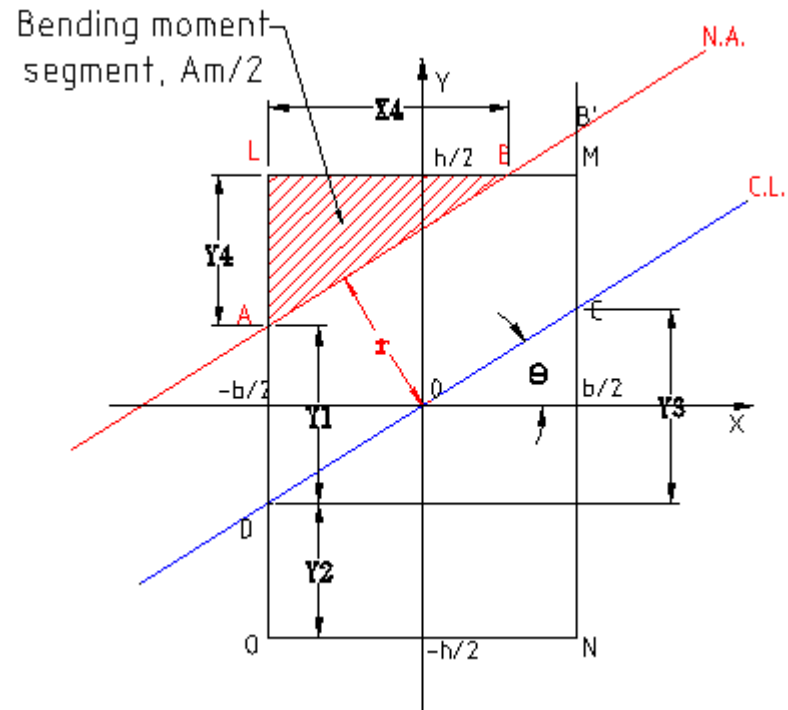


**Figure 22. Solid rectangular section, case #2**

Find  $y_4$

Observe  $\Delta_{ALB}$ :

$$\Delta_{ALB} = \frac{1}{2} AL \times LB = \frac{1}{2} y_4 x_4$$

But,

$$x_4 = y_4 / \tan(\theta)$$

Then,

$$\Delta_{ALB} = \frac{1}{2} y_4^2 / \tan(\theta)$$

Also,

$$\Delta_{ALB} = A_m/2$$

Then,

$$y_4 = \tan(\theta) \sqrt{\frac{A_m}{\tan(\theta)}}$$

Hence,

$$y_A = h - \tan(\theta) \sqrt{\frac{A_m}{\tan(\theta)}}$$

$$B(x_B, y_B)$$

$$x_B = x_4 - b/2$$

$$x_B = -\frac{b}{2} + \sqrt{\frac{A_m}{\tan(\theta)}}$$

$$y_B = h/2$$

**CASE#3:  $\theta > \theta_2$**

The interest region in this case is the polygon  $AOLB$ . Its area can be computed by knowing the coordinates of its vertices.

- $O(x_O, y_O) = (-\frac{b}{2}, -\frac{h}{2})$
- $L(x_L, y_L) = (-\frac{b}{2}, \frac{h}{2})$
- $A(x_A, y_A)$

$$y_A = -h/2$$

$$x_A = -\frac{b}{2} + x_4$$

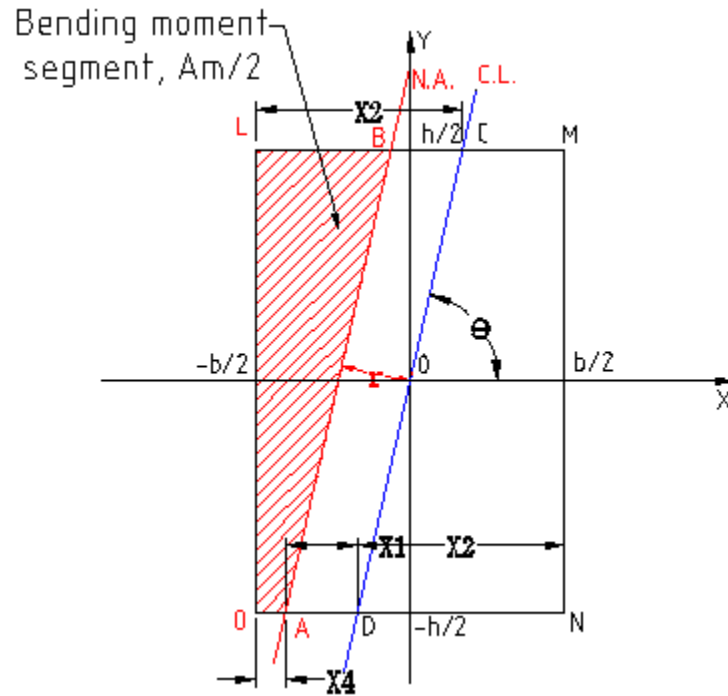


Figure 23. Solid rectangular section, case #3

Find  $x_4$

$$x_4 = b - (x_1 + x_2)$$

$$x_1 = R/\sin(\theta)$$

Observe: polygon  $ABCD$

$$Area_{ABCD} = r \times CD$$

$$CD = h/\sin(\theta)$$

However,

$Area_{ABCD}$  is also equal to half of area subjected to axial forces  $A_p/2$ .

Then,



$$r = \frac{A_p \sin(\theta)}{2h}$$

So,

$$x_1 = \frac{A_p}{2h}$$

$$x_2 = (b + x_3)/2$$

But,

$$x_3 = h \times \cot(\theta)$$

Then,

$$x_2 = (b + h \times \cot(\theta))/2$$

So,

$$x_4 = b - \left( \frac{A_p}{2h} + \frac{b + h \times \cot(\theta)}{2} \right)$$

$$x_A = -\frac{b}{2} + b - \left( \frac{A_p}{2h} + \frac{b + h \times \cot(\theta)}{2} \right)$$

$$x_A = -\frac{h \cot(\theta)}{2} - \frac{A_p}{2h}$$

- $B(x_B, y_B)$

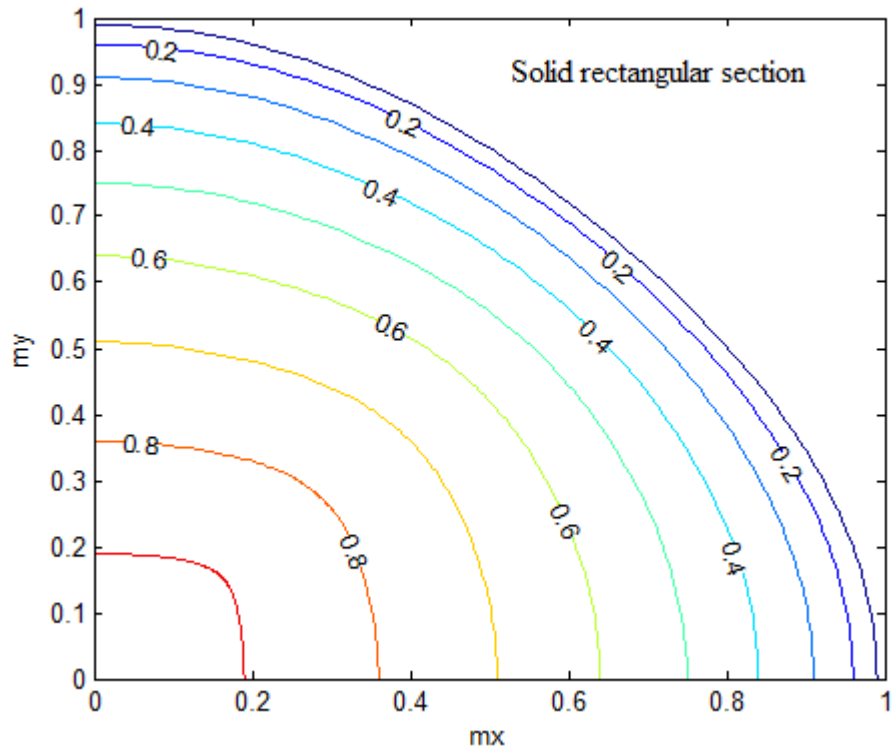
$$x_B = -\frac{b}{2} + (x_2 - x_1)$$

$$x_B = -\frac{b}{2} + \frac{b + h \times \cot(\theta)}{2} - \frac{A_p}{2h}$$

$$y_B = \frac{h}{2}$$

### 4.1.2 RESULTS

The theoretical yield surface of a solid rectangular section is the same for any proportions of solid rectangular section. The interaction curves (traces of the theoretical yield surface) of a solid rectangular yield surface are shown in Fig. 24a. They are identical to interaction curves for the solid rectangular section calculated by Chen and Atsuta that are shown in Fig. 24b. The comparison between the major- and the minor-axis bending interaction curves of the theoretical, regression and MASTAN2 are shown in Fig. 25.



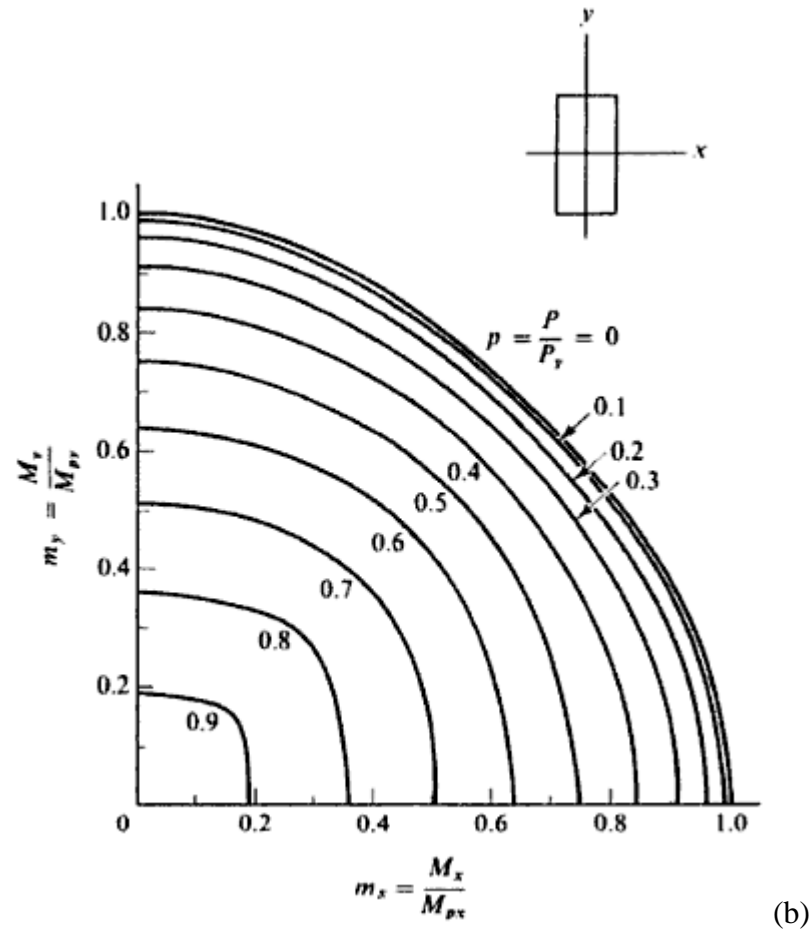
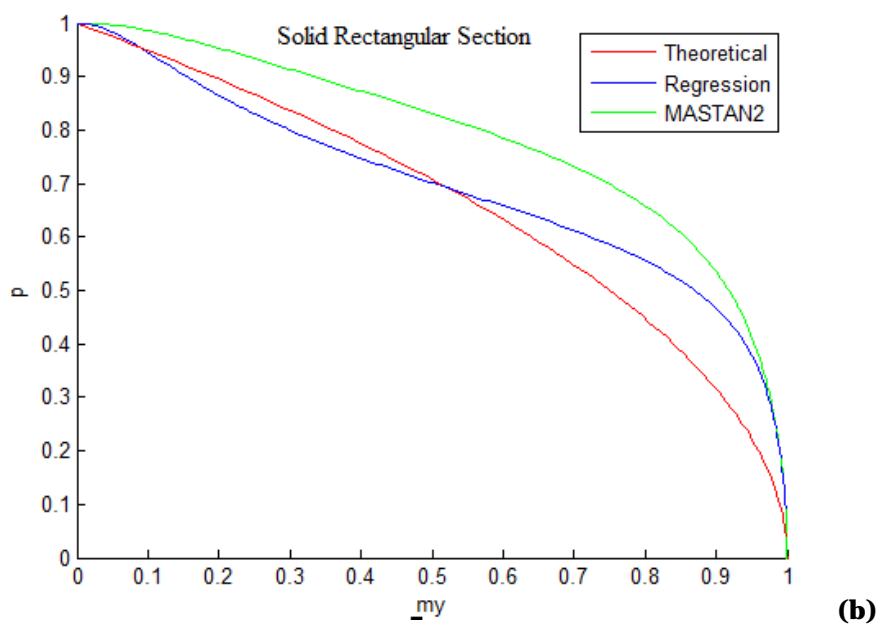
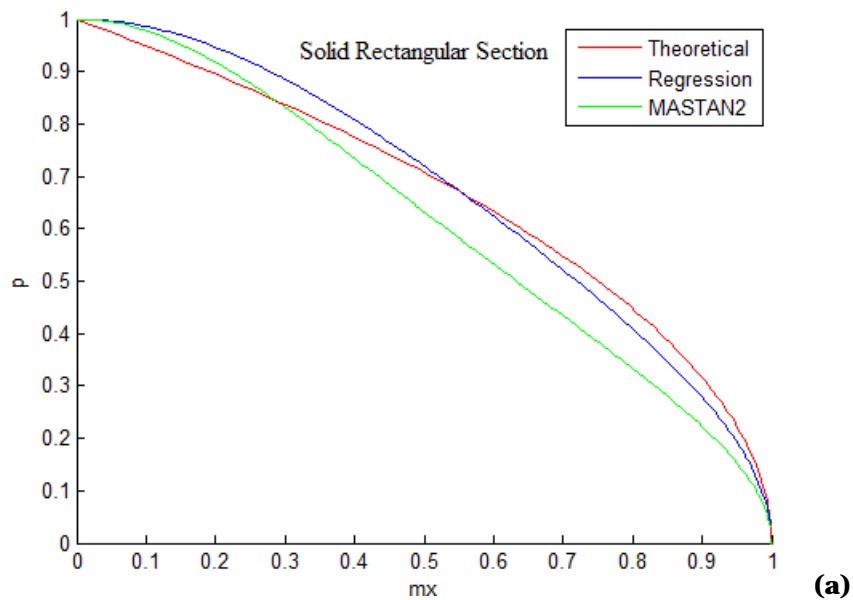


Figure 24. Top views of theoretical interaction curves for solid rectangular section (a) calculated in this study and (b) calculated by Chen and Atsuta (adopted from reference [2]).



**Figure 25. Interaction curves for a solid rectangular section ( $h/b=10$ ), (a) major-axis and (b) minor-axis.**

For major-axis, the regression curve underestimates the theoretical curve when  $p=[0,0.65]$  and overestimates the theoretical curve when  $p=[0.65,1]$ . The MASTAN2 curve underestimates the theoretical curve when  $p=[0,0.83]$  and overestimates the theoretical curve when  $p=[0.83,1]$ . For minor-axis behavior, the regression curve overestimates the theoretical curve when  $p=[0,0.69]$ , just overestimates the theoretical curve when  $p=[0.95,1]$ , and underestimates the theoretical curve when  $p=[0.69,0.95]$ . The MASTAN2 curve overestimates the theoretical curve for all values of  $p$ .

The results of the analysis of solid rectangular section are shown in Table A.1. MASTAN2's coefficients provide a negative  $R^2$  value of -0.5842 and the yield surface that is completely convex. This indicates that the general form of Eq. 7 cannot be used to model the theoretical yield surface of a solid rectangular section. The regression coefficients found with and without using weighting factors all provide with an  $R^2$  value at a maximum of 0.24 and the yield surface that is convex almost entirely. This shows the improvement of regression equation over MASTAN2 equation; however, only 24% of the theoretical yield surface data can be explained by the regression equation. Therefore, it can be concluded from these results that the customized MASTAN2 equation is not a good model for the yield surface of solid rectangular section.

## **4.2 HOLLOW RECTANGULAR SECTION**

### **4.2.1 METHOD**

Inputs: cross-section dimensions:

$h$  = depth of the shape

$b$  = width of base

$t$  = wall-thickness

$F_y$  = yield strength of material

Output: arrays of  $p$ ,  $m_x$ , and  $m_y$ .

### **STEP #1 CROSS SECTION PROPERTIES ( $A, M_{px}, M_{py}$ )**

By the principle of superposition, the properties of a hollow rectangular shape can be determined from the two solid rectangular shapes by

*hollow rectangle = outer rectangle – inner rectangle.*

Inputs: cross-section dimensions:

$$h_{outer} = h \quad h_{inner} = h - t \quad \text{Eq.(20)}$$

$$b_{outer} = b \quad b_{inner} = b - t$$

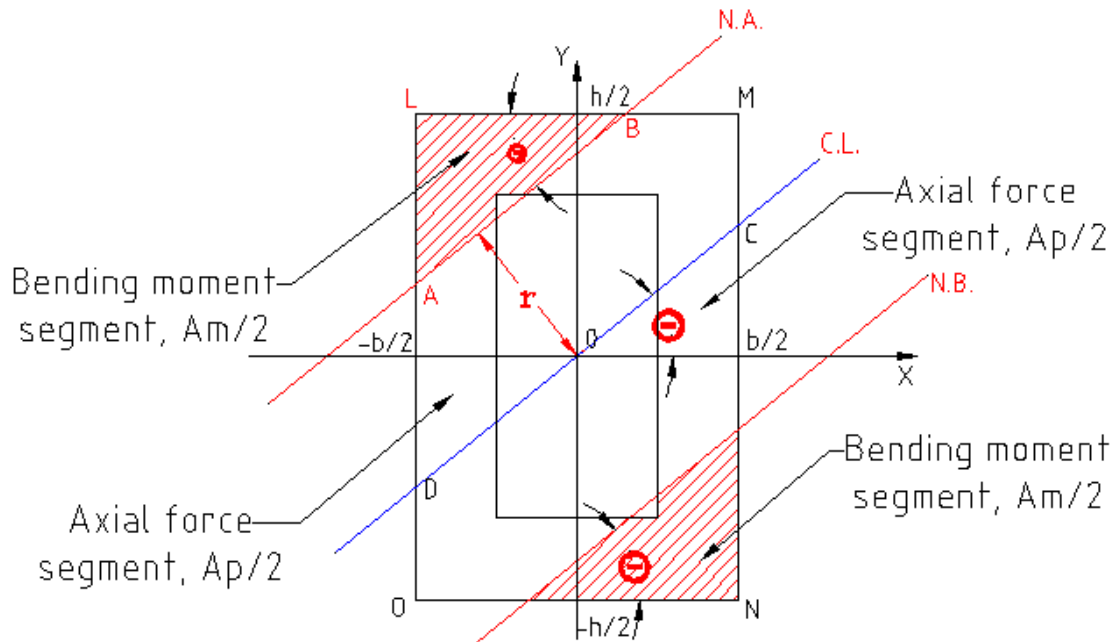


**Figure 26. Hollow rectangular section**

Apply superposition to cross-section properties/capacities:

- Cross-sectional area,  $A_{hollow} = A_{outer} - A_{inner}$
- Plastic Moment,  $M_{p(hollow)} = M_{p(outer)} - M_{p(inner)}$

Apply superposition to applied forces/moments:

- Bending Moment,  $M_{hollow} = M_{outer} - M_{inner}$

By applying the superposition principle,  $(m_z, m_y, p)$  of the hollow rectangular section can be generated from two solid rectangular shapes being analyzed simultaneously (Fig. 27).

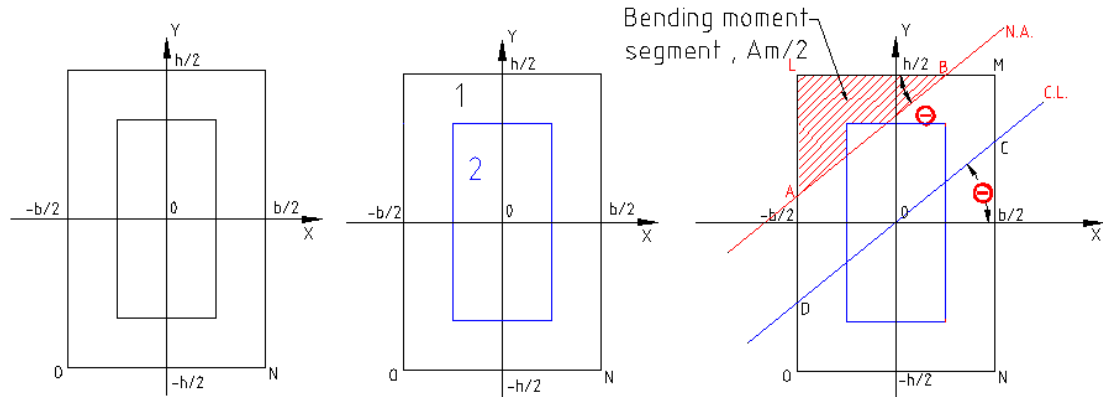


**Figure 27. Rectangular section as an assemblage of rectangles.**

### **STEP #2 BENDING SEGMENT'S VERTICES AND CENTROID**

Unfortunately, studying the different locations of the N.A. and using above the trapezoidal technique can only be done with one solid rectangular section. Because different sizes of solid rectangular sections are being considered together, a given location of N.A. can fall into more than one trapezoidal area which increases significantly the number of required cases that need to be considered. In most cases, it is difficult to find the critical angles to distinguish between these cases. Furthermore, the geometry of bending moment segment for these cases makes it nearly impossible to calculate the coordinates of the vertices of the bending segment.

With this in mind, a new technique was derived in this study to avoid the above shortcomings and provides a general solution to finding coordinates of vertices of bending moment segment for all kinds of cross sections that can be considered as the assemblage of rectangles. This new technique is called the “interpolating technique” and takes advantage of the MATLAB linear interpolation function “interp1.”



In this technique, the unique line N.A., for a given bending moment area  $AA$  ( $= A_m/2$  and corresponds to a given  $p$ ) and  $\theta$ , can be found by determining the parameter taken as the vertical intersection ( $yy$ ) of the line (N.A.):

$$y = \tan(\theta)x + yy \quad \text{Eq.(21)}$$

The unique line of the N.A. can be used to locate the vertices of the bending moment segment by determining the intersections between the line and any rectangles of the assemblage. An algorithm called “line\_intersect\_rect” was created in this thesis to find such intersections. The location  $yy$  can be found for any location of the N.A. by interpolating between only a few reference points that relate the area  $AA$  to the location  $yy$ . The illustration of such a relationship is shown in (Fig.28).

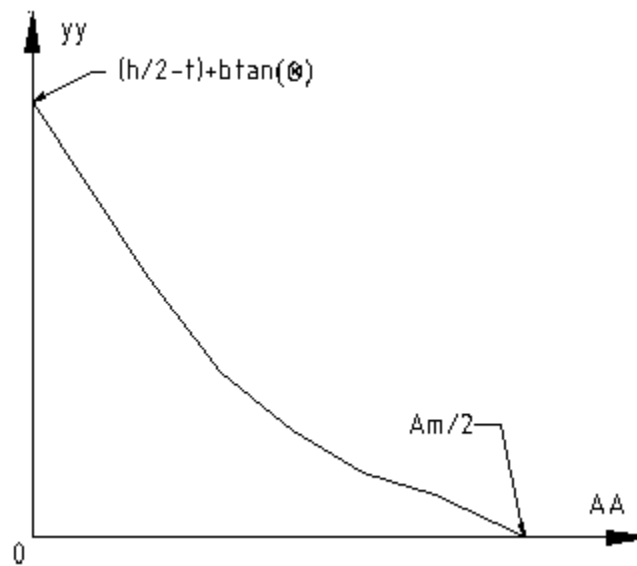


**Figure 28. Relationship between vertical interception of line N.A.:  $y = \tan(\theta)x + yy$  and bending moment area  $AA$ .**

The three reference points that are used in the interpolation to calculate  $yy$  from any given  $AA$  are identified below.

The first point is at  $(-b/2, h/2)$

$$AA = 0$$

$$yy = \frac{h}{2} + \frac{b}{2} \tan(\theta)$$

The second point is at  $(-\frac{b}{2}, \frac{h}{2} - t)$

There are two cases of  $\theta$  as shown in Fig. 29.

When  $\theta \geq \theta_c = \text{atan}\left(\frac{t}{b}\right)$

$$AA = \frac{t^2}{2 \tan(\theta)}$$

$$yy = \left(\frac{h}{2} - t\right) + \frac{b \tan(\theta)}{2}$$

When  $\theta < \theta_c = \text{atan}\left(\frac{t}{b}\right)$

$$AA = bt - \frac{b^2 \tan(\theta)}{2}$$

$$yy = \left(\frac{h}{2} - t\right) + \frac{b \tan(\theta)}{2}$$

The third point is at the origin:

$$AA = \frac{A}{2}$$

$$yy = 0$$

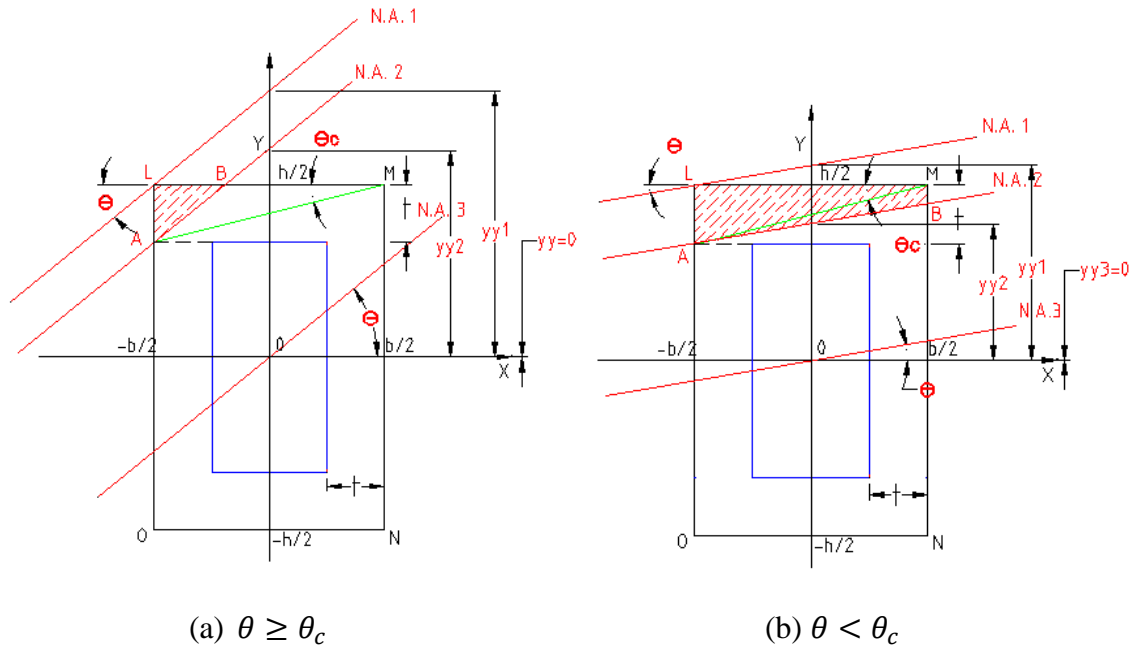


**Figure 29. Three reference points from the relationship between  $yy$  and  $AA$ .**

#### 4.2.2 RESULTS

The analyses of hollow rectangular sections provided similar results to the results of the solid rectangular section, as shown in Table A.2. On average the  $R^2$  values calculated from both the regression and MASTAN2 coefficients are close to zero. All of the yield surfaces are completely concave. The theoretical interaction curves for the hollow rectangular section with the ratio of height to base to wall thickness of 40:20:1 is shown in Fig. 30. The regression, the MASTAN2, and theoretical interaction curves are plotted together in Fig. 31. For major-axis behavior, the regression curve stays very close to the

MASTAN2 curve which both underestimate the theoretical curve when  $p=[0,0.7]$  and overestimate the theoretical curve when  $p=[0.7,1]$ . For minor-axis behavior, the MASTAN2 curve overestimates excessively the theoretical curve for all values of  $p$ . The regression curve starts off from  $p=0$  by staying close to the MASTAN2 curve until it starts to move away from the MASTAN2 curve at  $p=0.35$ . It directs toward the theoretical curve until it touches the theoretical curve when  $p=0.75$ . Then it stays close to the theoretical curve when  $p=[0.75,1]$ .

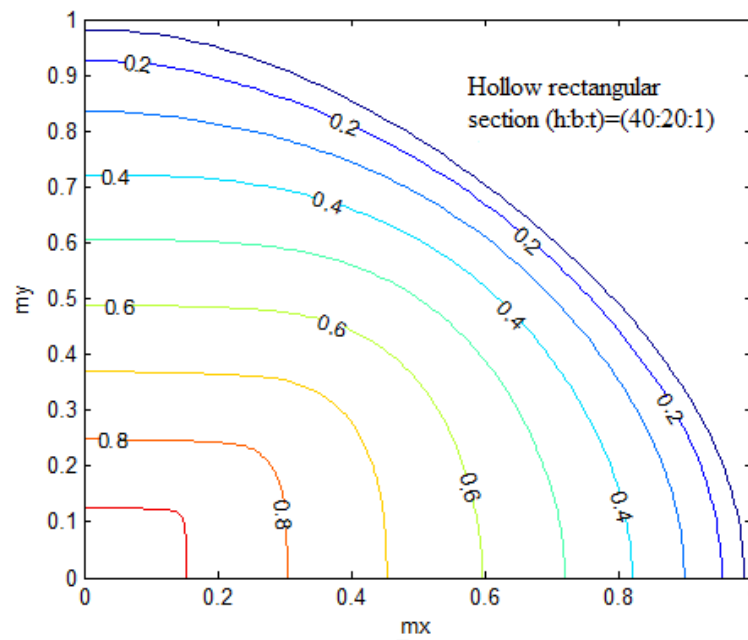


**Figure 30. The theoretical interaction curves for a hollow rectangular section.**

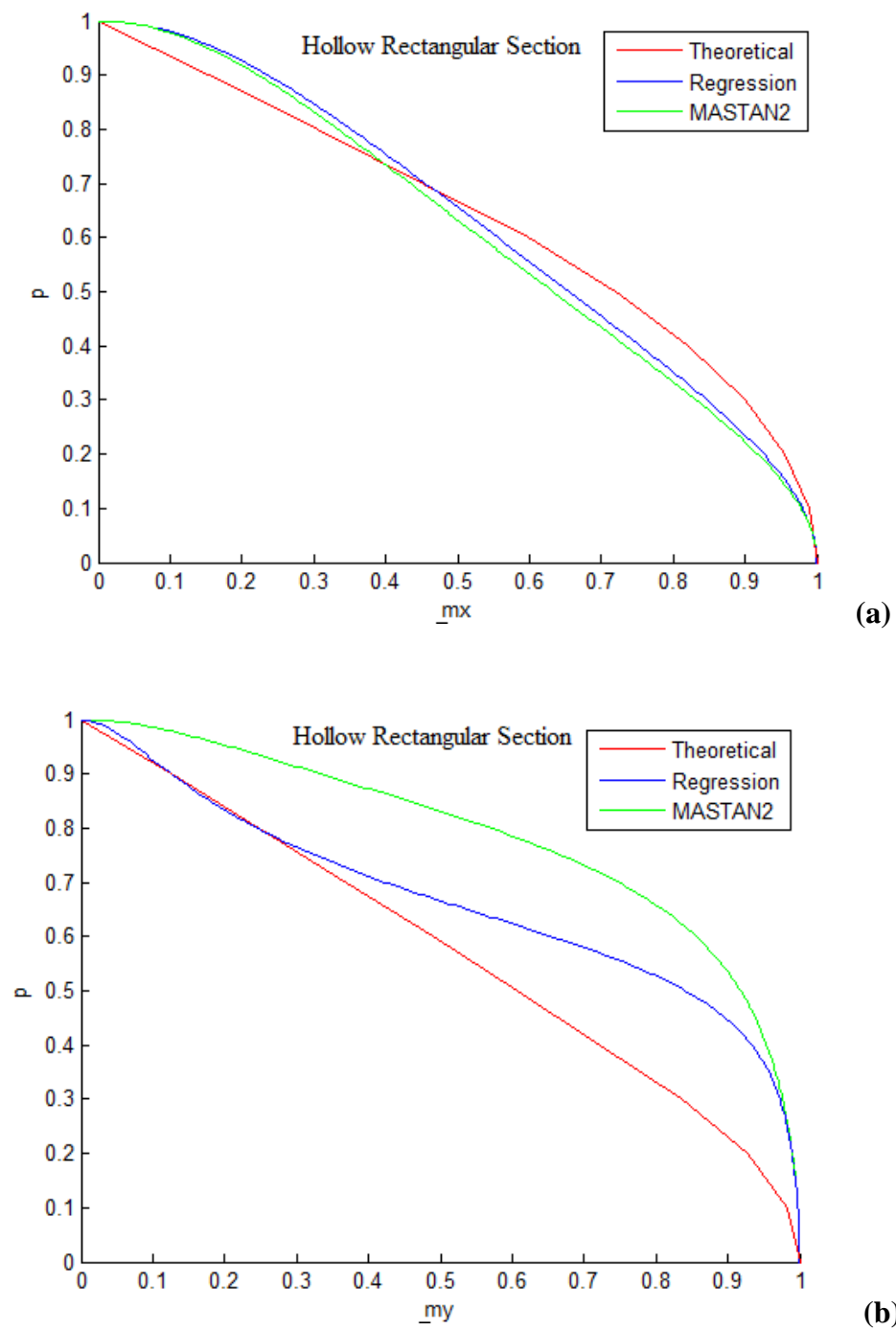


**Figure 31. The regression, MASTAN2, and theoretical interaction curves for a hollow rectangular section, (a) major-axis, (b) minor-axis.**

Although some improvement can be realized by customizing the MASTAN2 equation to the theoretical yield surface of hollow rectangular section, the resulting regression yield surface still cannot provide a good model for the theoretical yield surface of any corresponding hollow rectangular sections.

### 4.3 SOLID CIRCULAR SECTION

#### 4.3.1 METHOD

Inputs: cross-section dimensions:

$D$  = diameter of cross section ( $R = D/2$ )

$F_y$  = yield strength of material

Output: arrays of  $p$ ,  $m_x$ , and  $m_y$ .

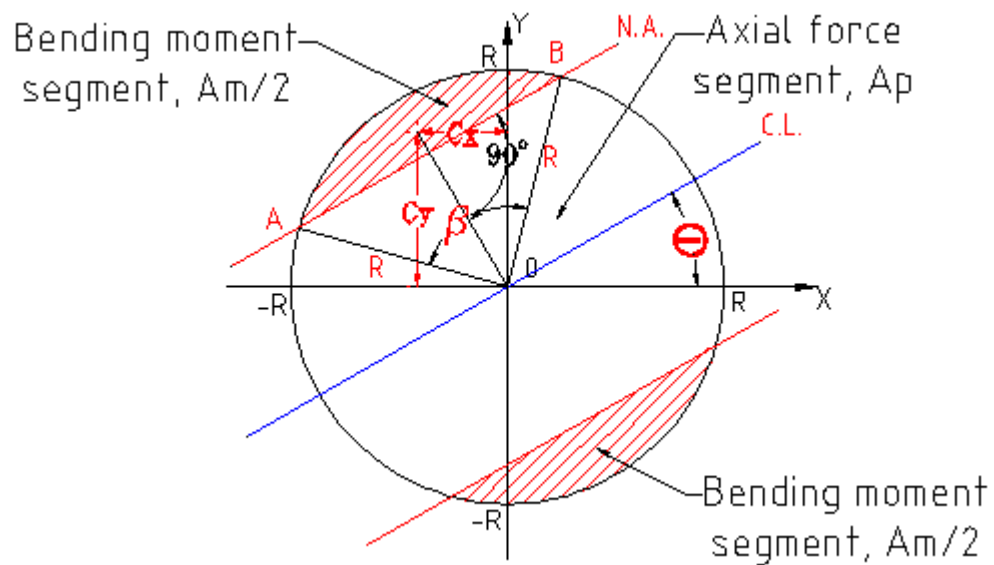


**Figure 32. Solid circular section**

### Step #1 CROSS SECTION PROPERTIES ( $A, M_{px}, M_{py}$ )

For circular shape:

- Cross-sectional area,  $A = \pi R^2$  Eq.(21)
- Plastic Moment,  $M_p = F_y \frac{4R^3}{3}$

### Step #2 BENDING MOMENT SEGMENT'S VERTICES AND CENTROID

The bending moment segment in this case is the shaded circular segment whose area is equal to  $A_m/2$ . Its moment arms can be calculated using the following equations

- x-component:  $C_x = \sin(\theta) \bar{y}$  Eq.(22)
- y-component:  $C_y = \cos(\theta) \bar{y}$

$$\text{where, } \bar{y} = \frac{4R \sin(\frac{\beta}{2})^3}{3(\beta - \sin(\beta))}$$

The area of the bending moment segment can be defined in terms of the circular radius  $R$  and the center angle  $\beta$  (in radians) by

$$A_m/2 = R^2 \frac{\beta - \sin(\beta)}{2} \quad \text{Eq.(23)}$$

with  $A_m = A - A_p = A(1 - p)$ , Eq.(23) can be rewritten as

$$R^2(\beta - \sin(\beta)) = A(1 - p) \quad \text{Eq.(24)}$$

With this,  $\beta$  can be solved from the above equation for the known values  $R$  and  $p$ .

### 4.3.2 RESULTS

The theoretical yield surface for solid circular section is the same for all sizes of a solid circular section. Its theoretical interaction curves are shown in Fig. 33. The comparison between the major- and the minor-axis interaction equations of the theoretical, regression, and MASTAN2 yield surfaces for a solid circular section is also shown in Fig. 34. The results of the regression analysis for a solid circular section are similar to the previous sections, as shown in Table A.3. The MASTAN2 coefficients provide a negative  $R^2$  value of -1.7474. The regression coefficients [ 2.0649 10.6746 1.9695] provide the corresponding  $R^2$  value of 0.1974.

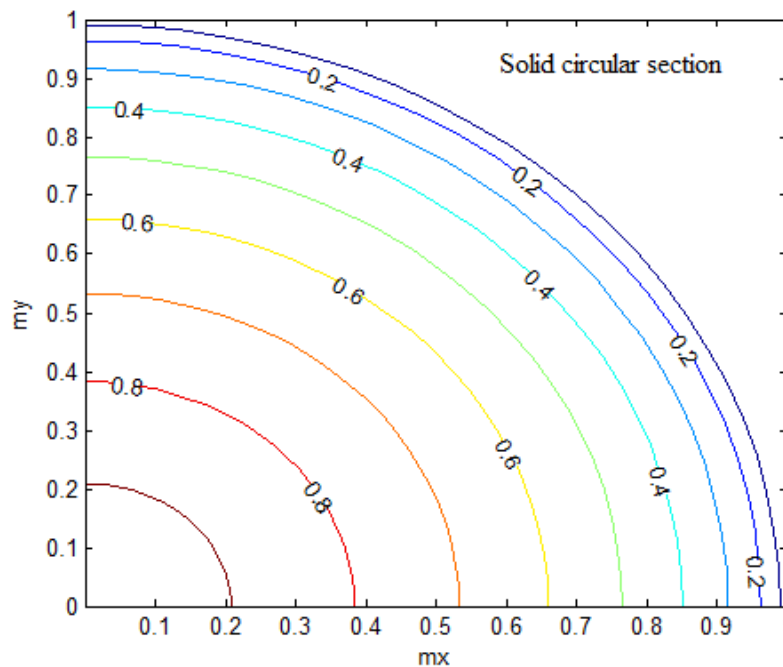


**Figure 33. The theoretical interaction curves for a solid circular section.**



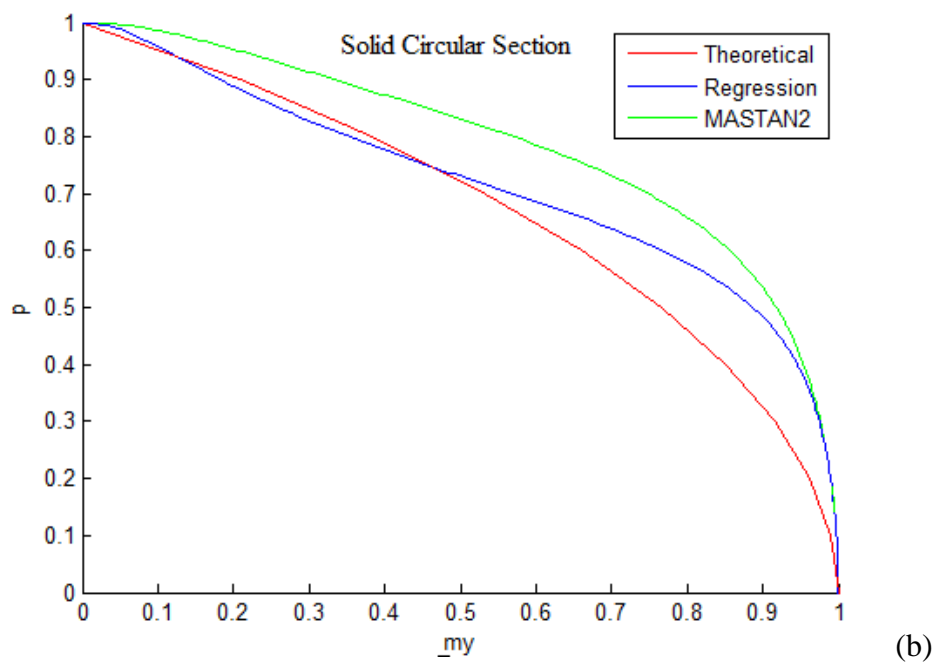
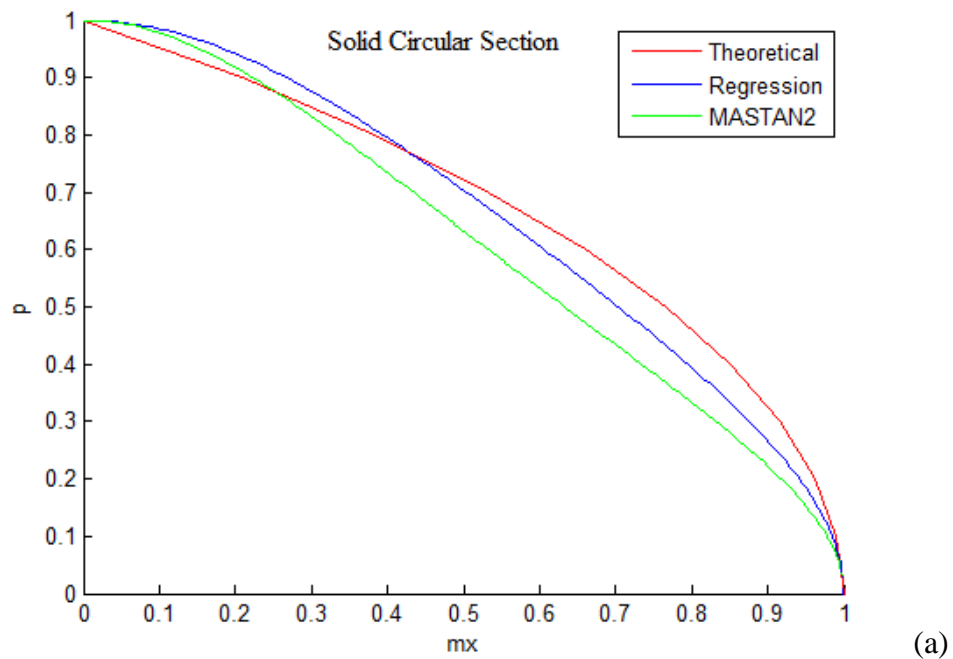


**Figure 32. The regression, MASTAN2, and theoretical interaction curves for a solid circular section, (a) major-axis, (b) minor-axis.**

This once again shows that the regression equation (Eq. 7) that results from fitting the MASTAN2 equation to fit the theoretical yield surface of a solid circular section cannot provide a good model for the theoretical yield surface of any solid circular sections. The regression and MASTAN2 curves of solid circular sections behave in a similar manner to that of the regression and MASTAN2 curves of hollow rectangular section with respect to their theoretical curves, as described in section 4.2.2. The same conclusion is reached, MASTAN2 cannot be used to give a good customized yield surface equation to model the theoretical yield surface of solid circular section.

## **4.4 HOLLOW CIRCULAR SECTION**

### **4.4.1 METHOD**

Inputs: cross-section dimensions:

$OD$  = Outside diameter

$t$  = thickness of pipe

$F_y$  = yield strength of material

Output: arrays of  $p$ ,  $m_x$ , and  $m_y$ .

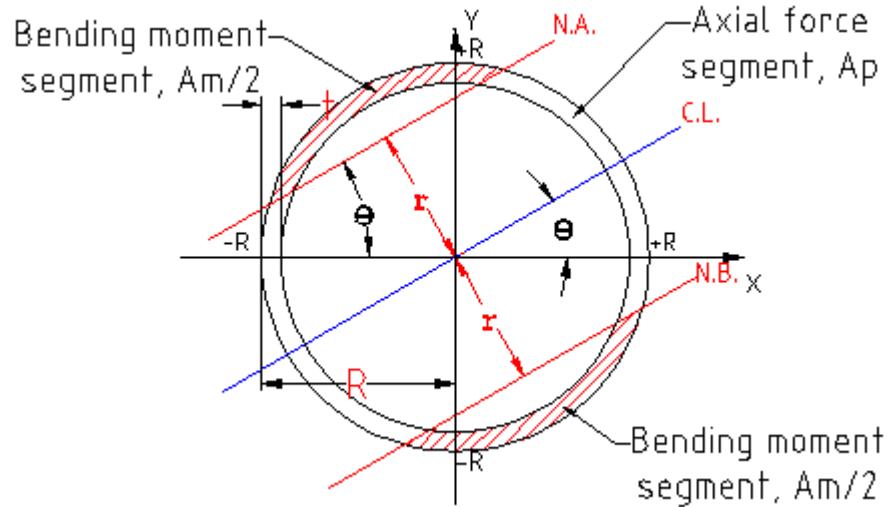


**Figure 33. Hollow circular section**

Similar to a hollow rectangular cross-section, the principle of superposition can be used to determine the properties of hollow rectangular cross-section from the corresponding properties of the outer and inner solid circular cross-sections.

$$\text{hollow pipe} = \text{outer pipe} - \text{inner pipe}$$

Inputs: cross-section dimensions:

$$R_{outer} = OD/2 \quad R_{inner} = OD/2 - t \quad \text{Eq.(25)}$$

Apply superposition to cross-section properties/capacities:

- Cross-sectional area,  $A_{hollow} = A_{outer} - A_{inner}$
- Plastic Moment,  $M_{p(hollow)} = M_{p(outer)} - M_{p(inner)}$

Apply superposition to applied forces/moments:

- Bending Moment,  $M_{hollow} = M_{outer} - M_{inner}$

Therefore,  $(m_z, m_y, p)$  of hollow rectangular shape can be generated from  $(m_z, m_y, p)$  of two solid rectangular shapes by applying the superposition principle.

### Step #2 BENDING MOMENT SEGMENT'S VERTICES AND CENTROID

The interpolating technique described above can be extended to determine the bending moment segment of the hollow circular section. This can be done by relating the hollow circular section  $r$  to the area  $AA$ . There are only two reference points that can be easily identified as shown below (Fig. 34). Due to the symmetry of a circle about any axis, these two points can be identified the same way for any given  $\theta$ .

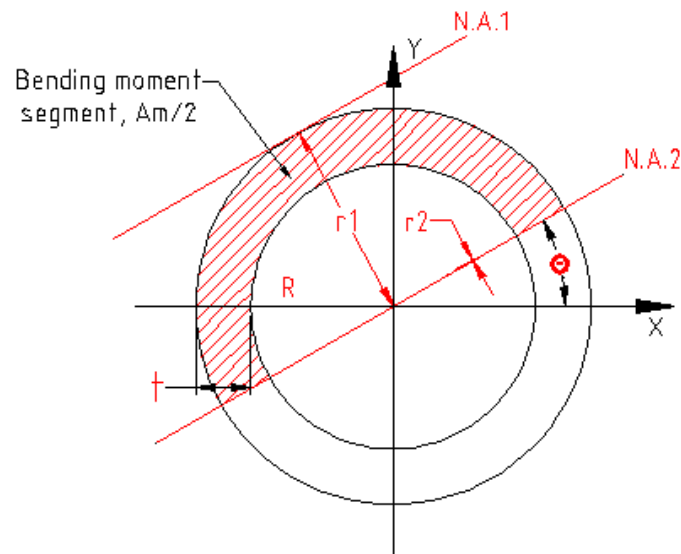


**Figure 34. Two reference points from the relationship between  $r$  and  $AA$ .**

The first point is located at any location on the outer circle:

$$AA = 0$$

$$r = R$$

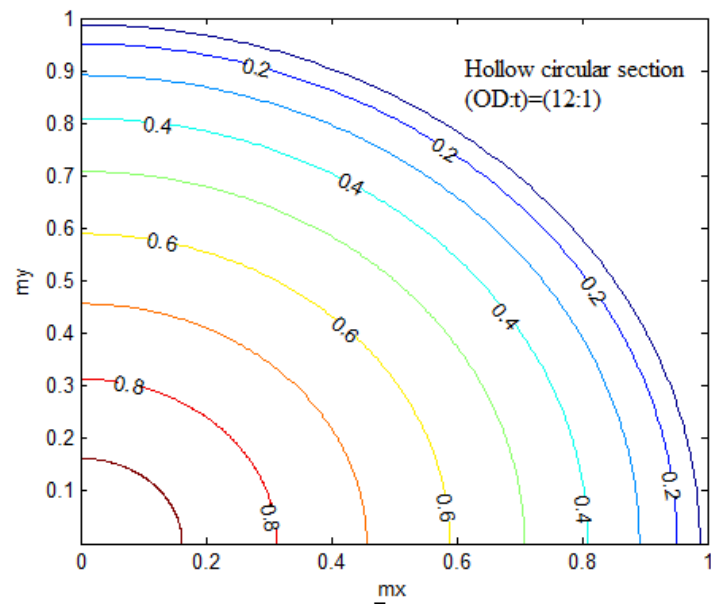
The second point is at the origin:

$$AA = A/2$$

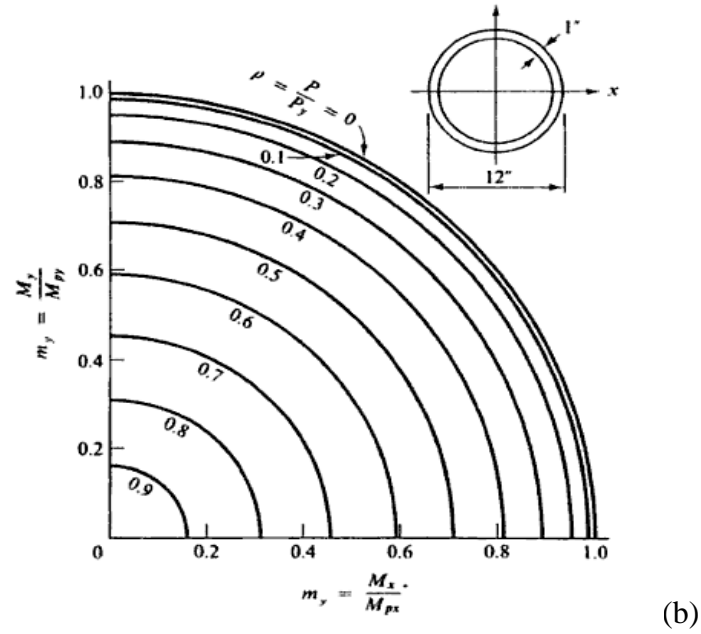
$$r = 0$$

#### 4.4.2 RESULTS

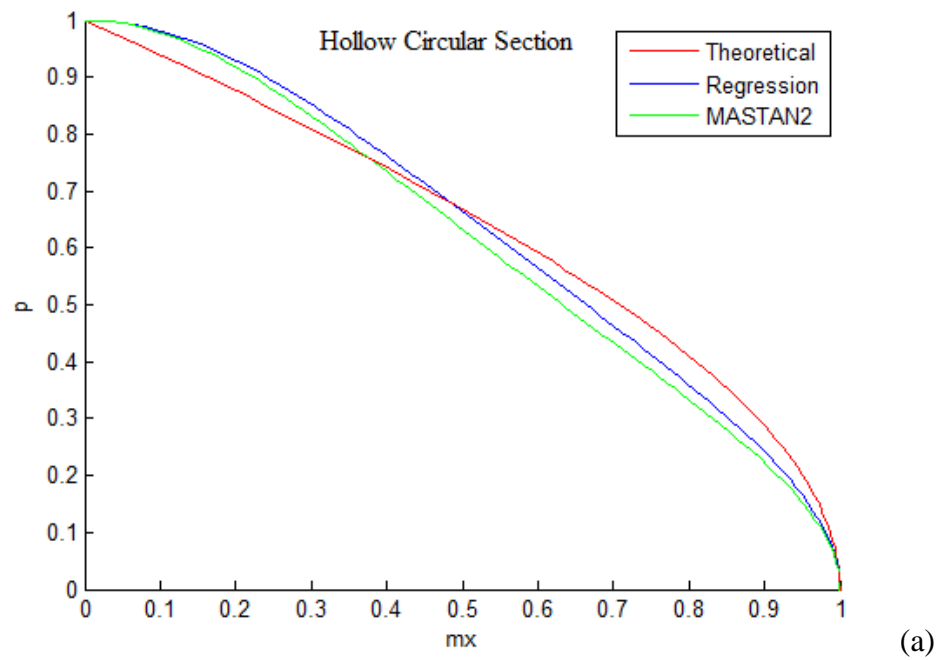
The theoretical interaction curves for a hollow circular section with the ratio of outside diameter to wall thickness of 12:1 are plotted to compare with the corresponding interaction curves calculated by Chen and Atsuta (Fig. 35). They are identical.



(a)



**Figure 35. The theoretical interaction curves for hollow circular section (a) calculated in this study and (b) calculated by Chen and Atsuta (adopted from reference [2])**



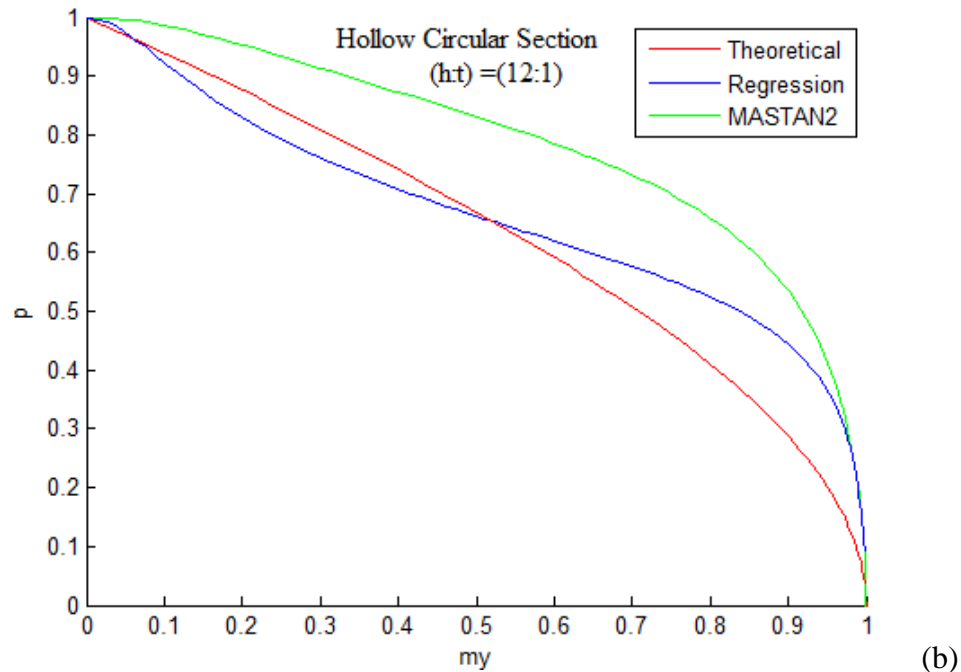


**Figure 36. The regression, MASTAN2, and theoretical interaction curves for a hollow circular section (OD/t=12/1), (a) major-axis, (b) minor-axis.**

The results of regression analysis for hollow circular sections are also similar to those of the previous sections, as shown in Table A.4. The regression and MASTAN2 yield surfaces did have some percentages of concavity. Similar to the findings in the above sections, the MASTAN2 yield surface equation cannot provide a good regression equation to model the corresponding theoretical yield surfaces of any hollow circular sections.

## 4.5 WIDE-FLANGE SECTION

### 4.5.1 METHOD

Inputs: cross-section dimensions:

$d$  = depth of the shape

$b_f$  = width of base

$t_w$  = width of the web

$t_f$  = width of the flange

Output: arrays of  $p$ ,  $m_x$ , and  $m_y$ .

### Step #1 CROSS SECTION PROPERTIES ( $A$ , $M_{px}$ , $M_{py}$ )

To simplify the analysis, a wide-flange cross-section can be broken into three rectangles.

The cross-section's yield surface ( $m_x, m_y, p$ ) is then the superposition of the behavior of these three rectangles (refer Fig.37).

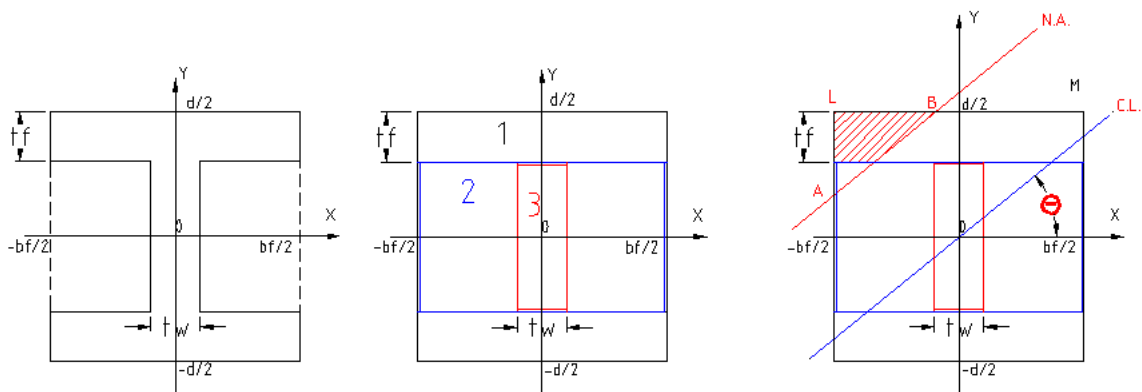


**Figure 37. Wide-flange section as the assemblage of rectangles.**

Rectangle 1: Outer rectangle



- Area,  $A_1 = b_f d$  Eq.(26)
- Plastic moment,  $M_{p(1)} = F_y (b_f d^2) / 4$

Rectangle 2: Inner rectangle

- Area,  $A_2 = b_f (d - 2t_f)$
- Plastic moment,  $M_{p(2)} = F_y [b_f (d - 2t_f)^2] / 4$

Rectangle 3: Web

- Area,  $A_3 = t_w (d - 2t_f)$
- Plastic moment,  $M_{p(3)} = F_y [t_w (d - 2t_f)^2] / 4$

### **STEP #2 BENDING MOMENT SEGMENT'S VERTICIES AND CENTROID:**

With the wide-flange section defined as an assemblage of rectangles, the bending moment segment can be determined by using the previously described interpolation technique. The parameter and reference points for the wide-flange section are almost identical to those for the hollow rectangular section.

The first point is at  $(-b_f/2, d/2)$

$$AA = 0$$

$$yy = \frac{d}{2} + \frac{b_f}{2} \tan(\theta)$$

The second point is at  $(-\frac{b_f}{2}, \frac{d}{2} - t_f)$ .

There are two cases of  $\theta$  as shown in Fig. 38.

When  $\theta \geq \theta_c = \text{atan}\left(\frac{t_f}{b_f}\right)$

$$AA = \frac{b_f^2}{2 \tan(\theta)}$$

$$yy = \left(\frac{d}{2} - t_f\right) + \frac{b_f \tan(\theta)}{2}$$

When  $\theta < \theta_c = \text{atan}\left(\frac{t_f}{b_f}\right)$

$$AA = b_f t_f - \frac{t_f^2 \tan(\theta)}{2}$$

$$yy = \left(\frac{d}{2} - t_f\right) + \frac{b_f \tan(\theta)}{2}$$

The third point is at the origin

$$AA = \frac{A}{2}$$

$$yy = 0$$

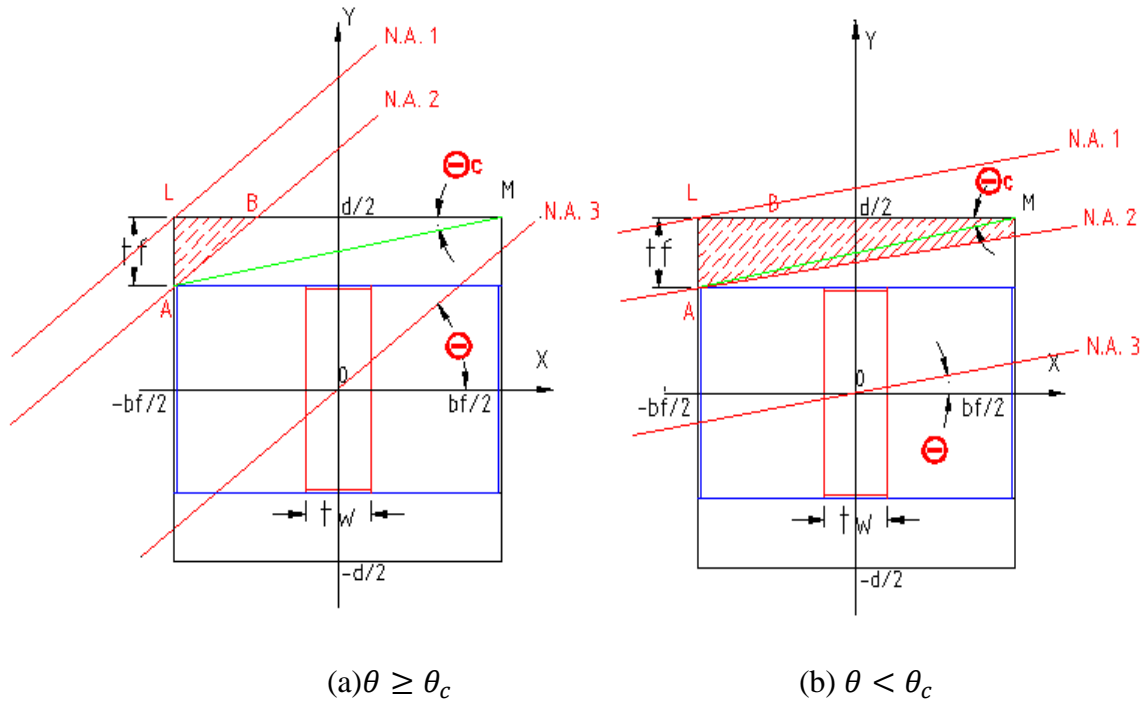
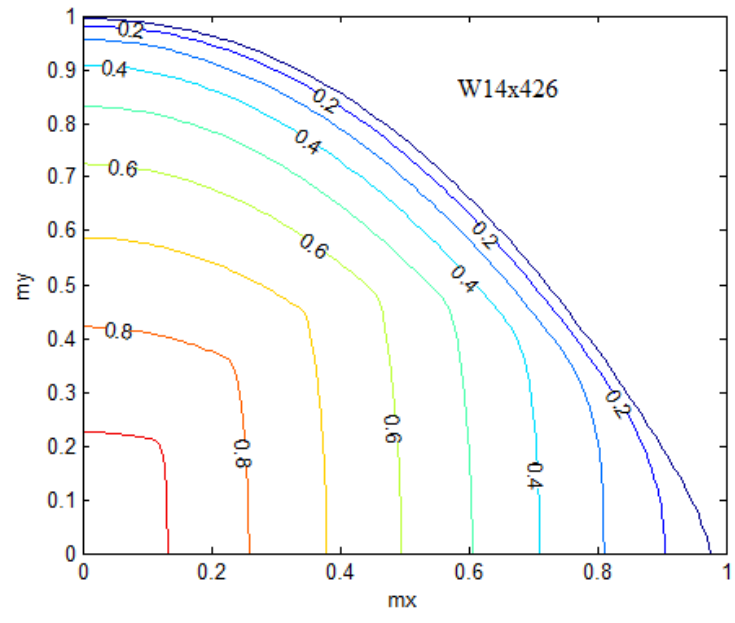


**Figure 38. Three reference points from the relationship between  $yy$  and  $AA$ .**

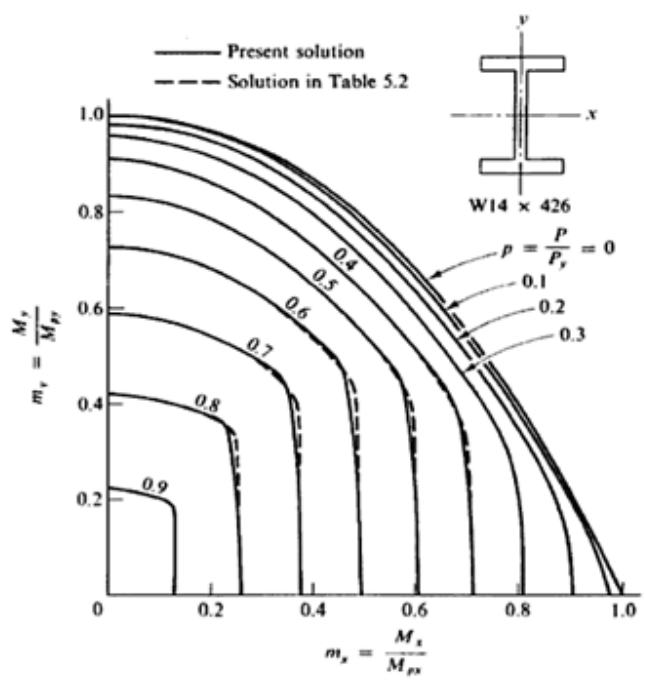
#### 4.5.2 RESULTS

The theoretical interaction curves for a W14x426 section generated in this study are compared to the interaction curves generated by Chen and Atsuta (Fig. 39). These two sets of interaction curves are identical. Table A. 5 shows complete results of the analysis of wide-flange sections. For all such sections, the  $R^2$  of the regression equation is closer to the ideal value of unit than the  $R^2$  of the MASTAN2 equation. Within the tolerance defined by using the percentage of concavity of the theoretical yield surface, both the MASTAN2 and regression yield surfaces were tested to contain zero percent concavity. In several cases, remarkable improvement can be observed. For example, a W24x55 results in regression coefficients defined [2.80 18.49 2.55] and the corresponding  $R^2$  is 0.79,

which is a significant improvement when compared to the MASTAN2  $R^2$  of 0.16. A comparison between the major- and the minor-axis interaction equations of the theoretical, regression, and MASTAN2 yield surfaces for W24x55 is shown in Fig. 40. Figure 41 provides three-dimensional surface plots of the theoretical, regression, and MASTAN2 yield surfaces.



(a)



(b)

Figure 39. The theoretical interaction curves of W14x426 calculated (a) using method derived in this study and (b) using Chen and Atsuta's Exact Method.

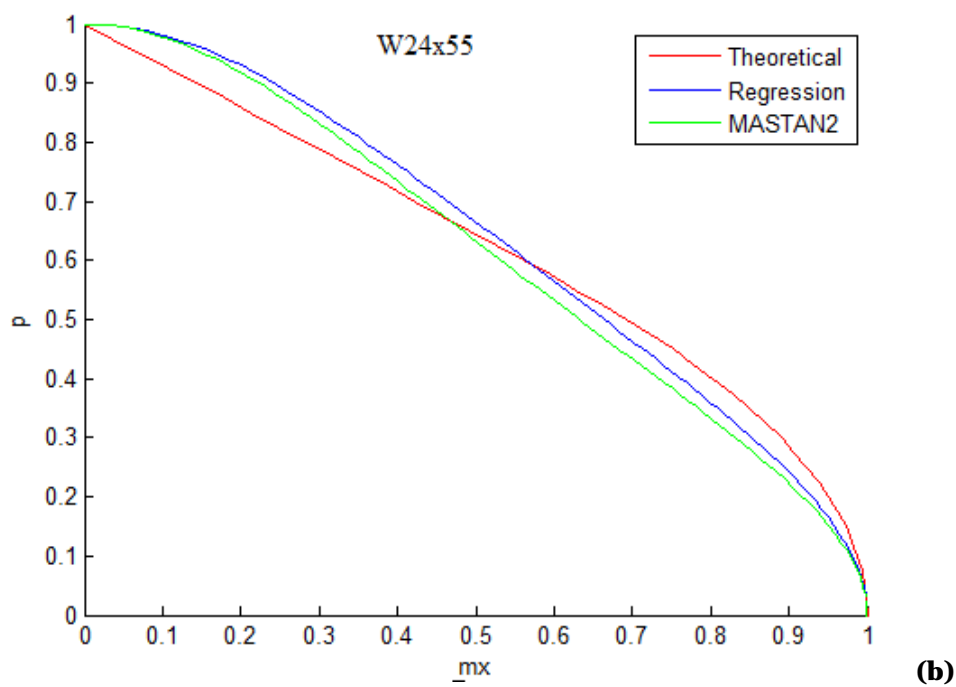
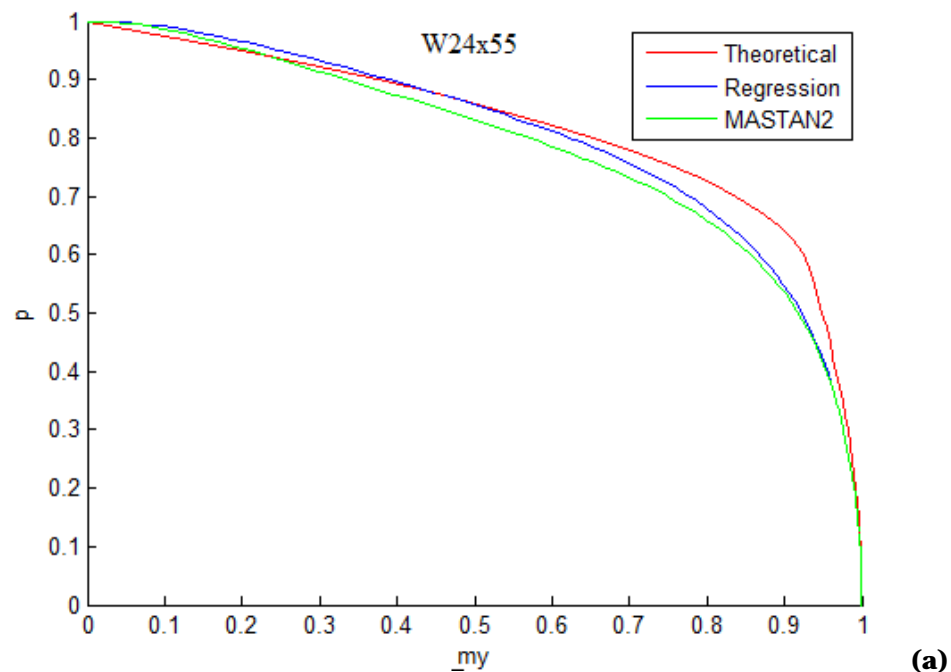
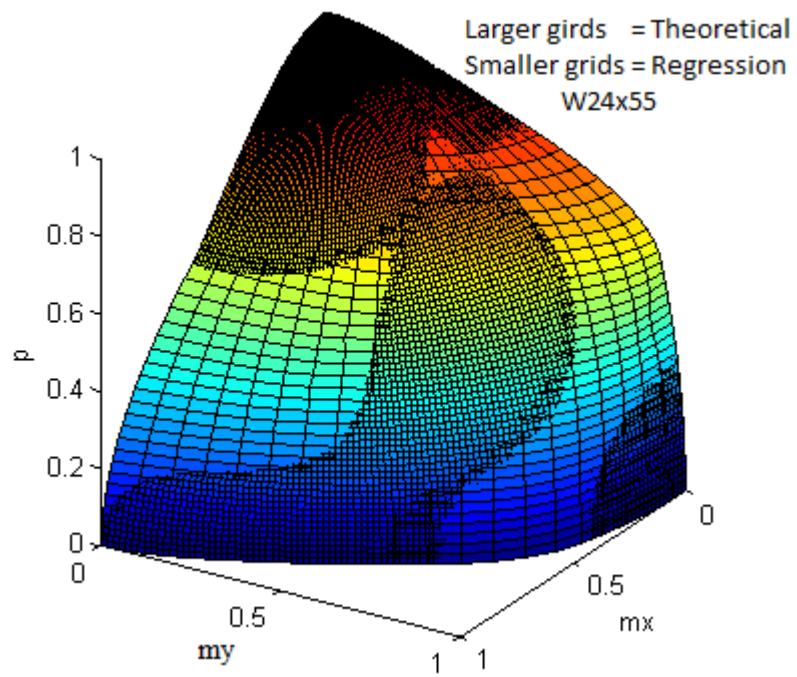
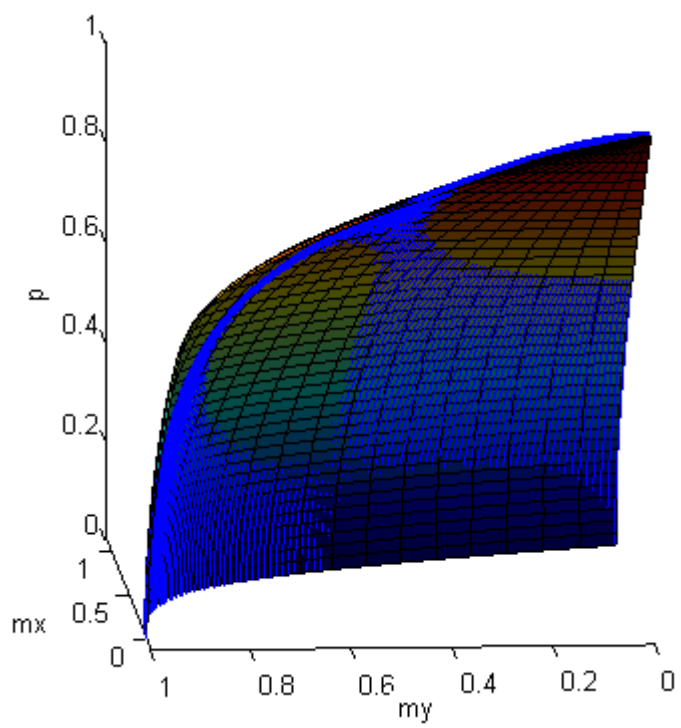


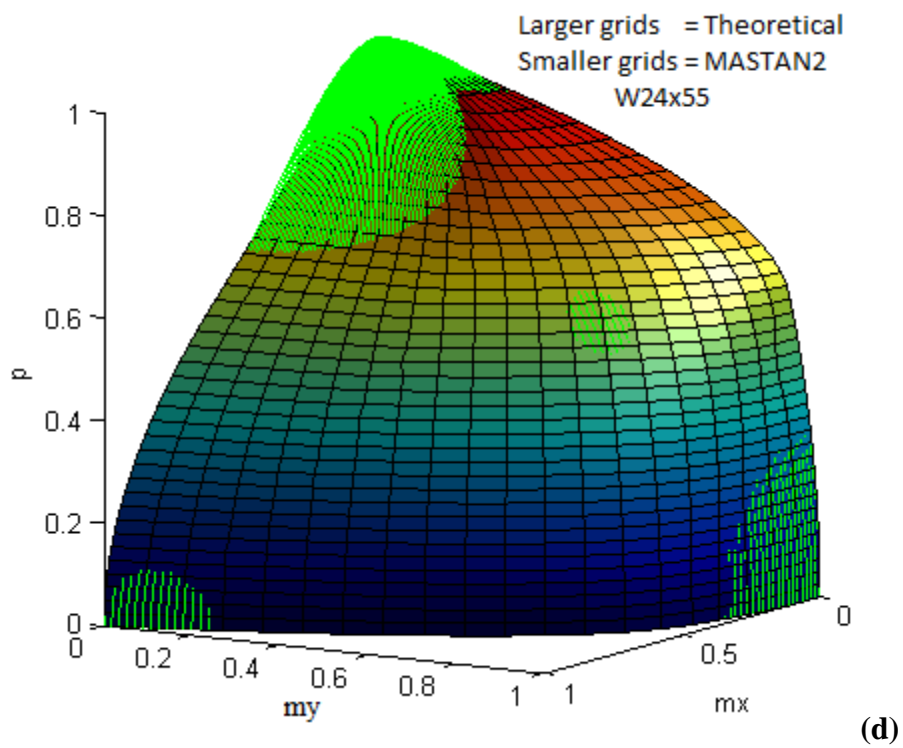
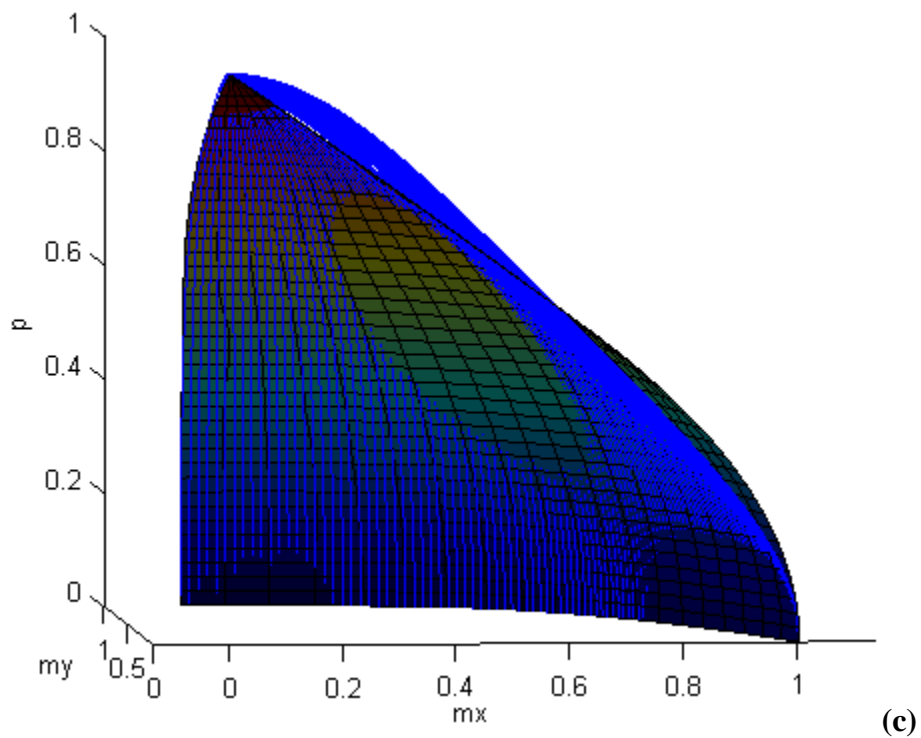
**Figure 40.** The regression, MASTAN2, and theoretical interaction curves for W24x55, (a) major-axis, (b) minor-axis.



(a)



(b)





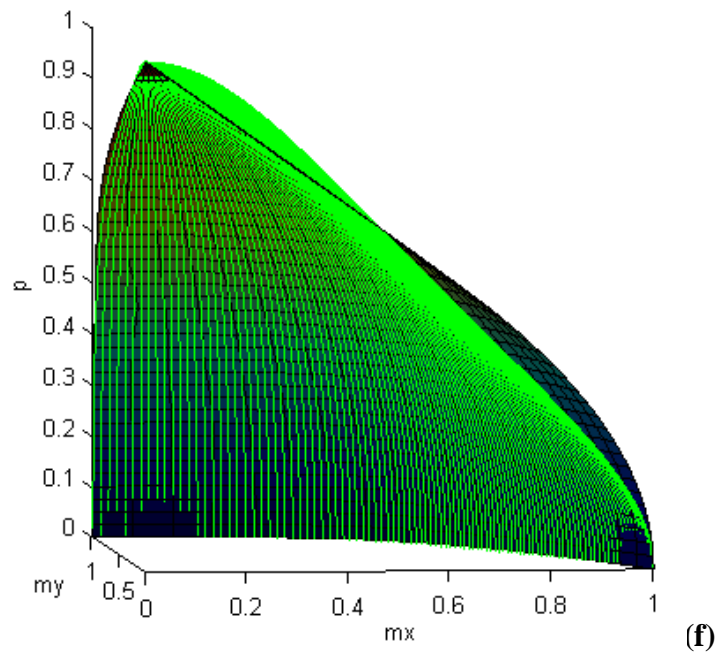
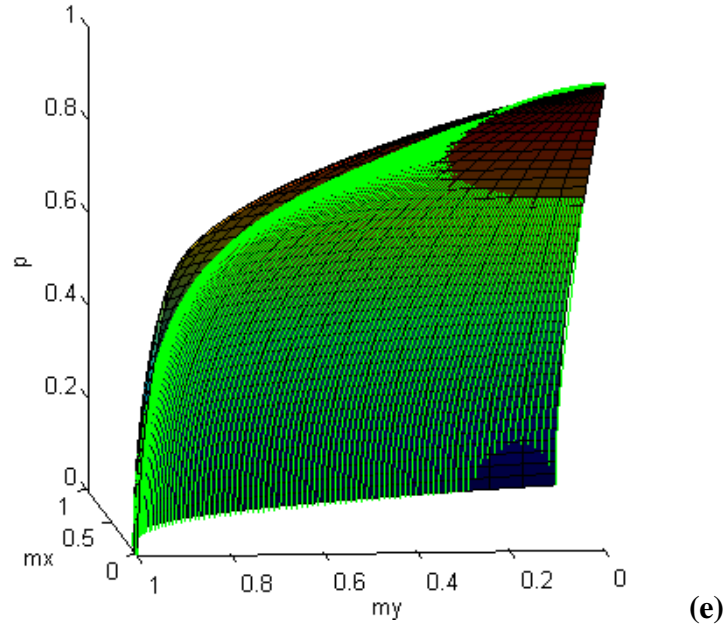


**Figure 41. (a), (b), and (c) surface plots comparing the theoretical and regression yield surfaces for W24x55. (d), (e), and (f) surface plots comparing the theoretical and MASTAN2 yield surfaces for W24x55.**

## 5 CONCLUSIONS

For wide-flange sections, coefficients found by performing a weighted regression analysis on theoretical data points always provides a better coefficient of determination  $R^2$  than MASTAN2. A better  $R^2$  indicates a better model because the value of  $R^2$  represents the percentage of the variation of theoretical data points that can be explained by the model. This study also proved that a small percent of concavity can always be found in the theoretical yield surfaces and their modeling equations. However, the degrees of concavity in the regression equations for wide-flange sections are insignificant.

For other shapes,  $R^2$  for both the regression and MASTAN2 equations are on average negative or close to zero. This indicates that MASTAN2 and its customized versions are not good representatives of the theoretical yield surfaces for solid and hollow rectangular and circular sections. The reason that customized versions of MASTAN2 for wide-flange sections provide better  $R^2$  than for other sections is simply that the MASTAN2 equation was derived from the theoretical yield surface of a wide-flange section, which is W12x31.

With this in mind, future work may include employing weighted regression analysis on other general forms of equations that are similar but the not the same as MASTAN2's yield surface equation. Hopefully this could produce that could be employed for cross-sectional shapes that are not wide-flange sections.

## BIBLIOGRAPHY

1. McGuire, W., Gallagher, R. H., & Ziemian, R. D. (2000). *Matrix structural analysis*. New York: John Wiley
2. Chen, W.F., & Atsuta, T. (1976). *Theory of beam columns*. New York: McGraw-Hill.
3. Ziemian, R. D., & McGuire, W. (2002). *Mastan2*. Web. 1 June 2011.  
<<http://www.mastan2.com>>.
4. Orbison, J.G., "Nonlinear Static Analysis of Three-Dimensional Steel Frames," Dissertation submitted in partial fulfillment for the degree of Doctor of Philosophy, Cornell University, Ithaca, NY, May 1982.
5. Ziemina, R.D., "Elastic-Plastic Analysis of Multi-Story Steel Frames," Cornell University, Ithaca, NY, May 1988.
6. Chapra, Steven C., and Raymond P. Canale. *Numerical Methods for Engineers: With Software and Programming Applications*. Boston: McGraw-Hill, 2002. Print.
7. Bourke, Paul. "Calculating the Area and Centroid of a Polygon." *Polygon Area and Centroid*. Web. 13 Sept. 2011. <<http://paulbourke.net/geometry/polyarea/>>.
8. Willett, J.B., and Judith D. S.(1988). Another Cautionary Note About  $R^2$ . *Its Use in Weighted Least-Squares Regression Analysis*. The American Statistician.

9. The MathWorks, Inc. (2012). *Surfnorm*. Web, 1 April 2012.

<<http://www.mathworks.com>>

# APPENDICES

## APPENDIX A: ANALYSIS RESULTS

**Table A1. Results of the analysis of the solid rectangular section.**

Solid Rectangular Section							
Weighting factors	c1	c2	c3	R squares		% concavity	
				Regression	MASTAN2	Regression	MASTAN2
Area	2.257	10.090	3.529	0.087	-0.584	0	0
Crowd	1.680	14.532	2.108	0.243	-1.774	11.12	0
Without	1.858	13.428	3.712	0.143	-0.584	0	0

**Table A2. Results of the analysis of the hollow rectangular sections.**

Hollow Rectangular Section (area weighting factors)								
h/b	b/t	c1	c2	c3	R squares		% concavity	
					Regression	MASTAN2	Regression	MASTAN2
1 2/5	7	2.505	27.359	3.862	-0.269	-1.266	0	0
1	8	2.962	24.809	3.748	-0.165	-1.156	0	0
1 1/4	9	2.659	27.002	3.805	-0.230	-1.233	0	0
1	10	2.962	24.812	3.748	-0.165	-1.156	0	0
1 1/5	11	2.714	26.608	3.789	-0.219	-1.219	0	0
1 2/5	12	2.514	28.091	3.860	-0.263	-1.270	0	0
1	13	2.963	24.814	3.748	-0.165	-1.156	0	0
1 1/3	14	2.576	27.629	3.834	-0.249	-1.254	0	0
1	15	2.963	24.816	3.748	-0.165	-1.156	0	0
1 1/4	16	2.660	27.010	3.805	-0.230	-1.233	0	0
1 1/3	17	2.576	27.639	3.834	-0.249	-1.254	0	0

1	18	2.976	25.148	3.745	-0.162	-1.161	0	0
1	19	2.976	25.153	3.745	-0.162	-1.162	0	0
1	20	2.980	25.245	3.744	-0.161	-1.163	0	0
1	21	2.982	25.312	3.743	-0.161	-1.164	0	0
1 1/3	22	2.582	28.187	3.832	-0.244	-1.258	0	0
1	23	2.982	25.316	3.743	-0.161	-1.164	0	0
1 1/3	24	2.582	28.192	3.832	-0.244	-1.258	0	0
1	25	2.985	25.406	3.743	-0.160	-1.166	0	0
1 1/5	26	2.725	27.245	3.786	-0.213	-1.225	0	0
1 2/5	27	2.520	28.770	3.858	-0.257	-1.274	0	0
1	28	2.985	25.410	3.743	-0.160	-1.166	0	0
1 1/5	29	2.725	27.250	3.786	-0.213	-1.225	0	0
1	30	2.990	25.548	3.741	-0.159	-1.168	0	0
1 1/4	31	2.671	27.810	3.802	-0.224	-1.240	0	0
1	32	2.990	25.554	3.741	-0.159	-1.168	0	0
1 1/8	33	2.819	26.752	3.765	-0.193	-1.206	0	0
1 1/4	34	2.671	27.816	3.802	-0.224	-1.240	0	0
1	35	2.993	25.645	3.741	-0.158	-1.169	0	0
1	36	2.993	25.648	3.741	-0.158	-1.169	0	0
1 2/7	37	2.634	28.202	3.814	-0.231	-1.250	0	0
1	38	2.997	25.770	3.740	-0.157	-1.171	0	0
1 1/3	39	2.586	28.704	3.831	-0.240	-1.262	0	0
1	40	2.997	25.773	3.740	-0.157	-1.171	0	0
1	41	2.997	25.774	3.740	-0.157	-1.171	0	0
1 1/3	42	2.586	28.708	3.831	-0.240	-1.262	0	0
1 1/3	43	2.586	28.712	3.831	-0.240	-1.262	0	0
1	44	2.997	25.778	3.740	-0.157	-1.171	0	0
1	45	3.000	25.880	3.739	-0.156	-1.173	0	0
1 1/4	46	2.675	28.173	3.801	-0.220	-1.243	0	0
1	47	3.000	25.883	3.739	-0.156	-1.173	0	0
1 1/4	48	2.675	28.176	3.801	-0.220	-1.243	0	0
1	49	3.001	25.945	3.738	-0.156	-1.174	0	0
1 1/5	50	2.733	27.827	3.784	-0.208	-1.231	0	0
1 2/5	51	2.523	29.391	3.856	-0.252	-1.278	0	0
1	52	3.001	25.949	3.738	-0.156	-1.174	0	0
1 1/5	53	2.733	27.832	3.784	-0.208	-1.231	0	0
1 2/5	54	2.523	29.396	3.856	-0.252	-1.278	0	0
1	55	3.003	26.014	3.738	-0.155	-1.175	0	0
1	56	3.003	26.017	3.738	-0.155	-1.175	0	0
1 2/7	57	2.637	28.613	3.813	-0.227	-1.253	0	0
1	58	3.004	26.054	3.738	-0.155	-1.176	0	0
1	59	3.004	26.057	3.738	-0.155	-1.176	0	0
1	60	3.005	26.080	3.737	-0.155	-1.176	0	0
1	61	3.007	26.187	3.737	-0.154	-1.178	0	0
1 1/4	62	2.677	28.512	3.800	-0.218	-1.246	0	0
1	63	3.007	26.188	3.737	-0.154	-1.178	0	0

1 1/5	64	2.735	28.090	3.784	-0.206	-1.234	0	0
1	65	3.007	26.189	3.737	-0.154	-1.178	0	0
1 1/3	66	2.589	29.177	3.829	-0.236	-1.265	0	0
1	67	3.007	26.190	3.737	-0.154	-1.178	0	0
1 1/4	68	2.677	28.515	3.800	-0.217	-1.246	0	0
1	69	3.007	26.190	3.737	-0.154	-1.178	0	0
1 2/5	70	2.524	29.675	3.855	-0.249	-1.280	0	0
1	71	3.007	26.192	3.737	-0.154	-1.178	0	0
1 1/8	72	2.829	27.422	3.762	-0.188	-1.214	0	0
1 1/4	73	2.677	28.517	3.800	-0.217	-1.246	0	0
1	74	3.007	26.192	3.737	-0.154	-1.178	0	0
1 1/3	75	2.589	29.181	3.829	-0.235	-1.265	0	0
1	76	3.009	26.293	3.736	-0.153	-1.180	0	0
1	77	3.010	26.314	3.736	-0.153	-1.180	0	0
1	78	3.010	26.317	3.736	-0.153	-1.180	0	0
2	5 3/4	2.120	29.052	4.126	-0.371	-1.374	0	0
1 1/2	6 7/8	2.421	27.786	3.904	-0.289	-1.288	0	0
1 1/2	8 3/5	2.429	28.733	3.901	-0.282	-1.293	0	0
2 1/3	8 5/8	1.984	32.461	4.257	-0.394	-1.418	0	0
2 1/3	10 1/3	1.980	33.156	4.253	-0.389	-1.418	0	0
2	11 1/2	2.117	32.231	4.113	-0.350	-1.379	0	0
2 1/3	13	1.976	33.822	4.248	-0.384	-1.417	0	0
1 1/2	13 3/4	2.435	29.998	3.897	-0.271	-1.299	0	0
2	14 3/8	2.115	32.768	4.110	-0.345	-1.379	0	0
1 1/2	17 1/6	2.435	30.366	3.895	-0.268	-1.300	0	0
2	21 1/2	2.111	33.422	4.104	-0.339	-1.379	0	0
2	21 5/9	2.111	33.427	4.104	-0.339	-1.379	0	0
2	23	2.111	33.505	4.104	-0.339	-1.379	0	0
2 1/3	25 6/7	1.967	35.011	4.237	-0.375	-1.414	0	0
1 1/2	27 1/2	2.435	30.867	3.893	-0.263	-1.302	0	0
2	28 3/4	2.109	33.732	4.101	-0.337	-1.378	0	0
2 1/3	34 1/2	1.964	35.283	4.234	-0.374	-1.410	0	0
1 2/3	41 1/4	2.305	32.200	3.960	-0.288	-1.330	0	0
1 1/2	46	2.433	31.167	3.892	-0.260	-1.301	0	0
2 1/2	5 3/4	1.942	30.572	4.330	-0.422	-1.433	0	0
3	6 8/9	1.816	32.950	4.505	-0.454	-1.473	0	0
2 6/7	7 1/2	1.842	33.182	4.455	-0.442	-1.463	0	0
3	8 5/8	1.805	34.185	4.500	-0.449	-1.473	0	0
3	10 1/3	1.798	34.951	4.495	-0.445	-1.472	0	0
2 1/2	11 1/2	1.923	34.020	4.316	-0.403	-1.433	0	0
2 6/7	12	1.825	35.139	4.443	-0.431	-1.461	0	0
3	13	1.791	35.684	4.489	-0.440	-1.470	0	0
2 1/2	13 7/9	1.919	34.523	4.311	-0.399	-1.433	0	0
2 6/7	15	1.819	35.733	4.438	-0.427	-1.460	0	0
3 1/3	17 1/4	1.719	37.110	4.586	-0.459	-1.486	0	0

2 6/7	20 1/9	1.813	36.306	4.431	-0.424	-1.457	0	0
3	20 5/8	1.780	36.709	4.479	-0.434	-1.466	0	0
3	23	1.778	36.876	4.476	-0.434	-1.464	0	0
3 1/3	25 6/7	1.710	37.795	4.578	-0.456	-1.477	0	0
2 1/2	27 1/2	1.909	35.664	4.299	-0.391	-1.427	0	0
2 6/7	30 1/6	1.807	36.839	4.425	-0.422	-1.450	0	0
2 1/2	34 1/2	1.906	35.878	4.297	-0.390	-1.423	0	0
4	5 3/4	1.688	33.042	4.780	-0.512	-1.524	0	0
4	6 7/8	1.673	34.450	4.784	-0.509	-1.523	0	0
4	8 3/5	1.656	35.801	4.781	-0.505	-1.522	0	0
4	10 1/3	1.646	36.648	4.777	-0.502	-1.520	0	0
3 1/2	11 1/2	1.705	36.299	4.644	-0.474	-1.498	0	0
4	11 1/2	1.640	37.074	4.774	-0.500	-1.519	0	0
4	12 7/8	1.635	37.463	4.772	-0.498	-1.517	0	0
4	13 3/4	1.633	37.665	4.770	-0.498	-1.516	0	0
4	17 1/4	1.625	38.252	4.764	-0.495	-1.512	0	0
3 1/2	23	1.685	37.959	4.628	-0.467	-1.487	0	0
5	5 3/4	1.613	33.914	4.981	-0.548	-1.553	0	0
5	6 7/8	1.594	35.400	4.988	-0.546	-1.553	0	0
5	8 3/5	1.574	36.820	4.989	-0.543	-1.551	0	0
5	11 1/2	1.555	38.178	4.985	-0.540	-1.546	0	0
5	13 3/4	1.546	38.823	4.981	-0.538	-1.542	0	0
5	17 1/6	1.536	39.446	4.976	-0.537	-1.535	0	0
6	6 7/8	1.546	36.053	5.143	-0.573	-1.571	0	0
6	8 3/5	1.524	37.533	5.147	-0.571	-1.569	0	0
6	11 1/2	1.502	38.966	5.145	-0.569	-1.562	0	0

**Table A3. Results of the analysis of the solid circular section.**

Solid Circular Section							
Weighting factors	c1	c2	c3	R squares		% concavity	
				Regression	MASTAN2	Regression	MASTAN2
Area	2.065	10.675	1.970	0.197	-1.747	[0]	[0]
Crowd	1.680	14.532	2.108	0.243	-1.774	[0]	[0]
Without	1.796	12.299	2.156	0.319	-1.774	[0]	[0]



**Table A4. Results of the analysis of hollow circular sections.**

Hollow Circular Section (area weighting factors)							
OD/t	c1	c2	c3	R squares		% concavity	
				Regression	MASTAN2	Regression	MASTAN2
10 1/5	2.696	23.675	2.155	0.107	-1.364	11.279	5.636
10 3/4	2.697	23.791	2.155	0.108	-1.365	11.276	5.636
11	2.698	23.829	2.155	0.108	-1.365	11.275	5.636
11 2/3	2.699	23.969	2.155	0.109	-1.366	11.271	5.636
11 5/6	2.700	23.989	2.155	0.110	-1.366	11.270	5.636
12	2.700	24.010	2.155	0.110	-1.366	11.269	5.636
12 1/3	2.700	24.064	2.155	0.110	-1.367	11.268	5.636
12 1/2	2.701	24.092	2.155	0.110	-1.367	11.267	5.636
12 3/4	2.701	24.121	2.155	0.111	-1.367	11.266	5.636
12 7/8	2.701	24.135	2.155	0.111	-1.367	11.266	5.636
12 8/9	2.701	24.137	2.155	0.111	-1.367	11.266	5.636
13	2.701	24.138	2.155	0.111	-1.367	11.266	5.636
13 2/3	2.702	24.224	2.155	0.111	-1.367	11.263	5.636
13 3/4	2.702	24.235	2.155	0.112	-1.368	11.263	5.636
14	2.702	24.268	2.155	0.112	-1.368	11.262	5.636
14 1/4	2.702	24.284	2.155	0.112	-1.368	11.262	5.636
14 1/3	2.702	24.293	2.155	0.112	-1.368	11.261	5.636
14 3/8	2.702	24.297	2.155	0.112	-1.368	11.261	5.636
14 7/9	2.703	24.334	2.155	0.112	-1.368	11.260	5.636
14 5/6	2.703	24.339	2.155	0.112	-1.368	11.260	5.636
15	2.703	24.345	2.155	0.112	-1.368	11.260	5.636
15 1/5	2.703	24.369	2.155	0.113	-1.369	11.259	5.636
15 3/4	2.703	24.410	2.155	0.113	-1.369	11.258	5.636
15 7/8	2.703	24.419	2.155	0.113	-1.369	11.258	5.636
16	2.703	24.424	2.155	0.113	-1.369	11.258	5.636
16 1/8	2.703	24.438	2.155	0.113	-1.369	11.257	5.636
16 1/2	2.703	24.460	2.155	0.113	-1.369	11.257	5.636
16 3/5	2.703	24.469	2.155	0.113	-1.369	11.256	5.636
17 1/9	2.703	24.502	2.155	0.113	-1.370	11.256	5.636
17 1/6	2.703	24.505	2.155	0.113	-1.370	11.255	5.636
17 1/5	2.703	24.506	2.155	0.113	-1.370	11.255	5.636
17 1/4	2.703	24.508	2.155	0.113	-1.370	11.255	5.636
17 2/5	2.703	24.516	2.155	0.113	-1.370	11.255	5.636
18 1/5	2.703	24.557	2.155	0.114	-1.370	11.254	5.636
18 1/2	2.703	24.573	2.155	0.114	-1.370	11.254	5.636
18 5/9	2.703	24.574	2.155	0.114	-1.370	11.254	5.636
19	2.703	24.594	2.155	0.114	-1.370	11.253	5.636

19 1/2	2.703	24.616	2.155	0.114	-1.370	11.252	5.636
19 2/3	2.703	24.624	2.155	0.114	-1.371	11.252	5.636
20	2.703	24.639	2.155	0.114	-1.371	11.252	5.636
20 1/9	2.703	24.641	2.155	0.114	-1.371	11.252	5.636
20 4/9	2.704	24.653	2.155	0.114	-1.371	11.251	5.636
20 1/2	2.704	24.654	2.155	0.114	-1.371	11.251	5.636
20 5/8	2.704	24.659	2.155	0.114	-1.371	11.251	5.636
20 2/3	2.704	24.662	2.155	0.114	-1.371	11.251	5.636
20 5/6	2.704	24.667	2.155	0.114	-1.371	11.251	5.636
21 2/7	2.703	24.682	2.155	0.114	-1.371	11.251	5.636
21 1/2	2.703	24.688	2.155	0.114	-1.371	11.250	5.636
21 5/9	2.703	24.691	2.155	0.114	-1.371	11.250	5.636
21 6/7	2.703	24.700	2.155	0.114	-1.371	11.250	5.636
22 3/4	2.703	24.727	2.155	0.115	-1.371	11.249	5.636
23	2.703	24.731	2.155	0.115	-1.371	11.249	5.636
23 1/8	2.703	24.736	2.155	0.115	-1.371	11.249	5.636
23 1/6	2.703	24.738	2.155	0.115	-1.371	11.249	5.636
23 5/8	2.703	24.748	2.155	0.115	-1.371	11.249	5.636
24	2.703	24.758	2.155	0.115	-1.372	11.249	5.636
24 1/5	2.703	24.761	2.155	0.115	-1.372	11.249	5.636
24 5/7	2.703	24.774	2.155	0.115	-1.372	11.248	5.636
24 7/9	2.703	24.775	2.155	0.115	-1.372	11.248	5.636
25	2.703	24.780	2.155	0.115	-1.372	11.248	5.636
25 1/2	2.703	24.790	2.155	0.115	-1.372	11.248	5.636
25 3/4	2.703	24.795	2.155	0.115	-1.372	11.248	5.636
25 7/9	2.703	24.795	2.155	0.115	-1.372	11.248	5.636
25 6/7	2.703	24.798	2.155	0.115	-1.372	11.248	5.636
27 3/7	2.703	24.826	2.155	0.115	-1.372	11.247	5.636
27 1/2	2.703	24.828	2.155	0.115	-1.372	11.247	5.636
27 4/7	2.703	24.829	2.155	0.115	-1.372	11.247	5.636
28 3/7	2.703	24.841	2.155	0.115	-1.372	11.246	5.636
28 2/3	2.703	24.846	2.155	0.115	-1.372	11.246	5.636
28 3/4	2.703	24.847	2.155	0.115	-1.372	11.246	5.636
29 1/2	2.703	24.858	2.156	0.115	-1.372	11.278	5.636
30	2.703	24.865	2.156	0.115	-1.372	11.277	5.636
30 1/9	2.703	24.866	2.156	0.115	-1.372	11.277	5.636
30 1/6	2.703	24.867	2.156	0.115	-1.373	11.277	5.636
30 4/5	2.702	24.874	2.156	0.115	-1.373	11.277	5.636
32	2.702	24.887	2.156	0.115	-1.373	11.277	5.636
32 1/5	2.703	24.890	2.156	0.115	-1.373	11.277	5.636
33	2.703	24.900	2.156	0.115	-1.373	11.276	5.636
34 3/8	2.702	24.913	2.156	0.115	-1.373	11.276	5.636
34 2/5	2.702	24.913	2.156	0.115	-1.373	11.276	5.636
34 1/2	2.702	24.914	2.156	0.115	-1.373	11.276	5.636
37	2.702	24.934	2.156	0.115	-1.373	11.275	5.636
38	2.702	24.942	2.156	0.115	-1.373	11.275	5.636

38 5/7	2.702	24.947	2.156	0.115	-1.373	11.275	5.636
38 4/5	2.702	24.948	2.156	0.115	-1.373	11.275	5.636
39 1/3	2.702	24.951	2.156	0.115	-1.373	11.275	5.636
39 1/2	2.702	24.953	2.156	0.115	-1.373	11.275	5.636
40 1/9	2.702	24.956	2.156	0.115	-1.373	11.275	5.636
40 2/9	2.702	24.957	2.156	0.115	-1.373	11.275	5.636
41 1/3	2.702	24.963	2.156	0.115	-1.373	11.275	5.636
43	2.702	24.972	2.156	0.115	-1.373	11.275	5.636
43 1/9	2.702	24.973	2.156	0.115	-1.373	11.275	5.636
44 6/7	2.702	24.982	2.156	0.115	-1.373	11.274	5.636
45 5/6	2.702	24.986	2.156	0.115	-1.373	11.274	5.636
46 1/7	2.702	24.987	2.156	0.115	-1.373	11.274	5.636
48 1/9	2.702	24.995	2.156	0.115	-1.373	11.274	5.636
49 4/7	2.702	25.001	2.156	0.115	-1.373	11.274	5.636
51 4/7	2.701	25.008	2.156	0.115	-1.374	11.274	5.636
51 5/7	2.701	25.008	2.156	0.115	-1.374	11.274	5.636
54 5/7	2.701	25.017	2.156	0.114	-1.374	11.273	5.636
55	2.701	25.018	2.156	0.114	-1.374	11.273	5.636
55 1/3	2.701	25.018	2.156	0.114	-1.374	11.273	5.636
57 1/9	2.701	25.023	2.156	0.114	-1.374	11.273	5.636
57 1/3	2.701	25.024	2.156	0.114	-1.374	11.273	5.636
57 1/2	2.701	25.024	2.156	0.114	-1.374	11.273	5.636
60	2.701	25.030	2.156	0.114	-1.374	11.273	5.636
60 1/3	2.701	25.031	2.156	0.114	-1.374	11.273	5.636
68 2/3	2.701	25.046	2.156	0.114	-1.374	11.273	5.636

**Table A5. Results of the analysis of wide-flange sections.**

Wide-flange Section (area weighting factors)							
Section Name	c1	c2	c3	R squares		% concavity	
				Regression	MASTAN2	Regression	MASTAN2
'W44X335'	[3.2899]	[3.7166]	[3.9617]	[0.7967]	[0.7647]	[0]	[0]
'W44X290'	[3.3812]	[3.7867]	[3.9390]	[0.8046]	[0.7731]	[0]	[0]
'W44X262'	[3.3862]	[3.6745]	[3.8383]	[0.8103]	[0.7761]	[0]	[0]
'W44X230'	[3.3430]	[3.4038]	[3.6414]	[0.8156]	[0.7682]	[0]	[0]
'W40X593'	[3.3452]	[5.0730]	[4.9643]	[0.6687]	[0.5652]	[0]	[0]
'W40X503'	[3.3693]	[4.7937]	[4.7452]	[0.7099]	[0.6346]	[0]	[0]

'W40X431'	[3.3801]	[4.5258]	[4.5357]	[0.7428]	[0.6892]	[0]	[0]
'W40X397'	[3.4224]	[4.4977]	[4.4770]	[0.7555]	[0.7033]	[0]	[0]
'W40X372'	[3.4176]	[4.3778]	[4.3880]	[0.7661]	[0.7212]	[0]	[0]
'W40X362'	[3.4323]	[4.3775]	[4.3747]	[0.7691]	[0.7239]	[0]	[0]
'W40X324'	[3.4606]	[4.2896]	[4.2798]	[0.7817]	[0.7401]	[0]	[0]
'W40X297'	[3.4486]	[4.1374]	[4.1682]	[0.7914]	[0.7557]	[0]	[0]
'W40X277'	[3.5506]	[4.3336]	[4.2336]	[0.7917]	[0.7447]	[0]	[0]
'W40X249'	[3.5633]	[4.2411]	[4.1476]	[0.7992]	[0.7555]	[0]	[0]
'W40X215'	[3.5776]	[4.1197]	[4.0354]	[0.8070]	[0.7662]	[0]	[0]
'W40X199'	[3.4219]	[3.5814]	[3.7241]	[0.8156]	[0.7769]	[0]	[0]
'W40X392'	[3.0416]	[4.0408]	[4.4320]	[0.6939]	[0.6494]	[0]	[0]
'W40X331'	[3.0505]	[3.7134]	[4.1571]	[0.7397]	[0.6956]	[0]	[0]
'W40X327'	[3.0794]	[3.7606]	[4.1749]	[0.7436]	[0.7034]	[0]	[0]
'W40X294'	[3.1034]	[3.6228]	[4.0398]	[0.7659]	[0.7235]	[0]	[0]
'W40X278'	[3.0755]	[3.4596]	[3.9207]	[0.7747]	[0.7206]	[0]	[0]
'W40X264'	[3.1053]	[3.4422]	[3.8820]	[0.7833]	[0.7307]	[0]	[0]
'W40X235'	[3.1877]	[3.4709]	[3.8396]	[0.7968]	[0.7515]	[0]	[0]
'W40X211'	[3.1897]	[3.3261]	[3.7098]	[0.8055]	[0.7490]	[0]	[0]
'W40X183'	[3.1847]	[3.1023]	[3.5120]	[0.8131]	[0.7314]	[0]	[0]
'W40X167'	[3.0331]	[2.5802]	[3.1433]	[0.8109]	[0.6056]	[0]	[0]
'W40X149'	[2.8658]	[1.9884]	[2.6618]	[0.7961]	[0.2982]	[0]	[0]
'W36X800'	[3.3709]	[5.9567]	[5.5085]	[0.5677]	[0.3554]	[0.9]	[0]
'W36X652'	[3.4337]	[5.5997]	[5.2428]	[0.6317]	[0.4662]	[0]	[0]
'W36X529'	[3.4955]	[5.3019]	[4.9969]	[0.6853]	[0.5558]	[0]	[0]
'W36X487'	[3.5043]	[5.1612]	[4.8928]	[0.7038]	[0.5902]	[0]	[0]
'W36X487'	[3.5043]	[5.1612]	[4.8928]	[0.7038]	[0.5902]	[0]	[0]
'W36X441'	[3.5325]	[5.0451]	[4.7870]	[0.7234]	[0.6217]	[0]	[0]
'W36X395'	[3.5569]	[4.9246]	[4.6789]	[0.7414]	[0.6511]	[0]	[0]
'W36X361'	[3.5692]	[4.8107]	[4.5843]	[0.7550]	[0.6748]	[0]	[0]
'W36X330'	[3.5971]	[4.7539]	[4.5173]	[0.7652]	[0.6887]	[0]	[0]
'W36X302'	[3.6038]	[4.6398]	[4.4247]	[0.7761]	[0.7082]	[0]	[0]
'W36X282'	[3.6074]	[4.5606]	[4.3604]	[0.7829]	[0.7204]	[0]	[0]
'W36X262'	[3.5767]	[4.3748]	[4.2424]	[0.7923]	[0.7421]	[0]	[0]
'W36X247'	[3.5603]	[4.2585]	[4.1642]	[0.7979]	[0.7536]	[0]	[0]
'W36X231'	[3.5497]	[4.1551]	[4.0900]	[0.8028]	[0.7625]	[0]	[0]
'W36X256'	[3.2065]	[3.7636]	[4.0746]	[0.7775]	[0.7450]	[0]	[0]
'W36X232'	[3.2184]	[3.6363]	[3.9563]	[0.7904]	[0.7548]	[0]	[0]
'W36X210'	[3.1398]	[3.2588]	[3.6909]	[0.8026]	[0.7363]	[0]	[0]
'W36X194'	[3.1490]	[3.1746]	[3.6073]	[0.8078]	[0.7326]	[0]	[0]

'W36X182'	[3.1465]	[3.0862]	[3.5287]	[0.8108]	[0.7238]	[0]	[0]
'W36X170'	[3.1382]	[2.9789]	[3.4368]	[0.8128]	[0.7090]	[0]	[0]
'W36X160'	[3.1146]	[2.8381]	[3.3244]	[0.8133]	[0.6819]	[0]	[0]
'W36X150'	[3.0751]	[2.6536]	[3.1807]	[0.8119]	[0.6345]	[0]	[0]
'W36X135'	[2.9512]	[2.1906]	[2.8151]	[0.8012]	[0.4423]	[0]	[0]
'W33X387'	[3.5822]	[5.1764]	[4.8374]	[0.7205]	[0.6034]	[0]	[0]
'W33X354'	[3.5969]	[5.0629]	[4.7443]	[0.7356]	[0.6302]	[0]	[0]
'W33X318'	[3.6304]	[4.9827]	[4.6574]	[0.7500]	[0.6514]	[0]	[0]
'W33X291'	[3.6374]	[4.8729]	[4.5708]	[0.7614]	[0.6729]	[0]	[0]
'W33X263'	[3.6544]	[4.7814]	[4.4874]	[0.7720]	[0.6907]	[0]	[0]
'W33X241'	[3.5945]	[4.4830]	[4.3114]	[0.7870]	[0.7300]	[0]	[0]
'W33X221'	[3.5776]	[4.3352]	[4.2099]	[0.7950]	[0.7467]	[0]	[0]
'W33X201'	[3.5504]	[4.1435]	[4.0800]	[0.8035]	[0.7635]	[0]	[0]
'W33X169'	[3.2974]	[3.5781]	[3.8365]	[0.8057]	[0.7689]	[0]	[0]
'W33X152'	[3.2236]	[3.2302]	[3.5936]	[0.8126]	[0.7481]	[0]	[0]
'W33X141'	[3.1669]	[2.9817]	[3.4151]	[0.8141]	[0.7136]	[0]	[0]
'W33X152'	[3.2236]	[3.2302]	[3.5936]	[0.8126]	[0.7481]	[0]	[0]
'W33X141'	[3.1669]	[2.9817]	[3.4151]	[0.8141]	[0.7136]	[0]	[0]
'W33X130'	[3.0966]	[2.6886]	[3.1968]	[0.8123]	[0.6470]	[0]	[0]
'W33X118'	[3.0110]	[2.3394]	[2.9221]	[0.8046]	[0.5228]	[0]	[0]
'W30X391'	[3.5983]	[5.5326]	[5.0662]	[0.6850]	[0.5256]	[0]	[0]
'W30X357'	[3.6320]	[5.4451]	[4.9801]	[0.7026]	[0.5528]	[0]	[0]
'W30X326'	[3.6493]	[5.3282]	[4.8861]	[0.7188]	[0.5824]	[0]	[0]
'W30X292'	[3.6861]	[5.2450]	[4.7973]	[0.7346]	[0.6062]	[0]	[0]
'W30X261'	[3.6802]	[5.0566]	[4.6681]	[0.7519]	[0.6437]	[0]	[0]
'W30X235'	[3.7226]	[5.0283]	[4.6109]	[0.7613]	[0.6540]	[0]	[0]
'W30X211'	[3.6720]	[4.7374]	[4.4385]	[0.7782]	[0.6995]	[0]	[0]
'W30X191'	[3.6601]	[4.5811]	[4.3289]	[0.7883]	[0.7218]	[0]	[0]
'W30X173'	[3.6475]	[4.4337]	[4.2248]	[0.7966]	[0.7397]	[0]	[0]
'W30X148'	[3.2943]	[3.6588]	[3.9090]	[0.8009]	[0.7672]	[0]	[0]
'W30X132'	[3.1898]	[3.2055]	[3.6004]	[0.8107]	[0.7418]	[0]	[0]
'W30X124'	[3.1724]	[3.0753]	[3.4968]	[0.8130]	[0.7266]	[0]	[0]
'W30X116'	[3.1222]	[2.8557]	[3.3347]	[0.8135]	[0.6864]	[0]	[0]
'W30X108'	[3.0514]	[2.5697]	[3.1176]	[0.8108]	[0.6071]	[0]	[0]
'W30X99'	[2.9772]	[2.2659]	[2.8730]	[0.8033]	[0.4837]	[0]	[0]
'W30X90'	[2.9860]	[2.1963]	[2.7970]	[0.7985]	[0.4588]	[0]	[0]
'W27X539'	[3.4821]	[6.4003]	[5.6741]	[0.5522]	[0.2799]	[0]	[0]
'W27X368'	[3.6138]	[5.8164]	[5.2358]	[0.6565]	[0.4602]	[0]	[0]
'W27X336'	[3.6505]	[5.7244]	[5.1483]	[0.6758]	[0.4904]	[0]	[0]

'W27X307'	[3.6614]	[5.5829]	[5.0478]	[0.6940]	[0.5263]	[0]	[0]
'W27X281'	[3.7053]	[5.5383]	[4.9822]	[0.7082]	[0.5443]	[0]	[0]
'W27X258'	[3.7137]	[5.4100]	[4.8886]	[0.7232]	[0.5745]	[0]	[0]
'W27X235'	[3.7044]	[5.2359]	[4.7755]	[0.7389]	[0.6106]	[0]	[0]
'W27X217'	[3.7489]	[5.2442]	[4.7437]	[0.7458]	[0.6145]	[0]	[0]
'W27X194'	[3.7526]	[5.0967]	[4.6348]	[0.7598]	[0.6441]	[0]	[0]
'W27X178'	[3.6721]	[4.7404]	[4.4407]	[0.7780]	[0.6991]	[0]	[0]
'W27X161'	[3.6779]	[4.6390]	[4.3578]	[0.7864]	[0.7149]	[0]	[0]
'W27X146'	[3.6762]	[4.5219]	[4.2681]	[0.7942]	[0.7306]	[0]	[0]
'W27X129'	[3.3551]	[3.8551]	[4.0203]	[0.7972]	[0.7669]	[0]	[0]
'W27X114'	[3.2702]	[3.4368]	[3.7366]	[0.8094]	[0.7642]	[0]	[0]
'W27X102'	[3.2606]	[3.2800]	[3.6056]	[0.8139]	[0.7556]	[0]	[0]
'W27X94'	[3.2062]	[3.0307]	[3.4260]	[0.8151]	[0.7248]	[0]	[0]
'W27X84'	[3.1203]	[2.6652]	[3.1548]	[0.8115]	[0.6451]	[0]	[0]
'W24X370'	[3.5709]	[6.2053]	[5.5014]	[0.6004]	[0.3529]	[0]	[0]
'W24X335'	[3.6055]	[6.0623]	[5.3921]	[0.6262]	[0.3971]	[0]	[0]
'W24X306'	[3.6456]	[5.9618]	[5.3007]	[0.6478]	[0.4311]	[0]	[0]
'W24X279'	[3.6694]	[5.8352]	[5.2037]	[0.6678]	[0.4672]	[0]	[0]
'W24X250'	[3.7129]	[5.7380]	[5.1072]	[0.6882]	[0.4987]	[0]	[0]
'W24X229'	[3.7236]	[5.6013]	[5.0092]	[0.7052]	[0.5327]	[0]	[0]
'W24X207'	[3.7482]	[5.4941]	[4.9173]	[0.7211]	[0.5607]	[0]	[0]
'W24X192'	[3.7693]	[5.4292]	[4.8556]	[0.7314]	[0.5778]	[0]	[0]
'W24X176'	[3.7750]	[5.3197]	[4.7749]	[0.7429]	[0.6018]	[0]	[0]
'W24X162'	[3.7648]	[5.1615]	[4.6711]	[0.7560]	[0.6328]	[0]	[0]
'W24X146'	[3.7398]	[4.9547]	[4.5418]	[0.7702]	[0.6690]	[0]	[0]
'W24X131'	[3.6869]	[4.6638]	[4.3691]	[0.7857]	[0.7119]	[0]	[0]
'W24X117'	[3.6618]	[4.4642]	[4.2361]	[0.7963]	[0.7369]	[0]	[0]
'W24X104'	[3.6418]	[4.2865]	[4.1123]	[0.8044]	[0.7547]	[0]	[0]
'W24X103'	[3.3569]	[3.8652]	[4.0269]	[0.7968]	[0.7665]	[0]	[0]
'W24X94'	[3.3269]	[3.6464]	[3.8683]	[0.8057]	[0.7715]	[0]	[0]
'W24X84'	[3.2949]	[3.4156]	[3.6956]	[0.8124]	[0.7659]	[0]	[0]
'W24X76'	[3.2380]	[3.1395]	[3.4981]	[0.8153]	[0.7410]	[0]	[0]
'W24X68'	[3.1456]	[2.7576]	[3.2220]	[0.8130]	[0.6700]	[0]	[0]
'W24X62'	[2.8605]	[2.1412]	[2.8211]	[0.8035]	[0.3695]	[0]	[0]
'W24X55'	[2.8017]	[1.8489]	[2.5485]	[0.7927]	[0.1642]	[0]	[0]
'W21X201'	[3.8190]	[5.9541]	[5.1615]	[0.6864]	[0.4632]	[0]	[0]
'W21X182'	[3.8384]	[5.8334]	[5.0694]	[0.7026]	[0.4945]	[0]	[0]
'W21X166'	[3.8787]	[5.7922]	[5.0110]	[0.7138]	[0.5088]	[0]	[0]
'W21X147'	[3.7609]	[5.2498]	[4.7377]	[0.7472]	[0.6146]	[0]	[0]

'W21X132'	[3.7840]	[5.1764]	[4.6658]	[0.7575]	[0.6316]	[0]	[0]
'W21X122'	[3.8005]	[5.1138]	[4.6064]	[0.7652]	[0.6450]	[0]	[0]
'W21X111'	[3.8040]	[5.0157]	[4.5315]	[0.7737]	[0.6630]	[0]	[0]
'W21X101'	[3.8281]	[4.9789]	[4.4834]	[0.7794]	[0.6707]	[0]	[0]
'W21X93'	[3.2906]	[3.8244]	[4.0520]	[0.7891]	[0.7590]	[0]	[0]
'W21X83'	[3.3177]	[3.7367]	[3.9536]	[0.7995]	[0.7680]	[0]	[0]
'W21X73'	[3.3349]	[3.6251]	[3.8424]	[0.8077]	[0.7726]	[0]	[0]
'W21X68'	[3.3163]	[3.4880]	[3.7399]	[0.8117]	[0.7700]	[0]	[0]
'W21X62'	[3.2813]	[3.2796]	[3.5865]	[0.8150]	[0.7571]	[0]	[0]
'W21X68'	[3.3163]	[3.4880]	[3.7399]	[0.8117]	[0.7700]	[0]	[0]
'W21X62'	[3.2813]	[3.2796]	[3.5865]	[0.8150]	[0.7571]	[0]	[0]
'W21X55'	[3.1802]	[2.8604]	[3.2897]	[0.8142]	[0.6946]	[0]	[0]
'W21X48'	[3.0488]	[2.3530]	[2.9081]	[0.8026]	[0.5383]	[0]	[0]
'W21X57'	[3.0558]	[2.8132]	[3.3487]	[0.8107]	[0.6650]	[0]	[0]
'W21X50'	[2.9390]	[2.3353]	[2.9689]	[0.8072]	[0.4944]	[0]	[0]
'W21X44'	[2.8583]	[1.9741]	[2.6508]	[0.7959]	[0.2852]	[0]	[0]
'W18X311'	[3.6136]	[7.0538]	[5.9085]	[0.5193]	[0.1548]	[0]	[0]
'W18X283'	[3.6480]	[6.8635]	[5.7955]	[0.5482]	[0.2078]	[0]	[0]
'W18X258'	[3.6976]	[6.7510]	[5.7056]	[0.5727]	[0.2454]	[0]	[0]
'W18X234'	[3.7546]	[6.6653]	[5.6215]	[0.5954]	[0.2771]	[0]	[0]
'W18X211'	[3.7847]	[6.5043]	[5.5130]	[0.6196]	[0.3222]	[0]	[0]
'W18X192'	[3.8325]	[6.4217]	[5.4322]	[0.6387]	[0.3502]	[0]	[0]
'W18X175'	[3.8419]	[6.2603]	[5.3314]	[0.6580]	[0.3915]	[0]	[0]
'W18X158'	[3.8658]	[6.1299]	[5.2349]	[0.6765]	[0.4268]	[0]	[0]